CAPITAL UNIVERSITY OF SCIENCE AND TECHNOLOGY, ISLAMABAD

Effects of Magnetic Field Inclination and Joule Heating on Mixed Convective Nanofluid Flow in an Inclined Porous Channel

by

Hira Khalid

A thesis submitted in partial fulfillment for the degree of Master of Philosophy

in the

Faculty of Computing
Department of Mathematics

2019

All dedications in the memory of my dearest father **Ch. Khalid Farooq** who always believed in me to be successful whatever the situation and his well wishes will remain with me throughout my life.

CERTIFICATE OF APPROVAL

Effects of Magnetic Field Inclination and Joule Heating on Mixed Convective Nanofluid Flow in an Inclined Porous Channel

by

Hira Khalid

(MMT171009)

THESIS EXAMINING COMMITTEE

S. No.	Examiner	Name	Organization
(a)	External Examiner	Dr. Tanvir Akbar Kiani	COMSATS University, Islamabad
(b)	Internal Examiner	Dr. Muhammad Sagheer	CUST, Islamabad
(c)	Supervisor	Dr. Shafqat Hussain	CUST, Islamabad

Dr. Shafqat Hussain
Thesis Supervisor
September, 2019

Dr. Muhammad Sagheer
Head
Dept. of Mathematics
September, 2019

Dr. Muhammad Abdul Qadir
Dean
Faculty of Computing
September, 2019

Author's Declaration

I, **Hira Khalid** hereby state that my M. Phil thesis titled "**Effects of Magnetic Field Inclination and Joule Heating on Mixed Convective Nanofluid Flow in an Inclined Porous Channel**" is my own work and has not been submitted previously by me for taking any degree from Capital University of Science and Technology, Islamabad or anywhere else in the country/abroad.

At any time if my statement is found to be incorrect even after my graduation, the University has the right to withdraw my M. Phil Degree.

Hira Khalid

(MMT171009)

Plagiarism Undertaking

I solemnly declare that research work presented in this thesis titled "***Effects of Magnetic Field Inclination and Joule Heating on Mixed Convective Nanofluid Flow in an Inclined Porous Channel***" is solely my research work with no significant contribution from any other person. Small contribution/help wherever taken has been dully acknowledged and that complete thesis has been written by me.

I understand the zero tolerance policy of the HEC and Capital University of Science and Technology towards plagiarism. Therefore, I as an author of the above titled thesis declare that no portion of my thesis has been plagiarized and any material used as reference is properly referred/cited.

I undertake that if I am found guilty of any formal plagiarism in the above titled thesis even after award of M. Phil degree, the University reserves the right to withdraw/revoke my M. Phil degree and that HEC and the University have the right to publish my name on the HEC/University website on which names of students are placed who submitted plagiarized work.

Hira Khalid

(MMT171009)

Acknowledgements

Starting with the name of Almighty **ALLAH** who is most gracious and omnipresent, who makes the mankind and created this world to reveal what is veiled. Also, the **Prophet Muhammad (Peace Be Upon Him)** who is a guidance in every aspect of life for the betterment of Humanity.

I would like to say a big thanks to my supervisor **Dr. Shafqat Hussain**, Associate Professor in Capital University of Science and Technology, for not only letting my mind to explore this problem but also helping me throughout the research and compilation of my dissertation. I would appreciate his continuous support, motivation, enthusiasm and immense knowledge. I would really acknowledge him for being such a resourceful mentor. He brought me to the opportunities up to my level and provided me the tools that drag me to the right direction and helped me to accomplish my thesis. He supported me greatly and was always there to help me. It was a great honour for me to work and study under his care and guidance.

Beside this, I would like to express my deep and sincere gratitude to our honourable head of department **Dr. Muhammad Sagheer** for providing us such an invaluable environment. I would also be thankful to my respected professors **Dr. Muhammad Afzal**, **Dr. Abdul Rehman Kashif** and **Dr. Rashid Ali** for their valuable guidance throughout this M. Phil session.

How could I forget my research fellows and seniors of this department who were always there as a source of encouragement for me. I am extremely grateful to my parents for their love and prayers especially my mother **Naheed Bashir** who always give me spiritual and moral support where I needed and to my lovable sister **Marwa Khalid** for being such a helpful companion throughout this journey.

Hira Khalid

(MMT171009)

Abstract

This thesis investigates MHD mixed convection of alumina-water nanofluid flow in an inclined porous channel. The effects of external inclined magnetic field and viscous dissipation due to Joule heating are inspected in this regard at a fixed cavity inclination. The influence of porous medium on heat convection is analyzed by Darcy-Brinkman-Forchheimer model. The left wall of cavity region is at T_h. The temperature of inlet opening of channel is T_c. The upper horizontal channel and the other walls of cavity are adiabatic. The governing system of PDEs is numerically simulated by Galerkin weighted residual based FEM. The space discretization of PDEs is performed by using LBB-stable finite element Q_2/P_1^{disc} pair, for which the velocity and temperature components are discretized by utilizing biquadratic (Q_2) element space whereas pressure is discretized in linear discontinuous (P_1^{disc}) finite element space. It leads to third order accuracy of Q_2 element and second order accuracy of P_1^{disc} element in L_2-norm. Governing physical parameters such as Reynolds number, Richardson number, Darcy number, Eckert number, porosity, magnetic field inclination and nanoparticles volume fraction are used to study the flow-temperature behaviour.

Contents

List of Figures

List of Tables

Abbreviations

PDEs	Partial differential equations
FEM	Finite element method
GFEM	Galerkin finite element method
FVM	Finite volume method
LBM	Lattice Boltzmann method
DBF	Darcy-Brinkman-Forchheimer
CCW	Counterclockwise
MHD	Magnetohydrodynamics
LBB	Ladyzhenskaya-Babuska-Brezzi

Symbols

C_ρ	Specific heat constant ($J\ kg^{-1}\ K^{-1}$)
$\mathbf{g}$	Gravitational acceleration ($m\ s^{-2}$)
$\frac{d\overline{Q}}{dt}$	Rate of heat transfer
A	Cross-sectional area normal to direction of heat flow (m^2)
$\hat{h}$	Enthalpy of system (J or $N\ m$)
H	Length of the square cavity (m)
u_0	Inlet velocity of flow ($m\ s^{-1}$)
Nu_{L}	Local Nusselt number
Nu_{avg}	Average Nusselt number
p	Dimensional pressure ($N\ m^{-2}$)
$\widehat{P}$	Non-dimensional pressure
Pr	Prandtl number ($\frac{\nu_f}{\alpha_f}$)
Ri	Richardson number ($\frac{GR}{Re^2}$)
Ha	Hartmann number ($B_0 H\sqrt{\sigma_f/\mu_{nf}}$)
Ec	Eckert number $\left(\frac{u_0^2}{C_p(T_h-T_c)}\right)$
Re	Reynolds number ($\frac{Hu_0}{\nu_f}$)
Gr	Grashof number ($\beta_f\ g\ \Delta T\ H^3/\nu_f^2$)
Da	Darcy number ($\frac{x}{H^2}$)
K	Permeability of porous medium (m^2)
C_f	Dimensionless drag force constant
$\mathbf{B}$	Strength of external magnetic field ($N\ m\ s^{-1}$)
T	Fluid's dimensional temperature (K)
T_h	Temperature of left hot wall (K)

T_c	Temperature of adiabatic walls (K)
R_f	Interfacial resistance of nanoparticles $(Km^2\ W^{-1})$
ΔT	Temperature gradient (K)
T_α	Object's surface temperature (K)
T_β	Temperature of fluid (K)
u	Dimensional velocity of flow in x-direction $(m\ s^{-1})$
v	Dimensional velocity of flow in y-direction $(m\ s^{-1})$
$\tilde{u}$	x-component of dimensional velocity in porous medium $(m\ s^{-1})$
$\tilde{v}$	y-component of dimensional velocity in porous medium $(m\ s^{-1})$
$\widehat{U}$	Dimensionless velocity component in x-direction
$\widehat{V}$	Dimensionless velocity component in y-direction
$\widehat{\theta}$	Dimensionless temperature component
(x, y)	Dimensional space coordinates (m)
(X, Y)	Dimensionless space coordinates

Greek symbols

α	Thermal diffusivity $(m^2\ s^{-1})$
β	Thermal expansion coefficient (K^{-1})
ϕ	Volume fraction of nanoparticles
θ	Non-dimensional temperature $\left(\frac{T-T_c}{T_h-T_c}\right)$
ρ	Density $(kg\ m^{-3})$
σ	Electrical conductivity $(\Omega\ m^{-1})$
μ	Dynamic viscosity $(kg\ m^{-1}\ s^{-1})$
ν	Kinematic viscosity $(m^2\ s^{-1})$
σ^*	Stefan-Boltzman constant $(K\ W\ m^{-2}\ k^{-4})$
ϵ	Porosity of medium
γ	Cavity inclination
ψ	Magnetic field inclination
κ	Thermal conductivity $(kg\ m\ s^3\ K^{-1})$
$\vec{\omega}$	Angular velocity (rad s^{-1})
τ^*	Stresses on flow (Nm^{-2})
$\hat{\varepsilon}$	Thermal emissivity of object

$\mathbf{\Phi}$	Viscous dissipation

Subscripts

avg	Average
c	Cold
h	Hot
f	Fluid
nf	Nanofluid
p	Nanoparticles
s	Solid medium particles
m	Porous medium

Chapter 1

Introduction

Heat transfer mechanism has been known for its great importance in many engineering and medical sciences for last many decades. Due to enormous benefits of heat energy for mankind, the field of thermodynamics is effectively linked with other disciplines. Heat transport process is imparting its noteworthy role in building designing [1], fuel filling system [2], air compressor [3], food industry [4], and in many other fields. In this regard fluid dynamics is playing an important role in thermal energy management by the usage of different fluids having good thermophysical properties. Researchers are emphasizing on different factors which are important for the augmentation of thermal process like involvement of porous medium, open and close cavities, implementation of magnetic effects, nanofluids, micro sized channel, etc., to enhance the thermal convection process. Our present study is focusing on the thermal energy transfer through open ended channel having cavity with the involvement of porous medium. The channel inclinations are considered here which has significant impacts in enhancement of heat distribution. Hence the thermal effects are maximized by using nanoparticles of Al_2O_3 along with the porous medium in view of Darcy-Brinkman-Forchheimer model and cavity inclinations. The extended work is focusing on the thermal flow controlling parameters for which MHD effects are incorporated. Magnetic field is rotating in counterclockwise direction for this case. The measurement of heat addition in system due to resistive effects by nanoparticles in the presence of uniform magnetic

field are observed in terms of Joule heating effects. To avoid complexity, power losses due to viscous dissipation by stresses as well as due to drag forces of porous medium are ignored.

1.1 Literature Review

1.1.1 Nanofluid and Heat Transfer

Research has distinctly shown that the thermal properties, boundary conditions and physical geometry of flow are used for the augmentation of heat convection process in fluids. The scope of 'micro' or 'nano' sized particles has been analyzed for better heat distribution in past decades [5]. Since the thermal conductive properties of solids are far better than liquid fluids, so the modern science technology is working on the use of nanometer sized solid particles usually with diameter less than 50 nm. Choi in [6] has used the term nanofluid for the first time, which is the colloidal mixture of nanoparticles and base fluid. Most of the research has shown that metallic particles transfer more heat energy as compared to non-metallic particles.

The comparative analysis on thermophysical properties was extesively studied by Hwang et al. in [7–9]. The study revealed that physical nature of nanoparticles (like shape, size and solid volume fraction) with base fluids (like water and ethylene glycol) has significant impacts on maximum heat transfer process. Buongiorno [10] investigated the seven velocity slip mechanisms due to the motion of nanoparticles. These were observed to be responsible for the abnormal increment in different thermal properties. Among all of these, velocity slips due to Brownian motion and thermophoresis seemed major contributor for incremented heat transport. Thermophysical aspects of aluminium oxide and copper oxide nanoparticles has been investigated by Zeinali et al. in [11]. The results illustrated that heat transfer coefficient has effective impacts on thermal conductivity and Peclet number. It was also concluded that Al_2O_3-water has shown better heat convection than

CuO-water nanofluid. The role of cavities with double-lid movements in mixed convection has been numerically explored by Mansour and Ahmed in [12]. It was observed that heat transport mechanism is strongly enhanced by the movements of enclosure's walls and with the increased solid volume concentration of particles.

1.1.2 Role of Mixed Convection in Heat Transfer

When heat transportation is arisen both by natural and forced convection, then another powerful mode of heat transfer is activated which is known as mixed convection. Mixed convection is responsible for many thermo-energy processes under the influence of balanced inertial forces of fluids (like shear, viscous, buoyancy forces etc.). Its implementations have been noticed in many processes of scientific importance like electrical cooling setups, industrial-chemical processes, dehydration of food technologies, engineering lubrication systems, food making reactions, etc., as discussed in [13].

Al-Amiri et al. [14] revealed that cavities with moving lid along the sinusoidal wavy wall at bottom has shown better mixed convection results. For numerical study, GFEM has been used to discretize governing system of PDEs. Significant Nu_{avg} at the low Richardson number were found due to wavy surface at the bottom of cavity. Hence a significant heat transfer was observed at low Richardson number. A vertical flat plate problem was analyzed by Hossain and Takhar in [15] to explore the impacts of thermal radiations on mixed convective flow numerically by adopting implicit finite difference method. It has been concluded that local shear stress and local heat transfer was reduced with the increased radiation parameter. Higher rate of convective heat transfer was observed at the maximized values of Prandtl number. Kurtbas and Celik [16] conducted a research on a horizontal rectangular shaped channel to analyze the influence of foamed medium (porous in nature) on forced and mixed convective heat transport. Results evidently revealed the effects of different physical parameters like cavity aspect ratio, Grashof number, Reynolds number and Richardson number on Nu_{avg} for heat transfer. It was concluded that Nu_{avg} directly affected by the increasing Reynolds number and

cavity aspect ratio. Similarly buoyancy effects were also increased for growing values of Grashof number. The exploration about nanoparticles mean diameter and their distinguishable effects on mixed convective heat transfer has been presented by Mirmasoumi and Behzadmehr [17]. Two-phase model for nanofluids mixture has been used for this numerical investigation by using finite volume method. An enhanced convection process was observed for nanoparticles having smaller sized diameters with no visible disruption in skin friction. Alchaar et al. [18] performed numerical simulations to study buoyancy dominated convection (natural convection) inside shallow rectangular shaped cavity in the presence of transverse magnetic field by applying finite difference scheme. Heat distribution over the flow geometry has been studied by different dimensionless physical parameters like Rayleigh number, Prandtl number, Hartmann number and cavity aspect ratio. There was a noticeable enhancement in Nu_{avg} for growing values of Rayleigh number. Horizontal open channel with open enclosure has been used to investigate different modes of mixed convective nanofluid flow (assisting, opposing and horizontal forced flow) by Mancca et al. [19] numerically. The results of simulations clearly depicted that maximum convection was occured for opposing forced flow case. Maximized thermal convection was noticed for the decreasing values of Reynolds and Richardson numbers. Lid-driven cavity with obstacle problem has been presented by Hemmat et al. [20] to study mixed convection with Al_2O_3-water nanofluid. The solution for governing PDEs was achieved by finite volume method. Augmented heat convection process was inspected for the incremented amount of Al_2O_3 particles. Growth in Richardson number resulted in the reduced values of Nu_{avg}.

1.1.3 Inclined Enclosures and Mixed Convection

The utilization of mixed convection for many engineering and industrial processes in open cavities brought revolutionary changes in many applications like electrical cooling of micro and nano devices, heat exchangers, solar collectors , crystal growth, etc., [21, 22]. Many studies on open U-shaped cavities have also been

come out for different experimental investigations and to study thermodynamical processes [19].

Hussain et al. [23] discussed the mixed convection of nanofluid flow inside an inclined double lid-driven enclosure in the presence of discrete heating source. The space and time discretization of unsteady PDEs were performed by finite element method and the Crank–Nicolson scheme respectively. Significant and enhanced convection process for left heating source has been noticed with the increasing angles of inclined cavity, i.e., γ. More enhanced average Nusselt number has been found with the augmentation in Richardson number and solid volume fraction of particles. A noticeable reduction in entropy of system was also observed for the increased cavity inclinations. A numerical investigation was studied by Kumar and Eswaran [24] to analyze the effects of thermal radiations on natural convective flow in an inclined enclosure. The cavity tilt angles, i.e., 45° and 60° have been chosen as test angles to study the impacts of different parameters on heat flow behaviour. The numerical results were obtained by finite volume scheme. It was concluded that the flow pattern and temperature field were significantly affected by radiations. An overall declination was observed in flow rate and for total Nusselt number at slanted angle of 45°. Ghasemi et al. [25] have presented an analysis about natural convective copper oxide nanofluid flow with inclination impacts of cavity. Increased temperature distribution over flow was noticed for the increased concentration of nanoparticles. The ascending values of Ra at different cavity alignments have shown significant variations for flow-velocity profiles and temperature field. Oztop et al. [26] investigated the natural convective nanofluid flow by interpreting the impacts of cavity inclinations and porous medium in the presence of non-isothermal heating source at cavity wall. The inclined layouts of enclosure have figured out as a major heat controlling parameter over the flow field. Rise with the Grashof number resulted in the increased thermal convection process. Mehrez et al. [22] examined the mixed convection of assisting copper-water nanofluid flow to explore the influence of inclined angles of open cavity on thermal energy distribution as well as on the entropy by system. Governing dimensionless system of PDEs has been inspected numerically by using FVM. The

results were examined for different inclination angles ($0° \leq \gamma \leq 360°$), solid volume fraction ratios ($0 \leq \phi \leq 0.06$) and Re numbers (100, 300 and 500) with fixed Gr number, i.e., $Gr = 10^4$. It has been noticed that at angles from 135° to 225° conduction mode dominated due to which less heat transfer and less entropy was observed. The comparison study of Bejan number showed that maximum fluid friction was observed for inclined angles of 90° and 135° at different values of Re.

1.1.4 Impact of Porous Medium on Mixed Convection

Many industrial, engineering and biological fields are using porous medium for thermal energy management. Mnay fields related to engineering and geological sciences include exploring underground reservoirs, applications of porous solids, thermal insulation, oil-gas recovery technology, geothermal species transport [27] are directly depending on the involvement of porous medium. Other applications of porous medium in medical fields are found in peristaltic processes like transport of urine from kidney, swallowing of food through esophagus, lymph transport, etc., [28].

MHD mixed convective copper oxide/water nanofluid flow inside porous cavity under the influence of heat flux boundary conditions has been extensively studied by Sheikholeslami and Shehzad [29]. The FEM has been adopted to study the consequences of different pertinent quantities which included CuO volume fraction, Hartmann number and Rayleigh number on thermal convection process. Enhanced Nu_{avg} was noticed at growing values of Ra and ϕ . Gibanov et al. [30] explored the impacts of magnetic field alignments on mixed convective ferrofluid flow inside a cavity with horizontal porous layer having a moving lid. Extended DBF model is introduced to analyze the influence of porous medium in thermal energy distribution among fluid layers. It was noticed that the inclination of magnetic field and height of porous layer have played a distinguishable role to control different heat transfer parameters. Decreasing trend for Nu_{avg} has been examined at the growing values of Hartmann number, thickness of porous layer, Darcy number

and magnetic field inclinations. Mehmood et al. [31] examined numerical analysis about the role of nonlinear thermal radiations and magnetic field inclinations on MHD mixed convective nanofluid flow inside cavity saturated by porous media. Finite element technique based on Galerkin type weighted residuals has been adopted for numerical inspection. Variations in heat flow patterns were observed for values of different parameters like radiation parameter (Rd), temperature ratio parameter (Nr), Darcy number (Da) and porosity parameter (ϵ). Reduction in convection was notable for increasing values of magnetic field angles and increase in heat transfer was analyzed for the amplifying values of Da, ϕ, ϵ, Rd and Nr. Forced convection through a wavy porous channel using copper oxide nonaofluid in non-Darcy flow regime has been investigated by Rehena et al. [32]. Physical properties of heat flow process were studied by keeping in view the different parameters like Re (10 to 500), Da (0.01 to ∞) and ϕ (0% to 20%). It has been realized that for the increments in both Re and ϕ, the convection proces inside the channel was enhanced. An opposite impact has been observed for the increased values of Da. Hadim and Chen [33] explored a research about non-Darcy mixed convection inside a vertical channel embedded with porous medium. An admissible influence of Darcy number over heat-flow domain has been inspected. For augmented values of Da, reduced Nu_{avg} has been found specifically for non-Darcy dominated flow at $Da = 10^4$. Mahmud and Roydon [34] revealed an analysis on MHD natural convection of nanofluid and entropy analysis inside the cavity having porous medium. The numerical study for unsteady PDEs was performed by finite volume method and Crank-Nicolson scheme. It was concluded that both average Nusselt number (Nu_{avg}) and entropy generation parameter (Ns) were decreased with the gradual increments in Ha, i.e., Hartmann number. Entropy of system has also been reduced with the increasing strength of magnetic field. The study about natural convection in cavity with porous medium having isothermal wavy surface at the bottom wall of cavity was performed by Kumar et al. [35]. The governing equations have been analyzed numerically by finite element method to study different heat transfer parameters. It has been noticed that sinusoidal bottom surface with undulations was responsible for the reduction in heat transfer

process in porous enclosure. A marginal increment in heat fluxes were observed for increasing values of Rayleigh number (Ra) and nanoparticles volume fraction (ϕ). Increasing Hartmann number resulted in low values of temperature gradient. Sheikholeslami [36] has greatly studied about the natural convection of nanofluid flow under the impacts of electrical field strength inside a cavity having porous medium. Numerical investigation has been inspected to analyze different thermophysical parameters by finite element method. A noticeable distortion in heat isotherms has been seen with the variations of Darcy number, Coulomb force and radiation parameter. More incremented values of Nu_{avg} were found for the ascending strength of buoyancy force and radiation parameter.

1.1.5 MHD Effects and Mixed Convection

MHD is the abbreviation of magneto-hydro-dynamics, in which the study of electrically active flows like plasma, liquid metals and salt water are studied with induced magnetic field effects (external or internal) [27]. Many research have already carried out in studying the role of MHD effects for the improvement of heat transport mechanism.

Makulati et al. [37] explored a research about the impacts of C-shaped cavity inclinations along with varying magnetic field on natural convective nanofluid flow by numerical inspection. The results obtained by finite volume method distinctly show that with the increasing Ha number, the Nu_{avg} has been reduced. Amplified convective heat transfer was obtained with the augmentation in physical quantities like cavity aspect ratio, cavity tilts and solid particles volume fractions. Convective heat transfer was more amplified for higher cavity aspect ratios as compared to the rise in tilted angles of enclosure. Another MHD flow problem by Yirga and Tesfay [38] demonstrated the impacts of viscous dissipation and chemical reaction on MHD mixed convective nanofluid flow passing over permeable stretching sheet. Comparative numerical analysis for copper-water and silver-water nanofluid was performed by using Keller box method. It has been inferred that skin friction of

silver-water was high as compared to copper-water nanofluid. Hence it was deduced that copper-water nanoliquid has shown a higher rate of convective heat transfer than silver-water nanoliquid. Thick thermal boundary layer for silver-water fluid has been noticed at the rising values of solid volume fraction and Eckert number. Buoyancy force dominated convective flow has been numerically studied by Grosan et al. [39] to explore the impacts of external magnetic field and effects of internal heat generation inside a rectangular enclosure having porous medium. The governing parameters like inclination angle (γ), Hartmann number (Ha), Rayleigh number (Ra) and cavity aspect ratio (a) have been analyzed. The convective heat distribution was reduced due to external magnetic field variations. For the increasing value of γ, decreased average Nusselt number has been obtained. Sheikholeslami et al. [40] have adopted Lattice Boltzmann method for the investigation of MHD mixed convective nanofluid for heat flow simulations inside a semi-annulus shaped cavity. Stronger convective heat transfer has been found at high Rayleigh number (Ra) and nanoparticles volume fractions (ϕ). It was noticed that Lorentz force became dominant for higher Hartmann number which lead to the retardation of convection process.

Another useful study by considering the effects of Lorentz forces on copper oxide-water nanofluid flow is presented by Sheikholeslami et al. [41] to inspect MHD mixed convection process. Augmentation in thermal energy transport has been noticed for the rising values of Hartmann number with the gradual increase in Nu_{avg} while an opposite relation was noted at the increasing Rayleigh number. The impacts of magnetic field variations on natural convective nanofluid flow inside rectangular shaped cavity have been elaborately discussed by Rudraiah et al. [42]. Numerical outcomes were used to inspect physical parameters like Grashof and Hartmann number at fixed Prandtl number, i.e., $Pr = 0.733$ to study free convection. It has been deduced from results that the rate of thermal convection is reduced at the variation of magnetic field effects. Most reduced average Nusselt number has been noticed at the higher Hartmann numbers.

1.2 Thesis Contribution

The leading motivation for present work is to investigate the impacts of external magnetic field inclinations and viscous dissipation due to Joule heating on MHD mixed convective flow of alumina-water nanofluid in an inclined open channel with cavity enclosed by porous medium. Numerical analysis of dimensionless governing PDEs is performed by using Galerkin weighted residual based FEM. For this, the governing PDEs are discretized in terms of LBB-stable Q_2/P_1^{disc} finite elements. In which biquadratic (Q_2) space is utilized for the discretization of velocity and temperature components while linear discontinuous (P_1^{disc}) finite space is used for pressure component. The physical characteristics of flow pattern are analyzed by studying different dimensionless parameters like Reynolds, Richardson, Darcy, Eckert and Hartmann numbers. Further more, cavity inclinations and magnetic field inclinations are also studied as a controlling parameters for heat convection process. The rate of average heat transport throughout the fluid's domain is calculated by using another physical quantity, i.e., average Nusselt number. Magnetic field inclinations are inspected at field layouts, i.e., ($0° \leq \psi \leq 90°$). Joule heating is added to energy equation as a viscous dissipation term due to magnetic field. Visualization of velocity and temperature data is presented with the help of streamline contours and isothermal patterns by using ParaView. Comparative analysis of different physical parameters with average Nusselt number is explored by using MATLAB graphs.

1.3 Thesis Layout

This thesis is further composed of the following chapters:

Chapter 2 demonstrates the introductory basics of fluid dynamics. A brief discussion about the basic definitions, governing laws for fluid motion and governing equations have been illustrated. The solution methodology has also been demonstrated. Dimensionless physical quantities of interest are also mentioned briefly

related to the problems.

Chapter 3 interprets a review analysis of the study which has been performed by Hussain et al. [43]. This work has covered the scope related to mixed convective heat transfer in alumina-water nanofluid in inclined channel with cavity which is enclosed by porous medium. The Darcy-Brinkman-Forchheimer model has been adopted for the homogenous porous medium. Numerical investigation is performed for steady set of dimensionless governing equations by GFEM. In last section, the compilation of results for solution data is given in the form of streamlines, isotherms and MATLAB graphs.

Chapter 4 presents the extension to the forgoing work of Hussain et al. [43]. In this work the effects of external magnetic field inclination and resistive heat effects due to Joule heating are inspected by adding MHD effects to the preceding problem. The set of dimensionless PDEs are solved by Galerkin weighted residual FEM. Numerical outcomes are compared by using dimensionless parameters such as Re, Ri, ψ, γ, ϵ, Ec and Ha with solid volume fraction ϕ to study thermal energy distributions on fluid's domain. Moreover, effects of physical parameters are portrayed in terms of streamlines for velocity profiles, isotherms for heat distribution and graphical plots for average Nusselt numbers.

Chapter 5 summarizes the overall analysis of the work which is presented in this thesis. Concluding remarks and future suggestions are also written in this chapter.

Chapter 2

Fundamental Concepts in Fluid Dynamics

In this chapter we are going to discuss basic concepts, definitions and governing laws related to the fluid dynamics [44–52]. Dimensionless quantities are also discussed which seems to be helpful in the subsequent chapters. Moreover, a brief discussion has been done for the numerical methodology adopted for the solution of governing equations. A simple two-dimensional poisson problem is also solved here to explain the numerical procedure for the achievement of results.

2.1 Basic Definitions

Definition 2.1.1. (**Fluid**)
"A fluid is a substance that deforms continuously when subjected to anisotropic states of stress, i.e., shear stress."

Definition 2.1.2. (**Flow**)
"A material that undergoes deformation when certain forces act upon it and continuously increases without limit then such phenomenon is called flow."

Definition 2.1.3. (**Fluid Mechanics**)
"Fluid mechanics is the study of fluids either in motion (Fluid dynamics) or at

rest (Fluid statics)."

Fluids are usually classified as liquids and gases. Different fluids like blood, saliva, honey, paints, starch solutions, etc., are the most common examples from engineering and medical fields.

Definition 2.1.4. (**Newton's Law of Viscosity**)

Newton's law of viscosity states that:

"In a Newtonian fluid the stress is directly proportional to the velocity gradient."

If τ^* be the force per unit area, then for one-dimensional flow $u(y)$ it can be expressed as

$$\tau^* = \mu \left(\frac{du}{dy} \right).$$

In the above relation 'τ^*' and 'μ' are stress and dynamic viscosity respectively.

2.2 Classification of Fluids

Fluids are basically divided into two main classes that are: Ideal or Perfect fluids and Real fluids.

Definition 2.2.1. (**Ideal Fluids**)

"Ideal or perfect fluids are those fluids having viscosity equal to 0, i.e., $\mu = 0$."

Such fluids do not have shear forces and are fictitious in nature. These are incompressible and also known as inviscid fluids.

Definition 2.2.2. (**Real Fluids**)

"Real or viscous fluids have non-zero viscosity, i.e., $\mu \neq 0$."

These fluids always possess non-zero viscosity and are either compressible or incompressible in nature. Major real fluid classes are termed as Newtonian fluids and non-Newtonian fluids. A brief discussion is summarized below:

Definition 2.2.3. (**Newtonian Fluids**)

"The fluids that obey Newton's law of viscosity are called Newtonian fluids."

These fluids have constant viscosity. Constant viscosity means that viscosity profile is not affected by the changes in velocity but may vary with changes in temperature and pressure. Few examples of Newtonian fluids are water, air, alcohol, glycerol, etc.

Definition 2.2.4. (**Non-Newtonian Fluids**)
"Fluids that do not obey the Newton's linear law of viscosity are called non-Newtonian fluids."
These fluids are usually highly viscous in nature. Few typical examples are polymer solutions, thermoplastics, drilling fluids, paints, concrete, biological fluids like saliva, mucus, blood, etc. Further classification for non-Newtonian fluids is given below:

- Viscoplastic fluids or Bingham fluids
- Shear thickening fluid or dilatant fluids
- Shear thinning fluids or pseudoplastic
- Thixotropic fluids
- Rheopectic fluids or anti-thixotropic fluids
- Viscoelastic fluids

Definition 2.2.5. (**Viscoplastic or Bingham Fluids**)
"These fluids show a linear relationship between shear stress and shear strain but need a yield stress to flow."
Examples of Bingham fluids are tooth paste, granular materials and fresh concrete.

Definition 2.2.6. (**Shear Thickening Fluids**)
"A small group of real liquids for which the viscosity increases with the increasing shear rate such fluids are called shear thickening fluids."
Shear thickening fluids are also called dilatant fluids. Examples are corn starch and oobleck.

Definition 2.2.7. (**Shear Thinning Fluids**)

"The fluids for which viscosity decreases with an increase in the shear rate are known as shear thinning fluids"

Shear thinning fluids are also called pseudoplastic fluids. Few examples are polymer solutions, mayonnaise, etc.

Definition 2.2.8. (**Thixotropic Fluids**)

"For such type of fluids the shear stress decreases monotonically with increasing time at constant shear rate."

The properties of these fluids are time dependent. Most common examples include yogurt, paints, iron oxide gels, etc.

Definition 2.2.9. (**Rheopectic Fluids**)

"For such type of fluids, the shear stress increases monotonically with increasing time at constant shear rate."

Properties of these fluids are also time dependent. Gypsum paste is an example of rheopectic fluid.

Definition 2.2.10. (**Viscoelastic Fluids**)

"A fluid that returns (either fully or partially) to its original shape after applied stress is released is called viscoelastic fluid."

Some polymers and soap solutions are the common examples [53].

2.3 Types of Flow

Following are different types of fluid's flow depending upon its physics and status of channel.

Definition 2.3.1. (**Uniform Flow**)

"If the fluid velocity $\mathbf{V}(u, v, w)$ at a given instant of time does not vary with in the given length of channel L then the flow is called uniform flow."

Mathematically, it is written as

$$\frac{\partial \mathbf{V}}{\partial L} = 0,$$

where velocity $\mathbf{V}(u, v, w)$ is constant.

Definition 2.3.2. (**Non-Uniform Flow**)

"If the fluid velocity $\mathbf{V}(u, v, w)$ at a time varies with respect to distance L, then the flow is called non-uniform flow or varied flow."

Mathematical representation is given below

$$\frac{\partial \mathbf{V}}{\partial L} \neq 0.$$

Definition 2.3.3. (**Laminar Flow**)

"The flow of fluid is called laminar if the liquid particles appear to move in definite straight and parallel paths."

Definition 2.3.4. (**Turbulent Flow**)

"The flow is called turbulent, if the liquid particles move in irregular paths which are not fixed with respect to either space or time."

Definition 2.3.5. (**Steady Flow**)

"A flow in which the property of fluid flowing per second is constant. In other words time independent flow is called steady flow."

If η be any fluid property and t the time, then

$$\frac{\partial \eta}{\partial t} = 0.$$

Definition 2.3.6. (**Unsteady Flow**)

"A flow in which the property of fluid flowing per second is not constant. In other words time dependent flow is called unsteady flow."

For fluid property η and time t, it is represented as

$$\frac{\partial \eta}{\partial t} \neq 0,$$

in both definitions 2.3.5 and 2.3.6, 'η' belongs to fluid properties like velocity, density, temperature, volume, etc.

Definition 2.3.7. (**Incompressible Flow**)

"A flow of fluid with constant density ρ is called incompressible flow."

Following is the mathematical notation for such flow

$$\rho(x, y, z, t) = c.$$

Definition 2.3.8. (**Compressible Flow**)

"A flow of fluid for which there may be significant changes in the density ρ with respect to time as well as with respect to pressure and temperature is called compressible flow."It can be written as

$$\rho(x, y, z, t) \neq c.$$

Definition 2.3.9. (**Rotational Flow**)

"A flow with velocity $\mathbf{V}$ in which fluid particles rotate about their own axis during the flow, i.e., fluid particles have non-zero angular velocity and vorticity then such flow is called rotational flow." Mathematical representation is given below

$$\vec{\omega} = \frac{1}{2}\nabla \times \mathbf{V} \neq 0 \Rightarrow \vec{\zeta} = \nabla \times \mathbf{V} \neq 0.$$

Definition 2.3.10. (**Irrotational Flow**)

"A flow with velocity $\mathbf{V}$ in which fluid particles do not spin about their axis as they move, i.e., they have zero angular velocity and vorticity, such flows are called irrotational flows." It can be expressed as

$$\vec{\omega} = \frac{1}{2}\nabla \times \mathbf{V} = 0 \Rightarrow \vec{\zeta} = \nabla \times \mathbf{V} = 0.$$

Here in both definitions 2.3.9 and 2.3.10, $\vec{\omega}$ and $\vec{\zeta}$ are used to represent angular velocity and vorticity.

Definition 2.3.11. (**Open Channel Flow**)

"The flow in an open channel having a free surface and moves under the influence of gravity is called open channel flow."

Definition 2.3.12. (**Closed Channel Flow**)

"The flow in a close conduit having or not having a free surface and moves under the influence of pressure is called closed channel flow."

2.4 Nanofluids

Definition 2.4.1. (**Nanofluids**)

This category of fluids can be defined as

"Nanofluids are relatively new class of fluids which consist of a base fluid with nano sized particles (1-100 nm) suspended within them. These particles are generally metal or metal oxide, increase conduction and convection processes by allowing more heat to transfer [54, 55]."

Various types of powders like metallic, non metallic and polymeric particles can

Types of particles	Examples [56]
Metallic oxides	Al_2O_3, TiO_2
Nitride ceramics	AlN, SiN
Carbide ceramic	SiC
Paramagnetic particles	Al_2O_3
Ferromagnetic particles	Fe_2O_4, Fe_2O_3, CuO
Semiconductor particles	GaN, GaP, ZnO
Carbon nanoparticles	$SWCNT$, $DWCNT$, $MWCNT$
Alloyed nanoparticles	Fe-Ni, Pt-Ag

Table 2.1: Classification of nanoparticles.

be added to fluids to form slurries and suspensions. Moreover, these are also used as coolants due to their cooling capabilities in many engineering fields. Nanoparticles are broadly divided into various categories depending on their morphology, properties and applications. Some of the well known types are given in **Table** 2.1.

2.5 Properties of Fluids

Depending upon different types of fluids, the following properties are of great importance for our present study.

Definition 2.5.1. (**Viscosity**)
"When a fluid moves relative to a solid or two fluids move relative to each other, then the internal resistance of fluid particles to motion is called viscosity."

Definition 2.5.2. (**Dynamic Viscosity**)
"It is the internal resistance between fluid layers which is the tangential force per unit area. It is also called absolute viscosity."
Mathematically, it is expressed by a linear relationship between shear stress and velocity gradient.

$$\tau^* = \mu \left(\frac{\partial u}{\partial y} \right),$$

where μ is called "dynamic viscosity".

Definition 2.5.3. (**Kinematic Viscosity**)
"The ratio of dynamic viscosity μ to the density ρ of fluid without the involvement of force is called kinematic viscosity". It is symbolized by ν and mathematically formulated as

$$\nu = \frac{\mu}{\rho}.$$

Definition 2.5.4. (**Vorticity**)
"Vorticity corresponds to the rotation of the particles of fluid."
The vorticity $\vec{\zeta}$ of fluid is mathematically denoted by

$$\vec{\zeta} = \nabla \times \mathbf{V}.$$

Definition 2.5.5. (**Shear Stress**)
"In shear stress a force is tending to cause deformation in a material or fluid. The direction of force in this case is always parallel to the material."

It is represented by τ and generally given by following relation

$$\tau = \frac{\mathbf{F}_{\shortparallel}}{A},$$

in fluids it can also be represented by the formulations as in definitions 2.1.4 and 2.5.2.

Definition 2.5.6. (**Normal Stress**)
"The stress in which force is acting perpendicular to the unit area of material's surface." It is represented by σ.

$$\sigma = \frac{\mathbf{F}_{\perp}}{A}.$$

In definitions 2.5.5 and 2.5.6, parallel and perpendicular components of force are represented as $\mathbf{F}_{\shortparallel}$ and $\mathbf{F}_{\perp}$.

Definition 2.5.7. (**Density**)
"Density is defined as mass per unit volume. It is represented by ρ."
Let m be the mass of fluid and V be the volume, then density is given by

$$\rho = \frac{m}{V}.$$

Definition 2.5.8. (**Pressure**)
"A normal force $\mathbf{F}$ exerted by a fluid per unit area A is called pressure."
It is formulated as

$$p = \frac{\mathbf{F}}{A}.$$

Definition 2.5.9. (**Thermal Conductivity**)
According to Fourier's law:
"The heat transfer rate q^{**} in any direction $\overline{\mathbf{n}}$ per unit area is measured normal to $\overline{\mathbf{n}}$." It is given by

$$q^{**} = -\kappa \left(\frac{\partial T}{\partial \overline{\mathbf{n}}} \right),$$

where κ is called "thermal conductivity" which is an important thermal property of fluid.

Definition 2.5.10. (**Thermal Diffusivity**)

"It is the ratio of the thermal conductivity of fluid or material to the specific heat capacity of fluid or material". It is represented by α.

$$\alpha = \frac{\kappa}{\rho C_\rho}.$$

Definition 2.5.11. (**Velocity Field**)

"It is the representation of net motion of molecules of fluid from one point in space to another point as a function of time." It is expressed as

$$\mathbf{V} = u\,(x, y, z, t)\,\hat{i} + v\,(x, y, z, t)\,\hat{j} + w\,(x, y, z, t)\,\hat{k},$$

where $\mathbf{V}$ represents three-dimensional velocity field with respective components u, v and w.

Definition 2.5.12. (**Streamlines**)

"A streamline is a line that is every where tangent to velocity field of fluid." Streamlines show pictorial representation of flow. For a three-dimensional velocity field it can be written as

$$\frac{dx}{u} = \frac{dy}{v} = \frac{dz}{w}.$$

Definition 2.5.13. (**Substantial or Material Derivative**)

"If ξ represent any property of fluid, with dx, dy, dz and dt are arbitrary changes of four independent variables, then total differential change in ξ is given by

$$\frac{d\xi}{dt} = u\frac{\partial \xi}{\partial x} + v\frac{\partial \xi}{\partial y} + w\frac{\partial \xi}{\partial z} + \frac{\partial \xi}{\partial t}."$$

The above mathematical relation is called substantial derivative or material derivative.

Definition 2.5.14. (**Acceleration of Flow Field**)

"Acceleration is the rate of change of velocity of fluid with respect to time." Acceleration $\mathbf{a}$ of fluid is mathematically given by

$$\mathbf{a} = \frac{d\mathbf{V}}{dt},$$

similarly by definition 2.5.13, acceleration for a three-dimensional velocity flow field is written below

$$\mathbf{a} = u\frac{\partial \mathbf{V}}{\partial x} + v\frac{\partial \mathbf{V}}{\partial y} + w\frac{\partial \mathbf{V}}{\partial z} + \frac{\partial \mathbf{V}}{\partial t}.$$

Definition 2.5.15. (**Enthalpy**)
"It is the combination of internal energy of fluid $\widetilde{E}$ and pressure energy $\left(\frac{p}{\rho}\right)$. This fluid property is called enthalpy which is represented by $\hat{h}$."

$$\hat{h} = \left(\widetilde{E} + \frac{p}{\rho}\right).$$

2.6 Basic Governing Laws and Equations for Fluid Motion

For the solution of many real life fluid problems in practical fields, we need to study the behaviour of fluid in finite region of space. This finite region of space is called "Finite control volume". In the perspective of finite control volume we try to find the rate of change of different properties of fluid. For this purpose we need to satisfy the basic fundamental laws of physics which include mass conservation, momentum conservation (Newton's second law of motion) and energy conservation (First law of thermodynamics) to define the fluid dynamics [44, 47, 50].

2.6.1 Law of Conservation of Mass

The mass conservation law states as below
"The mass inside a system is conserved and does not change." or
"The time rate of change of mass inside system = 0."

$$\frac{Dm}{Dt} = 0,$$

where m is the mass of fluid flowing in system or control volume [44, 47].

2.6.1.1 Continuity Equation

After using Reynolds transport theorem over the control volume of system, the mathematical notation for the law of conservation of mass is given below:

$$\frac{\partial \rho}{\partial t} + \nabla.(\rho \mathbf{V}) = 0. \tag{2.1}$$

For the steady flow above Eq. (2.1) can be written as

$$\nabla.(\rho \mathbf{V}) = 0. \tag{2.2}$$

For incompressible flow, Eq. (2.2) becomes

$$\nabla.\mathbf{V} = 0. \tag{2.3}$$

For incompressible and irrotational flow, the Eq. (2.3) is transformed in terms of velocity potential ψ, which is given by

$$\nabla^2 \psi = 0. \tag{2.4}$$

Equation (2.4) is known as "Laplace equation".

2.6.2 Law of Conservation of Momentum

To study the momentum equation, Newton's second law is of great importance. Newton's law of motion states that:
"The rate of change of momentum of body is equal to net forces acting on the body."
This statement leads to law of conservation of momentum, which states that:
"The momentum of a system remains constant when the net force acting on it is zero."

2.6.2.1 Momentum Equation

The principle of conservation of momentum can be expressed in the form of "momentum equation", which is formulated as [50]

$$\rho\left(\frac{\partial \mathbf{V}}{\partial t} + \mathbf{V}.(\nabla \mathbf{V})\right) = -\nabla p + \nabla.\tau_{ij}^{*} + \mathbf{F}_g, \tag{2.5}$$

where p, τ_{ij}^{*}, $\mathbf{F}_g = \rho\mathbf{g}$ are termed as hydrostatic pressure, viscous stress tensor and body force.

Viscous sress tensor 'τ_{ij}^{*}', is a tensor of rank 2 having nine stress components. It is written as

$$\tau_{ij}^{*} = \begin{pmatrix} \tau_{xx}^{*} & \tau_{xy}^{*} & \tau_{xz}^{*} \\ \tau_{yx}^{*} & \tau_{yy}^{*} & \tau_{yz}^{*} \\ \tau_{zx}^{*} & \tau_{zy}^{*} & \tau_{zz}^{*} \end{pmatrix}, \tag{2.6}$$

or

$$\tau_{ij}^{*} = \begin{pmatrix} \sigma_x & \tau_{xy}^{*} & \tau_{xz}^{*} \\ \tau_{yx}^{*} & \sigma_y & \tau_{yz}^{*} \\ \tau_{zx}^{*} & \tau_{zy}^{*} & \sigma_z \end{pmatrix}. \tag{2.7}$$

In Eq. (2.7), τ_{xy}^{*}, τ_{xz}^{*}, τ_{yx}^{*}, τ_{yz}^{*}, τ_{zx}^{*} and τ_{zy}^{*} are known as shear stresses while σ_x, σ_y and σ_z are called normal stresses.

In the case of incompressible and inviscid flows, the stress term in Eq. (2.5) is avoided to get the most simplified equation. Such momentum equation is known as the "Eulers momentum equation". It can be written as

$$\rho\left(\frac{\partial \mathbf{V}}{\partial t} + \mathbf{V}.(\nabla \mathbf{V})\right) = -\nabla p + \mathbf{F}_g. \tag{2.8}$$

2.6.2.2 Navier-Stokes Equation

By redefining Eq. (2.5), given below is the most well known form of momentum equation, usually known as "Navier-Stokes equation". It was first introduced

by "Claude-Louis Navier" in 1821 and further improved by "Sir George Gabriel Stokes" [44, 50].

$$\rho\left(\frac{\partial \mathbf{V}}{\partial t} + \mathbf{V}.\left(\nabla \mathbf{V}\right)\right) = \nabla.\overline{\mathbf{T}}_{ij} + \mathbf{F}_g, \tag{2.9}$$

where $\overline{\mathbf{T}}_{ij}$ is called "Cauchy stress tensor" and $\mathbf{F}_g$ is known as body force term. Cauchy stress tensor is further defined as below

$$\overline{\mathbf{T}}_{ij} = \underbrace{-p\mathbf{I}}_{\text{(pressure distribution term)}} + \underbrace{\tau^*_{ij}}_{\text{(deviatoric stress tensor term)}}. \tag{2.10}$$

In Eq. (2.10) the deviatoric stress tensor, i.e., τ^*_{ij} for Newtonian fluids is given below

$$\tau^*_{ij} = \mu \mathbf{A_1}, \tag{2.11}$$

where A_1 is called "first Rivlin Ericksen tensor" [57] and its formulation is given by

$$\mathbf{A_1} = \nabla \mathbf{V} + \left(\nabla \mathbf{V}\right)^\top. \tag{2.12}$$

The complete constitutive relation in Eq. (2.10) can be expressed as

$$\overline{\mathbf{T}}_{ij} = -p\mathbf{I} + \mu\left[\nabla \mathbf{V} + \left(\nabla \mathbf{V}\right)^\top\right]. \tag{2.13}$$

The gradient relation of three-dimensional velocity field $\mathbf{V}(u, v, w)$ is written as

$$\nabla \mathbf{V} = \begin{pmatrix} \frac{\partial u}{\partial x} & \frac{\partial v}{\partial x} & \frac{\partial w}{\partial x} \\ \frac{\partial u}{\partial y} & \frac{\partial v}{\partial y} & \frac{\partial w}{\partial y} \\ \frac{\partial u}{\partial z} & \frac{\partial v}{\partial z} & \frac{\partial w}{\partial z} \end{pmatrix},$$

and

$$(\nabla \mathbf{V})^{\top} = \begin{pmatrix} \frac{\partial u}{\partial x} & \frac{\partial u}{\partial y} & \frac{\partial u}{\partial z} \\ \frac{\partial v}{\partial x} & \frac{\partial v}{\partial y} & \frac{\partial v}{\partial z} \\ \frac{\partial w}{\partial x} & \frac{\partial w}{\partial y} & \frac{\partial w}{\partial z} \end{pmatrix}.$$

By substituting these relations into Eq. (2.12),

$$A_1 = \begin{pmatrix} 2\frac{\partial u}{\partial x} & \frac{\partial v}{\partial x} + \frac{\partial u}{\partial y} & \frac{\partial w}{\partial x} + \frac{\partial u}{\partial z} \\ \frac{\partial u}{\partial y} + \frac{\partial v}{\partial x} & 2\frac{\partial v}{\partial y} & \frac{\partial w}{\partial y} + \frac{\partial v}{\partial z} \\ \frac{\partial u}{\partial z} + \frac{\partial w}{\partial x} & \frac{\partial v}{\partial z} + \frac{\partial w}{\partial y} & 2\frac{\partial w}{\partial z} \end{pmatrix}. \tag{2.14}$$

Substitution of Eq. (2.14) into Eq. (2.11) leads to the following

$$\tau_{ij}^{*} = \begin{pmatrix} 2\mu\frac{\partial u}{\partial x} & \mu\left(\frac{\partial v}{\partial x} + \frac{\partial u}{\partial y}\right) & \mu\left(\frac{\partial w}{\partial x} + \frac{\partial u}{\partial z}\right) \\ \mu\left(\frac{\partial u}{\partial y} + \frac{\partial v}{\partial x}\right) & 2\mu\frac{\partial v}{\partial y} & \mu\left(\frac{\partial w}{\partial y} + \frac{\partial v}{\partial z}\right) \\ \mu\left(\frac{\partial u}{\partial z} + \frac{\partial w}{\partial x}\right) & \mu\left(\frac{\partial v}{\partial z} + \frac{\partial w}{\partial y}\right) & 2\mu\frac{\partial w}{\partial z} \end{pmatrix}, \tag{2.15}$$

and from Eq. (2.10), pressure term is written in matrix form as

$$-pI = \begin{pmatrix} -p & 0 & 0 \\ 0 & -p & 0 \\ 0 & 0 & -p \end{pmatrix}. \tag{2.16}$$

By using Eqs. (2.15) and (2.16) into Eq. (2.10) we get,

$$\overline{\mathbf{T}}_{ij} = \begin{pmatrix} \overline{\mathbf{T}}_{xx} & \overline{\mathbf{T}}_{xy} & \overline{\mathbf{T}}_{xz} \\ \overline{\mathbf{T}}_{yx} & \overline{\mathbf{T}}_{yy} & \overline{\mathbf{T}}_{yz} \\ \overline{\mathbf{T}}_{zx} & \overline{\mathbf{T}}_{zy} & \overline{\mathbf{T}}_{zz} \end{pmatrix},$$

and following are the x, y and z components of $\nabla.\overline{\mathbf{T}}_{ij}$

$$\left(\nabla.\overline{\mathbf{T}}_{ij}\right)_x = -\frac{\partial p}{\partial x} + \mu\left(\frac{\partial^2 u}{\partial x^2} + \frac{\partial^2 u}{\partial y^2} + \frac{\partial^2 u}{\partial z^2}\right), \tag{2.17}$$

$$\left(\nabla.\overline{\mathbf{T}}_{ij}\right)_y = -\frac{\partial p}{\partial y} + \mu\left(\frac{\partial^2 v}{\partial x^2} + \frac{\partial^2 v}{\partial y^2} + \frac{\partial^2 v}{\partial z^2}\right), \tag{2.18}$$

$$\left(\nabla.\overline{\mathbf{T}}_{ij}\right)_z = -\frac{\partial p}{\partial z} + \mu\left(\frac{\partial^2 w}{\partial x^2} + \frac{\partial^2 w}{\partial y^2} + \frac{\partial^2 w}{\partial z^2}\right). \tag{2.19}$$

After the substitution of Eqs. (2.17) to (2.19) into Eq. (2.9), we will get a set of equations known as "Navier-Stokes equations" for Newtonian and incompressible flow, i.e.,

$$\rho\left(\frac{\partial \mathbf{V}}{\partial t} + \mathbf{V}.(\nabla \mathbf{V})\right) = -\nabla p + \mu \Delta \mathbf{V} + \mathbf{F}_g. \tag{2.20}$$

2.6.3 First Law of Thermodynamics

First law of thermodynamics is nothing more than the principle of conservation of energy. First law of thermodynamics states that:
"The variation in internal energy $\widetilde{E}$ of a system during any transformation is equal to the amount of energy that system receives from the environment and the work done by the system." Mathematically, it is represented as

$$\Delta \widetilde{E} = \widetilde{Q} - \widetilde{W},$$

where $\Delta\widetilde{E}$, $\widetilde{Q}$ and $\widetilde{W}$ are termed as change in internal energy, heat added to the system and work done by the system respectively.

2.6.3.1 Energy Equation

The energy conservation of a system can be expressed in rate form as:

Rate of change of energy in system or control volume = (Rate of in flow of energy-Rate of out flow of energy) + (Rate of heat addition due to conduction) + (Rate of internal heat generation with in control volume) + (Rate of work done by the

forces acting on control volume).

The energy equation in terms of first law of thermodynamics is written below [45, 51, 58]

$$\rho\frac{D\widetilde{E}}{Dt}+\nabla q^{**}-q^{***}+p\left(\nabla.\mathbf{V}\right)-\tau_{ij}^{*}.\left(\nabla\mathbf{V}\right)=0, \tag{2.21}$$

where

$$\begin{aligned}\tau_{ij}^{*}.\left(\nabla\mathbf{V}\right)=&\left(\sigma_x\frac{\partial u}{\partial x}+\tau_{xy}^{*}\frac{\partial u}{\partial y}+\tau_{xz}^{*}\frac{\partial u}{\partial z}\right)+\left(\tau_{yx}^{*}\frac{\partial v}{\partial x}+\sigma_y\frac{\partial v}{\partial y}+\tau_{yz}^{*}\frac{\partial v}{\partial z}\right)\\&+\left(\tau_{zx}^{*}\frac{\partial w}{\partial x}+\tau_{zy}^{*}\frac{\partial w}{\partial y}+\sigma_z\frac{\partial w}{\partial z}\right).\end{aligned} \tag{2.22}$$

Substituting the values from Eq. (2.15) into Eq. (2.22), we get

$$\begin{aligned}\tau_{ij}^{*}.\left(\nabla\mathbf{V}\right)=&\mu\Bigg[2\left(\left(\frac{\partial u}{\partial x}\right)^2+\left(\frac{\partial v}{\partial y}\right)^2+\left(\frac{\partial w}{\partial z}\right)^2\right)+\left(\frac{\partial u}{\partial y}+\frac{\partial v}{\partial x}\right)^2\\&+\left(\frac{\partial w}{\partial y}+\frac{\partial v}{\partial z}\right)^2+\left(\frac{\partial u}{\partial z}+\frac{\partial w}{\partial x}\right)^2\Bigg],\\=&\mu\mathbf{\Phi},\end{aligned} \tag{2.23}$$

where $\mathbf{\Phi}$ is called "viscous dissipation".

After applying Eq. (2.23) into Eq. (2.21), we get

$$\rho\frac{D\widetilde{E}}{Dt}+\nabla q^{**}-q^{***}+p\left(\nabla.\mathbf{V}\right)-\mu\mathbf{\Phi}=0, \tag{2.24}$$

where the rate of work done by pressure forces on fluid, i.e., $p\left(\nabla.\mathbf{V}\right)$ becomes zero due to the contribution of continuity equation, so

$$\rho\frac{\partial\widetilde{E}}{\partial t}+\rho\mathbf{V}.\left(\nabla\widetilde{E}\right)+\nabla q^{**}-q^{***}-\mu\mathbf{\Phi}=0. \tag{2.25}$$

Adopting the definition 2.5.15 of enthalpy into Eq. (2.25), it can be written as

$$\widetilde{E}=\left(\hat{h}-\frac{p}{\rho}\right),$$

$$\rho\left(\frac{\partial\left(\hat{h}-\frac{p}{\rho}\right)}{\partial t}\right)+\rho\mathbf{V}.\left(\nabla\left(\hat{h}-\frac{p}{\rho}\right)\right)+\nabla q^{**}$$
$$-q^{***}-\mu\mathbf{\Phi}=0, \tag{2.26}$$

$$\rho\frac{\partial\hat{h}}{\partial t}-\frac{\partial p}{\partial t}+\rho\vec{\mathbf{V}}.\left(\nabla\hat{h}\right)-\mathbf{V}.\left(\nabla p\right)=-\nabla q^{**}+q^{***}+\mu\mathbf{\Phi}. \tag{2.27}$$

After applying the definition of Fourier's law 2.5.9, we get

$$\rho\frac{\partial\hat{h}}{\partial t}-\frac{\partial p}{\partial t}+\rho\mathbf{V}.\left(\nabla\hat{h}\right)-\mathbf{V}.\left(\nabla p\right)=-\nabla.\left(-\kappa\nabla T\right)$$
$$+q^{***}+\mu\mathbf{\Phi}, \tag{2.28}$$
$$\rho\left(\frac{\partial\hat{h}}{\partial t}+\mathbf{V}.\left(\nabla\hat{h}\right)\right)=\left(\frac{\partial p}{\partial t}+\mathbf{V}.\left(\nabla p\right)\right)+\nabla.\left(\kappa\nabla T\right)$$
$$+q^{***}+\mu\mathbf{\Phi}. \tag{2.29}$$

Substituting another physical relationship of enthalpy $\hat{h}$, which is defined as [58]:

$$d\hat{h}=C_\rho dT,$$

then Eq. (2.29) will be transformed into

$$\rho C_\rho\left(\frac{\partial T}{\partial t}+\mathbf{V}.\left(\nabla T\right)\right)=\left(\frac{\partial p}{\partial t}+\mathbf{V}.\left(\nabla p\right)\right)+\kappa\left(\Delta T\right)+q^{***}+\mu\mathbf{\Phi}, \tag{2.30}$$
$$\rho C_\rho\left(\frac{DT}{Dt}\right)=\frac{Dp}{Dt}+\kappa\left(\Delta T\right)+q^{***}+\mu\mathbf{\Phi}. \tag{2.31}$$

If the fluid is viscous, incompressible and steady, also for simplicity by ignoring the internal heating and viscous dissipation effects we get the following most generalized form of energy equation:

$$\left(u\frac{\partial T}{\partial x}+v\frac{\partial T}{\partial y}+w\frac{\partial T}{\partial z}\right)=\frac{\kappa}{\rho C_\rho}\left(\frac{\partial^2 T}{\partial x^2}+\frac{\partial^2 T}{\partial y^2}+\frac{\partial^2 T}{\partial z^2}\right), \tag{2.32}$$
$$\left(u\frac{\partial T}{\partial x}+v\frac{\partial T}{\partial y}+w\frac{\partial T}{\partial z}\right)=\quad\alpha\left(\frac{\partial^2 T}{\partial x^2}+\frac{\partial^2 T}{\partial y^2}+\frac{\partial^2 T}{\partial z^2}\right), \tag{2.33}$$

where α is called "thermal diffusivity".

2.7 Porous Medium

A wide range of researches have been carried out for last many years to study the role of porous medium for the heat transfer processes in many engineering application. Its application is observed in the area of geothermal energy system, oil recovery process, sub soil water filtration and nuclear waste storages [59]. Filtration capacities of medium is effectively understood by the porosity which is an important property of such medium and it always depends on the factors like shape of particles, degree of packing and degree of particle's sorting.

Definition 2.7.1. (**Porous Medium**)
"A solid material having a solid frame or matrix with interconnected free spaces (usually called voids), is known as porous material [60]." A porous medium is of two types:

- Natural porous medium (sand, soil, sand stone, wood, human bone, etc.)
- Man made porous medium (ceramics, metallic foams, sponges, cheese, bread, etc.)

Definition 2.7.2. (**Porosity** (ϵ))
"It is a fraction of total volume of medium that is occupied by void spaces of medium [60]." It can be represented by

$$\epsilon = \frac{V_{\text{void}}}{V_{\text{solid}}},$$

where V_{void} and V_{solid} are called volume occupied by voids and total volume occupied by the solid particles of medium respectively.

Definition 2.7.3. (**Void Ratio**)
"It is a ratio of volume of voids ϵ to the volume of solid matrix of medium $(1 -$

ϵ) [60].” Mathematical representation is given below

$$\widetilde{e} = \frac{\epsilon}{1-\epsilon}.$$

2.8 Governing Laws for Flow in Porous Medium

As day by day the field of science is progressing, there is immensely need to propose new methods for the analysis of solution which can bring about positive changes in the enhancement of heat transport process of many devices. The researchers are trying to study different techniques in this regard like use of nanoparticles, porous media, etc. Nowadays the fluids with saturated porous media have become a key area, which is turning into an important tool to extravagant the heat transport process. In 1985, Darcy studied the heat transfer process in porous medium by adding the resistive force term into the momentum equation. Later on other models came into the competition to overcome the limitations of Darcy's model like Forchheimer-Darcy, Brinkman-Darcy, and Darcy-Brinkman-Forchheimer flow models. One of the most famous model came into the field as DBF-model. Below is a brief study of different laws related to DBF-model and their impacts on momentum equation.

2.8.1 Darcy's Law

Henry Darcy presented a proportional relationship between flow rate and applied pressure differences for flow in porous medium. In this situation flow has to face some additional pressure gradient forces probably known as drag forces along with hydrostatic pressure [60]. Darcy's law states that:
“Fluid flow is proportional to pressure drop and inversely proportional to fluid viscosity.”

$$\nabla p + \frac{\mu_{nf}\tilde{V}}{K} = 0, \tag{2.34}$$

where ∇p, μ_{nf} and K are pressure gradient force, dynamic viscosity, velocity of flow in porous medium and permeability of isotropic medium respectively. While $\tilde{V}(\tilde{u}, \tilde{v})$ is called Darcy velocity for fluid flow in porous medium. It is given by

$$\tilde{V} = -\frac{K}{\mu_{nf}} \nabla p. \tag{2.35}$$

On account of the above discussion, momentum conservation equation for porous medium flow problem under the influence of linear drag forces is represented as follows

$$\rho_{nf} (\mathbf{V}.\nabla \mathbf{V}) = -\nabla p + \mu_{nf} \left(\nabla^2 \mathbf{V}\right) + (\beta\rho)_{nf} (T - T_c) \mathbf{g} - \frac{\mu_{nf} \tilde{V}}{K}. \tag{2.36}$$

Darcy's law has limitations due to drag forces which are linearly proportional to the velocities and applicable only for the flows having low velocity.

2.8.2 Dupuit-Forchheimer Relationship

According to Dupuit-Forchheimer relationship whenever a fluid flows through porous medium its velocity changes with factor ϵ. This new velocity is known as seeping velocity or Darcy velocity of fluid [60].

$$\tilde{V}(\tilde{u}, \tilde{v}) = \epsilon \, \mathbf{V}(u, v), \tag{2.37}$$

$$\Rightarrow u = \frac{\tilde{u}}{\epsilon}, \quad \text{and} \quad v = \frac{\tilde{v}}{\epsilon}.$$

Under the consideration of this assumption the governing laws for mass and momentum conservation are redefined and expressed as below:

- **Continuity Equation**

$$\frac{1}{\epsilon} \left(\nabla . \tilde{V}\right) = 0, \tag{2.38}$$

- **Momentum Equation**

$$\frac{\rho_{nf}}{\epsilon^2}\left(\tilde{V}.\nabla\tilde{V}\right) = -\nabla p + \frac{\mu_{nf}}{\epsilon}\left(\nabla^2\tilde{V}\right) + (\beta\rho)_{nf}\,(T - T_c)\,\mathbf{g} - \frac{\mu_{nf}\tilde{V}}{K}. \quad (2.39)$$

2.8.3 Forchheimer's Quadratic Drag Force

For greater velocity profile flows, Forchheimer introduced the quadratic drag force term which intensify the resistive forces by medium [61]. Hence total drag effects of medium on flow became

$$\text{Drag}_{(\text{force})} = \text{Drag}_{(\text{linear})} + \text{Drag}_{(\text{quad})}.$$

The mathematical formulation for drag linear and quadratic forces are written below

$$\begin{aligned}\text{Drag}_{(\text{quad})} =& C_f K^{-\frac{1}{2}}\rho_{nf}|\tilde{V}|\tilde{V},\\ \text{Drag}_{(\text{linear})} =& -\frac{\mu_{nf}\tilde{V}}{K}.\end{aligned}$$

Above expression leads to a special Stoke's equation, which is well known as Forchheimer's equation. It can be written as

$$\nabla p + \frac{\mu_{nf}}{K}\tilde{V} + C_f K^{-\frac{1}{2}}\rho_{nf}|\tilde{V}|\tilde{V} = 0.$$

Here C_f is termed as "dimensionless drag constant" and it varies from material to material. After using Forchheimer's drag term, the momentum conservation equation can be written as

$$\begin{aligned}\frac{\rho_{nf}}{\epsilon^2}\left(\tilde{V}.\nabla\tilde{V}\right) =& -\nabla p + \frac{\mu_{nf}}{\epsilon}\left(\nabla^2\tilde{V}\right) + (\beta\rho)_{nf}\,(T - T_c)\,\mathbf{g} - \frac{\mu_{nf}\tilde{V}}{K}\\ & - C_f K^{-\frac{1}{2}}\rho_{nf}|\tilde{V}|\tilde{V}.\end{aligned} \quad (2.40)$$

Here $|\tilde{V}| = \sqrt{\tilde{u}^2 + \tilde{v}^2}$

2.8.4 Ergun's Relationship for Drag Constant

Further, Ergun defined C_f for bed of spherical particles which may be less or not appropriate for other type of porous medium [61] which is given below:

$$C_f = \frac{1.75}{\sqrt{150K}\epsilon^{\frac{3}{2}}}, \tag{2.41}$$

in the above equation ϵ notifies the "porosity of medium". After using assumption as in Eq. (2.41) into Eq. (2.40), the momentum equation for the flow activity inside homogeneous porous media can be defined as

$$\begin{aligned}\frac{\rho_{nf}}{\epsilon^2}\left(\tilde{V}.\nabla\tilde{V}\right) = &-\nabla p + \frac{\mu_{nf}}{\epsilon}\left(\nabla^2\tilde{V}\right) + (\beta\rho)_{nf}(T-T_c)\,\mathbf{g} - \frac{\mu_{nf}\tilde{V}}{K} \\ &- \frac{1.75\rho_{nf}}{\sqrt{150K}\epsilon^{\frac{3}{2}}}\sqrt{\tilde{u}^2+\tilde{v}^2}\tilde{V}.\end{aligned} \tag{2.42}$$

2.8.5 Brinkman's Superposition

Brinkman presented another momentum equation for the drag forces acting on flow by the medium. According to him, these medium dependent forces have significant effects on the viscosity of the convective or Laplacian term in momentum equation [60].

$$\nabla p + \frac{\mu_{nf}}{K}\tilde{V} - \frac{\widetilde{\mu}}{\epsilon}\left(\nabla^2\tilde{V}\right) = 0,$$

these equations are known as "Brinkman equations". Here $\widetilde{\mu}$ is called "effective viscosity". There seemed an obvious uncertainty in the literature regarding Brinkman's effective viscosity term. Better approximations were observed for medium with larger permeability, where this effective viscosity was treated as dynamic viscosity. This model seemed not valid and shown deviations for the medium with non-homogeneous porosity [62].

2.8.6 Energy Equation and Porous Medium

First law of thermodynamics is used to derive the energy equation as in Eq. (2.31). Two types of thermal energy processes are considered whenever fluid flows through porous medium. These processes involve heat transfer through fluid phase and heat transfer through solid phase of medium. Following assumptions are used to formulate energy equation in such system [60]:

- Isotropic medium is considered
- Nanofluid mixture is homogeneous
- Set thermal equilibrium between nanofluid phase and solid phase of system
- Ignore the thermal radiation and viscous dissipation effects
- Ignore Brownian motion, slip velocities and thermophoresis effects of nanoparticles

Consider T_{nf} and T_s are for thermal energy in fluid phase and thermal energy in solid phase respectively. With reference of Eq. (2.30), the energy equations for solid phase and fluid phase can be written as

$$(1-\epsilon)\left(\rho C_\rho\right)_s \frac{\partial T_s}{\partial t} = (1-\epsilon)\,\nabla.\left(\kappa_s \nabla T_s\right) + (1-\epsilon)\, q_s^{**}, \tag{2.43}$$

$$\epsilon\left(\rho C_\rho\right)_{nf}\left(\frac{\partial T_{nf}}{\partial t} + \left(\mathbf{V}.\nabla T_{nf}\right)\right) = \epsilon\nabla.\left(\kappa_{nf}\nabla T_{nf}\right) + \epsilon\ q_{nf}^{**}, \tag{2.44}$$

$$\epsilon\left(\rho C_\rho\right)_{nf}\frac{\partial T_{nf}}{\partial t} + \epsilon\left(\rho C_\rho\right)_{nf}\mathbf{V}.\nabla T_{nf} = \epsilon\nabla.\left(\kappa_{nf}\nabla T_{nf}\right) + \epsilon\ q_{nf}^{**}, \tag{2.45}$$

where ϵ belongs to volume of voids, i.e., porosity and $(1-\epsilon)$ refers to volume of solid matrix of medium. By setting thermal equilibrium T_{nf}=T_s=T we get

$$(1-\epsilon)\left(\rho C_\rho\right)_s \frac{\partial T}{\partial t} = (1-\epsilon)\,\nabla.\left(\kappa_s \nabla T\right) + (1-\epsilon)\, q_s^{**}, \tag{2.46}$$

$$\epsilon\left(\rho C_\rho\right)_{nf}\frac{\partial T}{\partial t} + \epsilon\left(\rho C_\rho\right)_{nf}\mathbf{V}.\nabla T = \epsilon\nabla.\left(\kappa_{nf}\nabla T\right) + \epsilon\ q_{nf}^{**}. \tag{2.47}$$

Using Eq. (2.37) into Eq. (2.47) we get

$$\epsilon\left(\rho C_{\rho}\right)_{nf}\frac{\partial T}{\partial t}+\left(\rho C_{\rho}\right)_{nf}\tilde{V}.\nabla T=\epsilon\nabla.\left(\kappa_{nf}\nabla T\right)+\epsilon\ q_{nf}^{**}, \tag{2.48}$$

where $\left(\rho C_{\rho}\right)_{s}$, κ_{s}, q_{s}^{**}, $(1-\epsilon)$, $\left(\rho C_{\rho}\right)_{nf}$, κ_{nf}, q_{nf}^{**}, $\tilde{V}.\nabla T_{nf}$ are termed as specific heat for solid matrix, thermal conductivity for solid matrix, volume of solid matrix, specific heat for nanofluid, heat production for nanofluid and convection term due to temperature changes respectively. By adding Eqs. (2.46) and (2.48)

$$\begin{aligned}&\left(\rho C_{\rho}\right)_{s}\frac{\partial T}{\partial t}-\epsilon\left(\rho C_{\rho}\right)_{s}\frac{\partial T}{\partial t}+\epsilon\left(\rho C_{\rho}\right)_{nf}\frac{\partial T}{\partial t}+\left(\rho C_{\rho}\right)_{nf}\tilde{V}.\nabla T=\\&\nabla.\left(\kappa_{s}\nabla T\right)-\epsilon\nabla\left(\kappa_{s}\nabla T\right)+q_{s}^{**}-\epsilon q_{s}^{**}+\epsilon\nabla\left(\kappa_{nf}\nabla T\right)+\epsilon q_{nf}^{**},\end{aligned} \tag{2.49}$$

$$\begin{aligned}&\frac{\partial T}{\partial t}\Big(\left(1-\epsilon\right)\left(\rho C_{\rho}\right)_{s}+\epsilon\left(\rho C_{\rho}\right)_{nf}\Big)+\left(\rho C_{\rho}\right)_{nf}\Big(\tilde{V}.\nabla T\Big)=\\&\Big(\left(1-\epsilon\right)\kappa_{s}+\epsilon\kappa_{nf}\Big)\nabla.\left(\nabla T\right)+\Big(\left(1-\epsilon\right)q_{s}^{**}+\epsilon q_{nf}^{**}\Big).\end{aligned} \tag{2.50}$$

Some important relations from Eq. (2.50) are given below [60]

$$\left(\rho C_{\rho}\right)_{m}=\left(1-\epsilon\right)\left(\rho C_{\rho}\right)_{s}+\epsilon\left(\rho C_{\rho}\right)_{nf}, \tag{2.51}$$

$$\kappa_{m}\quad=\left(1-\epsilon\right)\kappa_{s}+\epsilon\kappa_{nf}, \tag{2.52}$$

$$q_{m}^{**}\quad=\left(1-\epsilon\right)q_{s}^{**}+\epsilon q_{nf}^{**}. \tag{2.53}$$

Here $\left(\rho C_{\rho}\right)_{m}$, κ_{m} and q_{m}^{**} are called specific heat, thermal conductivity and heat production per unit volume for porous medium. Hence Eq. (2.50) can be expressed as

$$\left(\rho C_{\rho}\right)_{nf}\frac{\partial T}{\partial t}+\left(\rho C_{\rho}\right)_{nf}\Big(\tilde{V}.\nabla T\Big)=\nabla.\left(\kappa_{m}\nabla T\right)+q_{m}^{**}. \tag{2.54}$$

For steady and incompressible flow case, Eq. (2.54) is transformed into

$$\left(\rho C_{\rho}\right)_{nf}\Big(\tilde{V}.\nabla T\Big)=\nabla.\left(\kappa_{m}\nabla T\right), \tag{2.55}$$

$$\Big(\tilde{V}.\nabla T\Big)\quad=\frac{\kappa_{m}}{\left(\rho C_{\rho}\right)_{nf}}\nabla.\left(\nabla T\right). \tag{2.56}$$

By using Eq. (2.51), the above equation can be formulated below

$$\left(\tilde{V}.\nabla T\right)=\frac{\left(\left(1-\epsilon\right)\kappa_s+\epsilon\kappa_{nf}\right)}{\left(\rho C_\rho\right)_{nf}}\nabla.\left(\nabla T\right), \tag{2.57}$$

$$\left(\tilde{V}.\nabla T\right)=\frac{\kappa_{nf}}{\left(\rho C_\rho\right)_{nf}}\left(\left(1-\epsilon\right)\frac{\kappa_s}{\kappa_{nf}}+\epsilon\right)\nabla.\left(\nabla T\right), \tag{2.58}$$

$$\left(\tilde{V}.\nabla T\right)=\alpha_{nf}\left(\left(1-\epsilon\right)\frac{\kappa_s}{\kappa_{nf}}+\epsilon\right)\nabla.\left(\nabla T\right). \tag{2.59}$$

Finally, Eq. (2.59) can be written as

$$\left(\tilde{V}.\nabla T\right)=\alpha_{nf}\left(\frac{\kappa_m}{\kappa_{nf}}\right)\Delta T. \tag{2.60}$$

The differential form of Eq. (2.60) can be expressed as

$$\tilde{u}\frac{\partial T}{\partial x}+\tilde{v}\frac{\partial T}{\partial y}\quad=\alpha_{nf}\left(\frac{\kappa_m}{\kappa_{nf}}\right)\left(\frac{\partial^2 T}{\partial x^2}+\frac{\partial^2 T}{\partial y^2}\right). \tag{2.61}$$

2.9 Heat Transfer in Fluids

Heat is an important form of energy. It always transfers from hot region to cold region with or without the involvement of material medium. The ways through which it transfers from one body to another body are called "Modes of heat transfer". The common means for heat transfer are conduction, convection and radiation. These can be defined as given below:

Definition 2.9.1. (**Thermal Conduction**)

"Conduction is the mode of heat transfer in which it travels from one part of body to another part by the interaction of electrons. The direction of this flow is always from the region at higher temperature to the region at lower temperature. Thermal conduction is also known as diffusion."

Fourier's law is important to explain this process which leads to the following important mathematical relation [45]

$$\frac{d\overline{Q}}{dt}=-\frac{\kappa A}{\Delta L}\left(T-T_0\right),$$

where $\overline{Q}$, κ, A, ΔL and $(T - T_0)$ are known as amount of heat transfer, thermal conductivity, area of body, length difference and temperature difference respectively.

Definition 2.9.2. (**Thermal Convection**)

"Convection is the mode of heat transfer that relates to the transfer of heat from a bounding surface (container) to the fluid in motion. It is simply the flow of heat through fluids either liquids or gases."

Mostly convection process in fluids is simply represented by using Newton's law of cooling. It is expressed as [45]

$$\frac{d\overline{Q}}{dt} = hA\left(T_\alpha - T_\beta\right),$$

where h, A, T_α and T_β are commonly known as heat transfer coefficient, area of body, temperature of object's surface and the temperature of fluid.

Convection of heat in fluids is of mostly three types. It categorizes as free or natural convection, forced convection and mixed convection. Further brief definitions can be expressed as below:

Definition 2.9.3. (**Natural Convection**)

"The heat transfer between a surface and fluid moving over it with fluid motion entirely caused by the buoyancy forces that arises due to density changes that results from the temperature variations in flow [51]."

Definition 2.9.4. (**Forced Convection**)

"It is the type of convection in which some external source is used to induce a force on the fluid's system for the transportation of heat. External source may be a pump, fan, or a suction device [45]."

Definition 2.9.5. (**Mixed Convection**)

"When the heat transfer process is influenced both by natural convection as well as forced convection at the same time, then this process is called mixed convection."

Definition 2.9.6. (**Thermal Radiation**)

"This phenomenon of heat transfer takes place without the involvement of medium.

It is also called electromagnetic radiation which are emitted by the body due to the presence of internal energy [45, 63]."

Thermal radiation is effectively defined by Stefan-Boltzmann law which gives the following equation to define this process

$$\frac{d\overline{Q}}{dt} = \sigma^* A\, \hat{\varepsilon} \left(T_1^4 - T_2^4\right),$$

where in above relation σ^*, $\hat{\varepsilon}$ and A are used for Stefan-Boltzmann constant, thermal emissivity of object and area of object.

2.10 Dimensionless Quantities

The dimensionless quantity expresses either a simple ratio of two dimensionally equal quantities or product of quantities in the numerator and in the denominator [64]. The result of such quantities will always be a pure numerical value. Such quantities are formed by using most commonly used simple dimensionless quantities of physical measurements like length, mass, time, etc. These quantities help us in reducing the complexity of problem by simplifying the physical phenomenon. Following are the few dimensionless physical parameters which are being used in our present study.

Definition 2.10.1. (**Reynolds Number** (Re))

"This is the number which expresses the ratio of fluid's inertial forces to the viscosity. It determines the nature of flow (laminar, turbulent or transient)."

Following cases are of great importance while using this quantity in understanding flow's behaviour [64]:

- Laminar flow if Re<2000,
- Transient flow if 2000<Re<4000,
- Turbulent flow if Re>4000.

Mathematically, it can be written as

$$Re = \frac{\text{inertial forces}}{\text{viscous forces}},$$

$$Re = \frac{\rho\, u_0 H}{\mu}.$$

Here u_0, ρ, μ and H are termed as velocity of fluid, density of fluid, dynamic viscosity and length of object.

Definition 2.10.2. (**Grashofs Number** (Gr))

"This number expresses the buoyancy to viscous forces ratio and its action on a fluid. It characterizes the free convection of fluid due to density differences caused by temperature gradient." This ratio can be expressed by [64]

$$Gr = \frac{\text{buoyancy forces}}{\text{viscous forces}},$$

$$Gr = \frac{gH^3\beta\Delta T}{\nu^2},$$

where g, β, ΔT and ν are named as gravitational acceleration, thermal expansion, temperature difference and kinematic viscosity of fluid.

Definition 2.10.3. (**Prandtle Number** (Pr))

"It is the number which expresses the ratio of viscosity (momentum diffusivity) to the thermal diffusivity. It characterizes the physical properties of fluids with convective heat transfer and diffusive heat transfer." Following cases are of great importance while using this quantity in understanding the heat transfer process [64]:

- Heat transfer is dominated by conduction if $Pr << 1$,
- Heat transfer is dominated by convection if $Pr >> 1$,
- Similar heat transfer if $Pr = 1$.

Its formulation is given by the following ratio

$$Pr = \frac{\nu}{\alpha} \Rightarrow \frac{C_\rho \mu}{\kappa}.$$

In this expression specific heat, dynamic viscosity and thermal conductivity of fluid are symbolized as C_ρ, μ and κ.

Definition 2.10.4. (**Richardson Number** (Ri))

"This number gives the ratio of natural convection to the forced convection. It also characterizes the effects of the domination of buoyancy forces and inertial forces on the behaviour of flow." Following are the two possible behaviour of flow due to the change in Ri number [64]:

- If Ri increases, free convection will dominate due to the excess of buoyancy forces,
- If Ri decreases, forced convection will dominate due to the excess of inertial forces.

Mathematically, this number can be expressed as

$$Ri = \frac{\text{buoyancy forces}}{\text{inertial forces}} = \frac{\text{free convection}}{\text{forced convection}},$$

$$Ri = \frac{g\beta\Delta T H}{u_0^2} \Rightarrow \frac{Gr}{Re^2}.$$

Definition 2.10.5. (**Darcys Number** (Da))

"This dimensionless number gives the effects of permeability of medium versus its cross sectional area."

$$Da = \frac{K}{H^2}.$$

where "K" belongs to permeability of porous medium [64].

Definition 2.10.6. (**Nusselt Number** (Nu))

"It is the number which expresses a ratio of the total heat transfer by convection

in a system to the heat transfer by conduction [64]."

$$Nu = \frac{\text{heat transfer by convection}}{\text{heat transfer by conduction}},$$

$$Nu = \frac{hH}{\kappa},$$

where "h " is called heat transfer coefficient. For $Nu \gg 1$ more visible convective heat transfer occurs but if $Nu = 1$ heat transfer shifts towards conduction mode.

Definition 2.10.7. (**Hartmann Number** (Ha))

"It is a ratio of electromagnetic force to viscous force (molecular friction force)." It can be formulated as [64]

$$Ha = B_0 H \sqrt{\frac{\sigma}{\mu}},$$

where B_0, σ and μ are known as magnetic field strength, electrical conductivity and dynamic viscosity of fluid.

Definition 2.10.8. (**Eckert Number** (Ec))

"It is the ratio of kinetic energy of fluid to the thermal energy change." Mathematically, this ratio can be written as [64]

$$Ec = \frac{u_0^2}{C_\rho \Delta T}.$$

In this relation velocity, specific heat and temperature difference are symbolized by u_0, C_ρ and ΔT.

2.11 Finite Element Method (FEM)

FEM is a numerical technique which is used for solving differential and integral equations related to many engineering or scientific problems. Such PDEs may describe some complicated natural processes which are either linear or non-linear in nature. FEM efficiently analyzes the problem related to the stresses, elasticity,

vibrations, heat transfer process and other complicated fluid flow processes (like high velocity profile, temperature profile, shock waves, etc.). The main philosophy behind this method is to convert continuous problems into finite or discrete type problems which are easily solvable by computers [65].

2.11.1 Galerkin Weighted Residual Method

This method is commonly used to choose weight functions. In this method weight functions are selected by taking the derivative of an approximate solution say $\bar{\mathbf{v}}(y)$ with respect to the involved unknown coefficients a_i. Vriational form is then achieved by setting their product with residual R of equation and integrate over domain Ω. So for one-dimensional case

$$w_i = \frac{\partial \bar{\mathbf{v}}(y)}{\partial a_i} = \varphi_i, \quad \forall\, i = 1, \ldots, n.$$

$$\int_{\Omega} w_i \, R \, d\Omega = 0.$$

2.11.2 Galerkin Finite Element Method

This is a FEA technique which uses "Galerkin weighted residual method" to get variational formulation of continuous problem for each individual element. These elements are the subdomains of the whole physical domain Ω. Main steps of GFEM for one-dimensional problem are given below:

- Discretize the whole computational domain say $\Omega = [a, b]$ of physical problem into different number of small subdomains, i.e., $y_0 = a,\ y_1, \ldots,\ y_L = b$. Define the size for each subdomain say h_i such that $h_i = (y_{i+1} - y_i)$, for $i = 1,\ 2, \ldots, (L-1)$. Each subdomain is known as element 'e'. Here y_i's are nodal points or node values and h_i is called mesh size or element size. All the elements should be non-overlapping, i.e., $e_i \bigcap e_j = 0$, for $i \neq j$.

- The strong form of PDEs of the given problem is converted to weak form. To get weak formulation, multiply the differential equation by the weight

functions (test functions) say w. These test functions must satisfy the homogeneous Dirichlet boundary conditions for the Dirichlet boundary data. Apply integration by parts using Neumann and Robbin type boundary conditions to set boundary integrals if required.

- Approximate the infinite dimensional solution and test spaces say $\mathbf{v}$ and W respectively by constructing or defining finite dimensional spaces say $\mathbf{v}_h$ and W_h for the achievement of discrete solution. Let $\mathbf{v}_h \approx \mathbf{v}$ and $W_h \approx W$, where $\mathbf{v}_h$ and W_h are known as finite dimensional trial solution and test spaces respectively.

- Apply Galerkin discretization to approximate finite dimensional trial solution and trial test spaces. Choose the approximate solution function v_h as find $v_h \; \varepsilon \; (\mathbf{v}_h \; \subset \; \mathbf{v})$ such that $a \; (v_h, w_h) = b \; (w_h)$, for all $w_h \; \varepsilon \; (W_h \; \subset \; W)$. Here $a \; (v_h, w_h)$ represents bilinear formulation while $b \; (w_h)$ notifies linear formulation of the respective differential equation.

- Represent the approximate solution over an element with finite dimensional trial solution space $\mathbf{v}_h$ by setting the linear combination of basis function φ_j's with the nodal unknowns v_j's such that

$$v_h^e = \sum_{j=1}^{NEN} v_j^e \varphi_j^e. \qquad j = 1, \; 2, \ldots, \; NEN \tag{2.62}$$

  These basis functions φ_i's and interpolation polynomial are of same type (geometry). Similarly choose a set of linearly independent basis function φ_i's for finite dimensional trial test space W_h such that

$$w_h^e = \sum_{j=1}^{NEN} w_i^e \varphi_i^e. \qquad i = 1, \; 2, \ldots, \; NEN \tag{2.63}$$

- Substitute these approximate solution functions v_h^e and approximate test functions w_h^e from Eqs. (2.62) and (2.63) into variational formulation of problem which yields a linear elemental system of algebraic equations as given

below

$$c\left(\sum_{j=1}^{NEN} v_j^e \varphi_j^e, \varphi_i^e\right) = d\left(\varphi_i^e\right), \qquad (i,j) \;=\; 1,\; 2, \ldots,\; NEN \tag{2.64}$$

$$\sum_{j=1}^{NEN} c\left(\varphi_j^e,\; \varphi_i^e\right) v_j^e = d\left(\varphi_i^e\right), \qquad (i,j) \;=\; 1,\; 2, \ldots,\; NEN \tag{2.65}$$

where v_j^e are the solution values at respective nodal points of element e.

- The above formulations will generate an algebraic linear system of equations, which contains equal number of equations as the number of elemental nodes and will be written in compact form as

$$[A^e]\{\mathbf{v}^e\} = \{B^e\}. \tag{2.66}$$

- Combine all local elemental systems like in Eq. (2.66), to get a global system of equations which will give the approximate solution over the whole computational domain $\Omega = [a, b]$.

$$[A]\{\mathbf{v}\} = \{B\}. \tag{2.67}$$

- The global system of equations in Eq. (2.67) comprises of algebraic equations is then solved by using any linear solver to get the final approximate solution.

Consider a following two-dimensional poisson problem for the illustration of solution methodology by GFEM.

Example

Given below is a steady two-dimensional poisson equation over the domain Ω.

$$-\nabla.(\nabla S) = f \qquad \text{or} \tag{2.68}$$

$$-\left(\frac{\partial^2 S}{\partial x^2}+\frac{\partial^2 S}{\partial y^2}\right) = f \qquad \text{in } \Omega \tag{2.69}$$

$$S = 0 \qquad \text{on } \partial\Omega \tag{2.70}$$

- To make weak formulation, select test function $w(x,y)$ satisfying the homogenous Drichlet boundary condition, i.e., $w(x,y)=0$ on $\partial\Omega$. By multiplying Eq. (2.68) with test function and integrate over the elemental domain gives the following variational form

$$-\int_{\Omega^e} w\Delta S d\Omega = \int_{\Omega^e} w f d\Omega, \qquad \text{or} \tag{2.71}$$

$$-\int_{\Omega^e} w\frac{\partial}{\partial x}\left(\frac{\partial S}{\partial x}\right)d\Omega - \int_{\Omega^e} w\frac{\partial}{\partial y}\left(\frac{\partial S}{\partial y}\right)d\Omega = \int_{\Omega^e} w f d\Omega. \tag{2.72}$$

- Reduce second order derivatives of S in Eq. (2.72) to get first order derivatives by applying following Green's identity

$$\int_{\Omega} w\frac{\partial G}{\partial \vec{n}}d\Omega = -\int_{\Omega} G\frac{\partial w}{\partial \vec{n}}d\Omega + \oint_{\Gamma} w\, G\, \vec{n}\, d\Gamma, \tag{2.73}$$

we get the following elemental weak formulation

$$\int_{\Omega^e}\left(\frac{\partial w}{\partial x}\frac{\partial S}{\partial x}+\frac{\partial w}{\partial x}\frac{\partial S}{\partial x}\right)d\Omega = \int_{\Omega^e} w f d\Omega. \tag{2.74}$$

- Approximate the solution over the element e by using

$$S^e(x,y) = \sum_{j=1}^{NEN} S_j^e \varphi_j^e(x,y), \tag{2.75}$$

where S_j's are approximate solution values at the elemental nodal points and φ_j's are pre-selected basis functions.

- Substitute the approximate solution Eq. (2.75) into variational formulation Eq. (2.74) we get

$$\int_{\Omega^e} \left[\left(\sum_{j=1}^{NEN} S_j^e \frac{\partial \varphi_j^e}{\partial x} \right) \frac{\partial w}{\partial x} + \left(\sum_{j=1}^{NEN} S_j^e \frac{\partial \varphi_j^e}{\partial x} \right) \frac{\partial w}{\partial y} \right] d\Omega = \int_{\Omega^e} w f d\Omega. \quad (2.76)$$

- For Galerkin FEM approximation to choose weight function of type $w\ (x, y) = \phi_i^e\ (x, y)$ to get the following elemental system

$$\int_{\Omega^e} \left[\left(\sum_{j=1}^{NEN} S_j^e \frac{\partial \varphi_j^e}{\partial x} \right) \frac{\partial \varphi_i^e}{\partial x} + \left(\sum_{j=1}^{NEN} S_j^e \frac{\partial \varphi_j^e}{\partial x} \right) \frac{\partial \varphi_i^e}{\partial y} \right] d\Omega = \int_{\Omega^e} \varphi_i^e f d\Omega. \quad (2.77)$$

  Equation (2.77) gives

$$\sum_{j=1}^{NEN} \left[\int_{\Omega^e} \left(\frac{\partial \varphi_j^e}{\partial x} \frac{\partial \varphi_i^e}{\partial x} + \frac{\partial \varphi_j^e}{\partial y} \frac{\partial \varphi_i^e}{\partial y} \right) d\Omega \right] \{S_j^e\} = \int_{\Omega^e} \varphi_i^e f d\Omega. \quad (2.78)$$

- The i^{th} elemental system in Eq. (2.78) will generate a discrete system of algebraic i^{th} number of equations which is expressed as

$$[A^e]\{S^e\} = \{\bar{F}^e\}, \quad (2.79)$$

  where $[A^e]$, $\{S^e\}$, and $\{\bar{F}^e\}$ are elemental stiffness matrix, elemental solution and elemental force vector matrix respectively.

- All such local elemental systems combine to give global system as below, which will finally provide the approximate solution of problem in Eq. (2.68).

$$[A]\{S\} = \{\bar{F}\}. \quad (2.80)$$

Chapter 3

Study of Mixed Convection of Alumina-Water Flow in an Inclined Porous Channel

This chapter is a review study of entropy generation analysis of mixed convective alumina-water flow by Hussain et al. [43]. Here we are going to reinvestigate the governing laws and equations which are helpful in analyzing the heat convection of alumina-water nanofluid along with the porous medium. The Darcy-Brinkman-Forchheimer model is applied here to investigate the role of porous medium in the augmentation of heat transport process. The numerical analysis is performed by using the Galerkin weighted residual based FEM. Exploration of results is displayed in terms of streamline contours, isothermal patterns and MATLAB plots.

3.1 Problem Formulation

Figure 3.1 is the demonstration of single phase, two-dimensional, incompressible and steady mixed convective nanofluid flow. A viscous and Newtonian flow is taken in an inclined open ended channel having a cavity. The conduit is inclined in counterclockwise direction with an angle γ. The dimensions of open ended

channel are $\frac{H}{2}$, l and w respectively. Some measurements related to cavity are taken as H and $L = 2H$. The whole channel is enclosed by porous medium and soaked with alumina-water nanofluid. The flow is entering into the channel at inlet with velocity u_0 and temperature T_c. The left wall of rectangular cavity has temperature T_h due to the attached heat source. Porous medium particles are

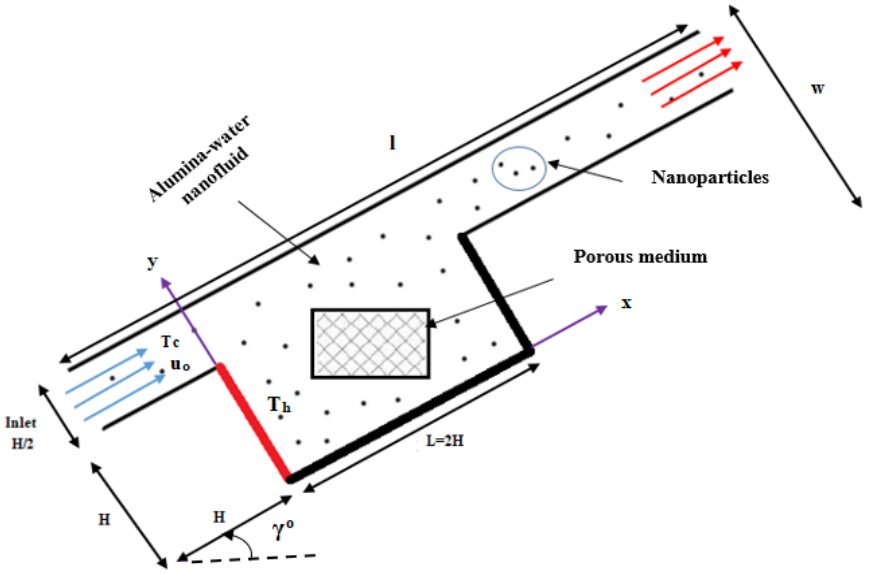

Figure 3.1: Physical geometry of the proposed problem.

isotropic solid which are of spherical in shape having uniform size. The mixture is supposed as a homogeneous combination of nanoparticles and base fluid. Base fluid (water) is chemically non-reactive towards Al_2O_3 particles. Both nanoparticles and the base fluid are in thermal equilibrium. Thermophysical properties of Al_2O_3 nanoparticles and water are kept constant. The cause of natural convection in present case arises due to the density variations for temperature differences. Boussinesq approximation is used to inspect natural convection [51].

3.1.1 Thermal and Physical Properties of Nanofluid

The different thermophysical properties of water and Aluminium oxide particles are given below in **Table** 3.1.

Properties	H_2O	Al_2O_3
C_ρ(J Kg^{-1} K^{-1})	4179	765
k(W m^{-1}K^{-1})	0.613	40
β(K^{-1})	21×10^{-5}	0.85×10^{-5}
$\sigma(\Omega\ \mathrm{m}^{-1})$	0.05	1×10^{-10}
ρ(kg m^{-3})	997.1	3970
d_p(nm)	-	47

Table 3.1: Thermal and physical properties of alumina-water.

3.2 Dimensional Governing Equations

On the account of the above discussion, now we are able to describe the dimensional form of the governing equations for the proposed problem. Boussinesq approximation is applied to body force term as $(\beta\rho)_{nf}(T - T_c)\mathbf{g}$. In which β represents thermal expansion and $\mathbf{g}$ is known as gravitational acceleration. For inclined channel the x and y components of $\mathbf{g}$ are $g\sin\gamma$ and $g\cos\gamma$ respectively. Given below is the governing system for the nanofluid flow in porous medium under Darcy-Brinkman-Forchheimer model together with respective boundary conditions [22, 43].

Continuity Equation:

$$\frac{1}{\epsilon}\left(\frac{\partial\tilde{u}}{\partial x} + \frac{\partial\tilde{v}}{\partial y}\right) = 0, \tag{3.1}$$

x-Component of Momentum Equation:

$$\begin{aligned}\frac{\rho_{nf}}{\epsilon^2}\left(\tilde{u}\frac{\partial\tilde{u}}{\partial x} + \tilde{v}\frac{\partial\tilde{u}}{\partial y}\right) = &-\frac{\partial p}{\partial x} + \frac{\mu_f}{\epsilon(1-\phi)^{2.5}}\left(\frac{\partial^2\tilde{u}}{\partial x^2} + \frac{\partial^2\tilde{u}}{\partial y^2}\right)\\ &+ (\beta\rho)_{nf}\, g\,(T - T_c)\sin\gamma - \frac{\mu_{nf}}{K}\tilde{u}\\ &- \frac{1.75\rho_{nf}}{\sqrt{150K}\epsilon^{3/2}}\left(\sqrt{\tilde{u}^2 + \tilde{v}^2}\right)\tilde{u},\end{aligned} \tag{3.2}$$

y-Component of Momentum Equation:

$$\frac{\rho_{nf}}{\epsilon^2}\left(\tilde{u}\frac{\partial\tilde{v}}{\partial x}+\tilde{v}\frac{\partial\tilde{v}}{\partial y}\right)=-\frac{\partial p}{\partial y}+\frac{\mu_f}{\epsilon(1-\phi)^{2.5}}\left(\frac{\partial^2\tilde{v}}{\partial x^2}+\frac{\partial^2\tilde{v}}{\partial y^2}\right)+(\beta\rho)_{nf}\,g\,(T-T_c)\cos\gamma-\frac{\mu_{nf}}{K}\tilde{v}-\frac{1.75\rho_{nf}}{\sqrt{150K}\epsilon^{3/2}}\left(\sqrt{\tilde{u}^2+\tilde{v}^2}\right)\tilde{v}, \tag{3.3}$$

Energy Equation:

$$\tilde{u}\frac{\partial T}{\partial x}+\tilde{v}\frac{\partial T}{\partial y}=\alpha_{nf}\left(\frac{\kappa_m}{\kappa_{nf}}\right)\left(\frac{\partial^2 T}{\partial x^2}+\frac{\partial^2 T}{\partial y^2}\right). \tag{3.4}$$

The momentum equations (3.2) and (3.3) are approximated by $\mu_{nf}=\frac{\mu_f}{(1-\phi)^{2.5}}$ which is presented by Brinkman in 1952 for concentrated suspensions and solutions [66]. The associated conditions for boundaries are given below:

- On the inlet side of channel:

$$\tilde{u}(x,y)=u_0, \qquad \tilde{v}(x,y)=0, \qquad T=T_c.$$

- On left wall of cavity:

$$\tilde{u}(x,y)=0, \qquad \tilde{v}(x,y)=0, \qquad T=T_h.$$

- On the horizontal adiabatic walls of channel and cavity:

$$\tilde{u}(x,y)=0, \qquad \tilde{v}(x,y)=0, \qquad \frac{\partial T}{\partial y}=0.$$

- On the vertical adiabatic walls of channel and cavity:

$$\tilde{u}(x,y)=0, \qquad \tilde{v}(x,y)=0, \qquad \frac{\partial T}{\partial x}=0.$$

- On the outlet side of channel:

$$\frac{\partial \tilde{u}}{\partial x} = 0, \qquad \frac{\partial \tilde{v}}{\partial y} = 0, \qquad \frac{\partial T}{\partial x} = 0.$$

3.3 Dimensionless Governing Equations

Given below are the physical relations used to transform the set of governing equations from (3.1) to (3.4) into the respective dimensionless form.

$$X = \frac{x}{H}, \qquad Y = \frac{y}{H}, \qquad \widehat{U} = \frac{\tilde{u}}{u_0}, \quad \widehat{V} = \frac{\tilde{v}}{u_0}, \quad \widehat{\theta} = \frac{T - T_c}{T_h - T_c}, \quad \widehat{P} = \frac{p}{\rho_{nf} {u_0}^2},$$

$$Re = \frac{u_0 H}{\nu_f}, \quad Da = \frac{K}{H^2}, \quad Pr = \frac{\nu_f}{\alpha_f}, \quad Ri = \frac{Gr}{Re^2}, \quad Gr = \frac{g\beta_f \Delta T H^3}{\nu_f^2}.$$

After conversion the set of transformed dimensionless equations can be written as

Continuity Equation:

$$\frac{\partial \widehat{U}}{\partial X} + \frac{\partial \widehat{V}}{\partial Y} = 0, \tag{3.5}$$

x-Component of Momentum Equation:

$$\begin{aligned}\frac{1}{\epsilon^2}\left(\widehat{U}\frac{\partial \widehat{U}}{\partial X} + \widehat{V}\frac{\partial \widehat{U}}{\partial Y}\right) = &-\frac{\partial \widehat{P}}{\partial X} + \frac{1}{\epsilon Re}\frac{\rho_f}{\rho_{nf}}\frac{1}{(1-\phi)^{2.5}}\left(\frac{\partial^2 \widehat{U}}{\partial X^2} + \frac{\partial^2 \widehat{U}}{\partial Y^2}\right) \\ &+ Ri\frac{\rho_f}{\rho_{nf}}\left((1-\phi) + \phi\frac{\rho_p \beta_p}{\rho_f \beta_f}\right)\sin\gamma\,\widehat{\theta} \\ &- \frac{\mu_{nf}}{\rho_{nf}\nu_f}\frac{1}{ReDa}\widehat{U} - \frac{1.75}{\sqrt{150Da}\epsilon^{3/2}}\left(\sqrt{\widehat{U}^2 + \widehat{V}^2}\right)\widehat{U},\end{aligned} \tag{3.6}$$

y-Component of Momentum Equation:

$$\frac{1}{\epsilon^2}\left(\widehat{U}\frac{\partial \widehat{V}}{\partial X}+\widehat{V}\frac{\partial \widehat{V}}{\partial Y}\right)=-\frac{\partial \widehat{P}}{\partial Y}+\frac{1}{\epsilon Re}\frac{\rho_f}{\rho_{nf}}\frac{1}{(1-\phi)^{2.5}}\left(\frac{\partial^2 \widehat{V}}{\partial X^2}+\frac{\partial^2 \widehat{V}}{\partial Y^2}\right)$$
$$+Ri\frac{\rho_f}{\rho_{nf}}\left((1-\phi)+\phi\frac{\rho_p\beta_p}{\rho_f\beta_f}\right)\cos\gamma\,\widehat{\theta}$$
$$-\frac{\mu_{nf}}{\rho_{nf}\nu_f}\frac{1}{ReDa}\widehat{V}-\frac{1.75}{\sqrt{150Da}\epsilon^{3/2}}\left(\sqrt{\widehat{U}^2+\widehat{V}^2}\right)\widehat{V}, \quad (3.7)$$

Energy Equation:

$$\widehat{U}\frac{\partial \widehat{\theta}}{\partial X}+\widehat{V}\frac{\partial \widehat{\theta}}{\partial Y}=\frac{1}{RePr}\frac{\alpha_{nf}}{\alpha_f}\frac{\kappa_m}{\kappa_{nf}}\left(\frac{\partial^2 \widehat{\theta}}{\partial X^2}+\frac{\partial^2 \widehat{\theta}}{\partial Y^2}\right). \quad (3.8)$$

The associated dimensionless boundary conditions are as follows:

- On the inlet side of channel:

$$\widehat{U}=1, \qquad \widehat{V}=0, \qquad \widehat{\theta}=0.$$

- On the left wall of cavity:

$$\widehat{U}=0, \qquad \widehat{V}=0, \qquad \widehat{\theta}=1.$$

- On the horizontal adiabatic walls of channel and cavity:

$$\widehat{U}=0, \qquad \widehat{V}=0, \qquad \frac{\partial \widehat{\theta}}{\partial Y}=0.$$

- On the vertical adiabatic walls of channel and cavity:

$$\widehat{U}=0, \qquad \widehat{V}=0, \qquad \frac{\partial \widehat{\theta}}{\partial X}=0.$$

- On the outlet side of channel:

$$\frac{\partial \widehat{U}}{\partial X}=0, \qquad \frac{\partial \widehat{V}}{\partial Y}=0, \qquad \frac{\partial \widehat{\theta}}{\partial X}=0.$$

3.4 Effective Properties of Nanofluid

According to a postulate by Koo and Kleinstreuer that Brownian motion of nanopaticles have significant impacts on thermal conduction of nanofluids. This property is mainly due to the nanoparticle's conventional static part and a Brownian motion part [67]. For this, a model is proposed by Koo and Keleinstreuer which has disclosed that thermal conduction and viscosity are directly influenced by the size, concentration volume and temperature dependency of nanoparticles. Both of these thermal properties are important for effective heat transport mechanism. It also accounts that not only the types and nature of particles but base fluid combinations have a great effect on the thermal conductivity and viscosity of nanofluid. A brief discussion of these are mentioned below [43, 68, 69].

- **Effective Thermal Conductivity**:

  According to literature the effective thermal conductivity is mathematically represented as

  $$\kappa_{\text{eff,nf}} = \kappa_{\text{static}} + \kappa_{\text{Brownian}},$$

  where κ_{static} belongs to the static part of nanofluid due to less heat gradients and κ_{Brownian} belongs to the dynamic part of fluid due to large temperature gradients [43, 68, 69]. Here κ_{static} is demonstrated by Maxwell in [70] as given below

  $$\kappa_{\text{static}} = \kappa_f \left[1 + \frac{3\left(\frac{\kappa_p}{\kappa_f} - 1\right)\phi}{\left(\frac{\kappa_p}{\kappa_f} + 2\right) - \left(\frac{\kappa_p}{\kappa_f} - 1\right)\phi}\right],$$

  where κ_f, κ_p, ϕ are notifying thermal conductivity of base fluid, thermal conductivity of nanoparticles and concentration fraction of nanoparticles. Now κ_{Brownian} is expressed by Koo-Kleinstreuer-Li as below

  $$\kappa_{\text{Brownian}} = 5 \times 10^4 \phi \rho_f \left(C_\rho\right)_f \sqrt{\frac{\kappa_b T_{\text{ref}}}{\rho_p d_p}} \acute{g}\left(T_{\text{ref}}, \phi, d_p\right).$$

  Here the terms $(C_\rho)_f$, ϕ, ρ_f, κ_b, T_{ref}, d_p are known as specific heat capacity for base fluid, volume fraction of nanoparticles, density of base fluid, Boltzmann

constant, reference temperature, density of nanoparticles and diameter of nanoparticles respectively.

The experimentally calculated value for the function $\acute{g}$ is given by following empirical formulation [43]:

$$\begin{aligned}\acute{g}\left(T_{\text{ref}}, \phi, d_p\right) =& \big(r_1 + r_2 \ln\left(d_p\right) + r_3 \ln\left(\phi\right) + r_4 \ln\left(\phi\right) \ln\left(d_p\right) + \\ & r_5 \ln\left(d_p\right)^2 \ln T_{\text{ref}} + \left(r_6 + r_7 \ln\left(d_p\right)\right) + r_8 \ln\left(\phi\right) + \\ & r_9 \ln\left(d_p\right) \ln\left(\phi\right) + r_{10} \ln\left(d_p\right)^2 \big).\end{aligned}$$

The constants r_1 to r_{10} are mentioned in **Table** 3.2. Another important

Coefficients	Values for alumina-water [43]
r_1	52.813488759
r_2	6.115637295
r_3	0.6955745084
r_4	0.041745555278
r_5	0.176919300241
r_6	-298.19819084
r_7	-34.532716906
r_8	-3.9225289283
r_9	-0.2354329626
r_{10}	-0.999063481

Table 3.2: The coefficient values of alumina-water nanofluid [43].

relation in this regard is "interfacial resistance" which is denoted by R_f. It is the resistance between the dissolved nanoparticles and base fluid. It is mathematically given by [43, 71]

$$R_f + \frac{d_p}{\kappa_p} = \frac{d_p}{\kappa_{\text{eff,p}}}. \tag{3.9}$$

For Al_2O_3 nanoparticles its value is 4×10^{-8} Km^2 W^{-1}. Equation (3.9) leads to another important relation, which gives the effective thermal conductivity

for isolated Al_2O_3 nanoparticles [71]. It is expressed as

$$\kappa_{\text{eff,p}} = \frac{d_p \kappa_p}{\kappa_p R_f + d_p},$$

where R_f, d_p, κ_p are representations for intrfacial thermal resistance, diameter and thermal conductivity for nanoparticles.

- **Effective Viscosity**:

  Effective viscosity for nanofluid has been demonstrated by Koo and Kleinstreuer and is illustrated as [43, 68, 69]

$$\mu_{\text{eff,nf}} = \mu_{\text{static}} + \mu_{\text{Brownian}},$$

  where μ_{Brownian} can be written as

$$\mu_{\text{Brownian}} = \frac{\kappa_{\text{Brownian}}}{\kappa_f} \times \frac{\mu_f}{Pr_f}.$$

  Here viscosity, Prandtle number and thermal conductivity of base fluid are symbolized by μ_f, Pr_f and κ_f. Brinkmann presented the static part of viscosity, which is given below

$$\mu_{\text{static}} = \frac{\mu_f}{(1-\phi)^{2.5}}.$$

  Hence by substituting Eqs. (3.4) and (4.13) into Eq. (3.4) gives the final expression for effective viscosity as below

$$\mu_{\text{eff,nf}} = \frac{\mu_f}{(1-\phi)^{2.5}} + \frac{\kappa_{\text{Brownian}}}{\kappa_f} \times \frac{\mu_f}{Pr_f}.$$

Some other effective properties which may affect and increase the heat transfer capacities of nanofluids are considered as follows

- **Effective Density**:

$$\rho_{nf} = (1-\phi)\,\rho_f + \phi \rho_p,$$

- **Effective Thermal Diffusivity**:

$$\alpha_{nf} = \frac{\kappa_{nf}}{(\rho \mathrm{C}_\rho)_{nf}},$$

- **Effective Specific Heat Capacity**:

$$(\rho \mathrm{C}_\rho)_{nf} = (1-\phi)\,(\rho \mathrm{C}_\rho)_f + \phi\,(\rho \mathrm{C}_\rho)_p\,,$$

- **Effective Electrical Conductivity**:

$$\sigma_{nf} = \sigma_f\big[1 + \frac{3\,(\sigma-1)\,\phi}{(\sigma+2)-(\sigma-1)\,\phi}\big], \qquad \sigma = \frac{\sigma_p}{\sigma_f}$$

- **Effective Thermal Expansion**:

$$(\rho\beta)_{nf} = (1-\phi)\,(\rho\beta)_f + \phi\,(\rho\beta)_p\,.$$

Some important effective thermal properties for porous medium of our interest are

- **Effective Specific Heat Capacity for Porous Medium**:

$$(\rho C_\rho)_m = (1-\epsilon)\,(\rho C_\rho)_s + \epsilon\,(\rho C_\rho)_{nf}\,,$$

- **Effective Thermal Conductivity for Porous Medium**:

$$\kappa_m = (1-\epsilon)\,\kappa_s + \epsilon\kappa_{nf}.$$

Heat Transfer Physical Parameters

To analyze the temperature distributions over alumina-water flow is the main purpose of this schemed problem. The most common parameter which is used to measure the rate of heat transfer throughout the geometry is Nusselt number.

It represents the ratio of total convective heat transfer in a system to the heat transfer by conduction.

The dimensionless local Nusselt number is given by

$$Nu_{\mathrm{L}} = -\frac{\kappa_{nf}}{\kappa_f}\left|\left(\frac{\partial\widehat{\theta}}{\partial X}\right)\right|_{X=0}.$$

Average Nusselt number is the mean of all local Nusselt numbers over entire heat transfer domain. It is obtained by integrating the local Nusselt numbers over the heated boundary.

$$Nu_{\mathrm{avg}} = \int_0^c Nu\, dY.$$

Here c represents the length of hot wall.

3.5 Numerical Solution

The set of dimensionless equations from Eqs. (3.5) to (3.8) forms a system of nonlinear coupled PDEs along with the associated boundary conditions. The solution is achieved by the discretization of nonlinear PDEs using the Galerkin finite element method. Galerkin weighted residual technique is applied to get the weight functions for trial test and trial solution spaces. The spatial discretization of governing PDEs is achieved by using higher order Ladyzhenskaya-Babuska-Brezzi stable finite element pair, i.e., Q_2/P_1^{disc} [65, 72].

The main steps for the methodology are further listed below:

3.5.1 Strong Form of Governing Equations

The set of governing PDEs from Eqs. (3.5) to (3.8) are initially known as strong form which are re-written as

$$a_1\left(\widehat{U}\frac{\partial\widehat{U}}{\partial X}+\widehat{V}\frac{\partial\widehat{U}}{\partial Y}\right)=-\frac{\partial\widehat{P}}{\partial X}+a_2\left(\frac{\partial^2\widehat{U}}{\partial X^2}+\frac{\partial^2\widehat{U}}{\partial Y^2}\right)+a_3\widehat{\theta}-a_4\widehat{U}-a_5\left(\sqrt{\widehat{U}^2+\widehat{V}^2}\right)\widehat{U}, \tag{3.10}$$

$$a_6\left(\widehat{U}\frac{\partial\widehat{V}}{\partial X}+\widehat{V}\frac{\partial\widehat{V}}{\partial Y}\right)=-\frac{\partial\widehat{P}}{\partial Y}+a_7\left(\frac{\partial^2\widehat{V}}{\partial X^2}+\frac{\partial^2\widehat{V}}{\partial Y^2}\right)+a_8\widehat{\theta}-a_9\widehat{V}-a_{10}\left(\sqrt{\widehat{U}^2+\widehat{V}^2}\right)\widehat{V}, \tag{3.11}$$

$$\frac{\partial\widehat{U}}{\partial X}+\frac{\partial\widehat{V}}{\partial Y}=0, \tag{3.12}$$

$$\widehat{U}\frac{\partial\widehat{\theta}}{\partial X}+\widehat{V}\frac{\partial\widehat{\theta}}{\partial Y}=a_{11}\left(\frac{\partial^2\widehat{\theta}}{\partial X^2}+\frac{\partial^2\widehat{\theta}}{\partial Y^2}\right). \tag{3.13}$$

In the set of equations, the values of a's are expressed as:

$a_1=a_6=\frac{1}{\epsilon^2}$, $\quad a_2=a_7=\frac{1}{\epsilon Re}\frac{\rho_f}{\rho_{nf}}\frac{1}{(1-\phi)^{2.5}}$,

$a_3=Ri\frac{\rho_f}{\rho_{nf}}\left((1-\phi)+\phi\frac{\rho_p\beta_p}{\rho_f\beta_f}\right)\sin\gamma$, $\quad a_4=a_9=\frac{\mu_{nf}}{\rho_{nf}\nu_f}\frac{1}{ReDa}$,

$a_8=Ri\frac{\rho_f}{\rho_{nf}}\left((1-\phi)+\phi\frac{\rho_p\beta_p}{\rho_f\beta_f}\right)\cos\gamma$, $\quad a_5=a_{10}=\frac{1.75}{\sqrt{150Da\epsilon^{3/2}}}$,

$a_{11}=\frac{1}{RePr}\frac{\alpha_{nf}}{\alpha_f}\frac{\kappa_m}{\kappa_{nf}}$.

3.5.2 Weak/Variational Formulation

Weak formulation is a variational method which is used to transform differential equations into integral form by multiplying the dependent variables with suitable test function and then integrated over the whole computational domain. Here $\widehat{U}$, $\widehat{V}$, $\widehat{\theta}$ and $\widehat{P}$ are solution spaces defined on continuously varying infinite dimensional space Ω, the matter of fact is that the achievement of the solution in such a large space is not possible. The main objective is to find some suitable spaces to get

functions with finite properties or parameters. To start with weak formulation we need to define some special functions, which we called test functions for the residuals to find approximate solution. Let $\mathbf{W}$ and Q be the test spaces of infinite dimensions in which $\mathbf{W} = [H_1(\Omega), H_1(\Omega), H_1(\Omega)]$ and $Q = L_2(\Omega)$. Let $\hat{w}$ and $\hat{q}$ be the respective test functions such that $\hat{w}\ \varepsilon\ \mathbf{W}$ and $\hat{q}\ \varepsilon\ Q$. For the variational formulation the components of momentum and energy equations are multiplied by test function $\hat{w}\ \varepsilon\ \mathbf{W}$ while the continuity equation is multiplied by test function $\hat{q}$ $\varepsilon\ Q$. The weak formulation of the strong form of governing PDEs from Eqs. (3.10) to (3.13) is written below:

Find $(\widehat{U},\widehat{V},\widehat{\theta},\widehat{P})\ \varepsilon\ (\mathbf{W}\times Q)$ such that

$$a_1\int_\Omega\left(\widehat{U}\frac{\partial\widehat{U}}{\partial X}+\widehat{V}\frac{\partial\widehat{U}}{\partial Y}\right)\hat{w}d\Omega-\int_\Omega\frac{\partial\widehat{P}}{\partial X}\hat{w}d\Omega+a_2\int_\Omega\left(\frac{\partial^2\widehat{U}}{\partial X^2}+\frac{\partial^2\widehat{U}}{\partial Y^2}\right)\hat{w}d\Omega$$
$$-a_3\int_\Omega\widehat{\theta}\hat{w}d\Omega+a_4\int_\Omega\widehat{U}\hat{w}d\Omega+a_5\left(\sqrt{\widehat{U}^2+\widehat{V}^2}\right)\int_\Omega\widehat{U}\hat{w}d\Omega=0, \tag{3.14}$$

$$a_6\int_\Omega\left(\widehat{U}\frac{\partial\widehat{V}}{\partial X}+\widehat{V}\frac{\partial\widehat{V}}{\partial Y}\right)\hat{w}d\Omega-\int_\Omega\frac{\partial\widehat{P}}{\partial Y}\hat{w}d\Omega+a_7\int_\Omega\left(\frac{\partial^2\widehat{V}}{\partial X^2}+\frac{\partial^2\widehat{V}}{\partial Y^2}\right)\hat{w}d\Omega$$
$$-a_8\int_\Omega\widehat{\theta}\hat{w}d\Omega+a_9\int_\Omega\widehat{V}\hat{w}d\Omega+a_{10}\left(\sqrt{\widehat{U}^2+\widehat{V}^2}\right)\int_\Omega\widehat{V}\hat{w}d\Omega=0, \tag{3.15}$$

$$\int_\Omega\left(\frac{\partial\widehat{U}}{\partial X}+\frac{\partial\widehat{V}}{\partial Y}\right)\hat{q}d\Omega=0, \tag{3.16}$$

$$\int_\Omega\left(\widehat{U}\frac{\partial\widehat{\theta}}{\partial X}+\widehat{V}\frac{\partial\widehat{\theta}}{\partial Y}\right)\hat{w}d\Omega+a_{11}\int_\Omega\left(\frac{\partial^2\widehat{\theta}}{\partial X^2}+\frac{\partial^2\widehat{\theta}}{\partial Y^2}\right)\hat{w}d\Omega=0, \tag{3.17}$$

for all $(\hat{w},\hat{q})\ \varepsilon\ (\mathbf{W}\times Q)$.

The infinite dimensional test and solution spaces are approximated by the finite dimensional spaces by Galerkin discretization scheme to ensure the accuracy requirements. These spaces are known as finite element spaces. Let the approximated solution components are $(\widehat{U}_\hbar,\widehat{V}_\hbar,\widehat{P}_\hbar,\widehat{\theta}_\hbar)\approx(\widehat{U},\widehat{V},\widehat{P},\widehat{\theta})$ whereas $(\mathbf{W}_\hbar,\ Q_\hbar)\approx(\mathbf{W}\times Q)$ are the finite dimensional test spaces.

Find $(\widehat{U}_\hbar,\widehat{V}_\hbar,\widehat{P}_\hbar,\widehat{\theta}_\hbar)\ \varepsilon\ (\mathbf{W}_\hbar,\ Q_\hbar)$ such that

$$a_1 \int_\Omega \left(\widehat{U}_\hbar \frac{\partial \widehat{U}_\hbar}{\partial X} + \widehat{V}_\hbar \frac{\partial \widehat{U}_\hbar}{\partial Y} \right) \hat{w}_\hbar d\Omega \quad + \quad a_2 \int_\Omega \left(\frac{\partial \widehat{U}_\hbar}{\partial X} \frac{\partial \hat{w}_\hbar}{\partial X} + \frac{\partial \widehat{U}_\hbar}{\partial Y} \frac{\partial \hat{w}_\hbar}{\partial Y} \right) d\Omega$$
$$- \int_\Omega \frac{\partial \widehat{P}_\hbar}{\partial X} \hat{w}_\hbar d\Omega \quad - a_3 \int_\Omega \widehat{\theta}_\hbar \hat{w}_\hbar d\Omega \quad + a_4 \int_\Omega \widehat{U}_\hbar \hat{w}_\hbar d\Omega$$
$$+ a_5 \left(\sqrt{\widehat{U}_\hbar^2 + \widehat{V}_\hbar^2} \right) \int_\Omega \widehat{U}_\hbar \hat{w}_\hbar d\Omega = 0, \tag{3.18}$$

$$a_6 \int_\Omega \left(\widehat{U}_\hbar \frac{\partial \widehat{V}_\hbar}{\partial X} + \widehat{V}_\hbar \frac{\partial \widehat{V}_\hbar}{\partial Y} \right) \hat{w}_\hbar d\Omega \quad + \quad a_7 \int_\Omega \left(\frac{\partial \widehat{V}_\hbar}{\partial X} \frac{\partial \hat{w}_\hbar}{\partial X} + \frac{\partial \widehat{V}_\hbar}{\partial Y} \frac{\partial \hat{w}_\hbar}{\partial Y} \right) d\Omega$$
$$- \int_\Omega \frac{\partial \widehat{P}_\hbar}{\partial Y} \hat{w}_\hbar d\Omega \quad - a_8 \int_\Omega \widehat{\theta}_\hbar \hat{w}_\hbar d\Omega \quad + a_9 \int_\Omega \widehat{V}_\hbar \hat{w}_\hbar d\Omega$$
$$+ a_{10} \left(\sqrt{\widehat{U}_\hbar^2 + \widehat{V}_\hbar^2} \right) \int_\Omega \widehat{V}_\hbar \hat{w}_\hbar d\Omega = 0, \tag{3.19}$$

$$\int_\Omega \left(\frac{\partial \widehat{U}_\hbar}{\partial X} + \frac{\partial \widehat{U}_\hbar}{\partial Y} \right) \hat{q}_\hbar d\Omega = 0, \tag{3.20}$$

$$\int_\Omega \left(\widehat{U}_\hbar \frac{\partial \widehat{\theta}_\hbar}{\partial X} + \widehat{V}_\hbar \frac{\partial \widehat{\theta}_\hbar}{\partial Y} \right) \hat{w}_\hbar d\Omega + a_{11} \int_\Omega \left(\frac{\partial \widehat{\theta}_\hbar}{\partial X} \frac{\partial \hat{w}_\hbar}{\partial X} + \frac{\partial \widehat{\theta}_\hbar}{\partial Y} \frac{\partial \hat{w}_\hbar}{\partial Y} \right) d\Omega = 0, \tag{3.21}$$

for all $(\hat{w}_\hbar, \hat{q}_\hbar)\ \varepsilon\ (\mathbf{W}_\hbar, Q_\hbar)$.

FEM approximation is achieved by using the approximate trial solution functions and trial test functions. These functions are the linear combination of nodal unknowns and shape functions which are linearly independent. Given below are the trial solution functions:

$$\widehat{U}_\hbar = \sum_{j=1}^{m} \widehat{U}_j \xi_j, \qquad \widehat{V}_\hbar = \sum_{j=1}^{m} \widehat{V}_j \xi_j, \qquad \widehat{\theta}_\hbar = \sum_{j=1}^{m} \widehat{\theta}_j \xi_j, \qquad \widehat{P}_\hbar = \sum_{j=1}^{l} \widehat{P}_j \eta_j.$$

Similarly following trial approximated functions are defined for test spaces:

$$\hat{w}_\hbar = \sum_{i=1}^{m} \hat{w}_i \xi_i, \qquad \hat{q}_\hbar = \sum_{i=1}^{l} \hat{q}_i \eta_i.$$

In all above relations ξ_j and η_j are the shape functions. The discretization of these finite element equations have been performed by introducing a higher order stable

Q_2/P_1^{disc} pair of finite elements.

For this, the biquadratic (Q_2) space is used to discretize the velocity and temperature components and discontinuous linear (P_1^{disc}) finite element is utilized for pressure field. Here the biquadratic (Q_2) are the elements with third order accuracy while discontinuous linear (P_1^{disc}) are the finite elements with second order accuracy in L_2-norm respectively. In this pair biquadratic Q_2 element has 9 local degrees of freedom for each velocity-temperature components whereas 3 local nodal unknowns are placed for discontinuous linear P_1^{disc} pressure component on each quadrilateral element. Hence each quadrilateral element is representing a total of 30 unknowns for velocity, temperature and pressure solution components. Integration in each elemental term is solved by using Gaussian quadrature rules.

By using these approximations in Eqs. (3.18) to (3.21), we get the discretized system of nonlinear algebraic equations as

$$[A^*(\widehat{U},\widehat{V})]\{X^*\} = \{\bar{F}^*\}.$$

The matrix notation of $A^*(\widehat{U},\widehat{V})$, X^* and $\bar{F}^*$ can be written as

$$\underbrace{\begin{bmatrix} \Upsilon^{11} & \Upsilon^{12} & \mathbf{B}_1 & \Upsilon^{14} \\ \Upsilon^{21} & \Upsilon^{22} & \mathbf{B}_2 & \Upsilon^{24} \\ \mathbf{B}_1^{\mathrm{T}} & \mathbf{B}_2^{\mathrm{T}} & \Upsilon^{33} & \Upsilon^{34} \\ \Upsilon^{41} & \Upsilon^{42} & \Upsilon^{43} & \Upsilon^{44} \end{bmatrix}}_{A^*} \underbrace{\begin{bmatrix} \widehat{U} \\ \widehat{V} \\ \widehat{P} \\ \widehat{\theta} \end{bmatrix}}_{X^*} = \underbrace{\begin{bmatrix} \bar{F}^1 \\ \bar{F}^2 \\ \bar{F}^3 \\ \bar{F}^4 \end{bmatrix}}_{\bar{F}^*}. \tag{3.22}$$

Here A^*, X^* and $\bar{F}^*$ are called block stiffness matrix, block solution vector and block load vector respectively. The local elemental entries of block stiffness matrix are given as

$$\Upsilon_{\mathrm{ij}}^{11} = a_1 \int_\Omega \left[\left(\sum_{j=1}^{m} \widehat{U}_j \xi_j \right) \frac{\partial \xi_j}{\partial X} + \left(\sum_{j=1}^{m} \widehat{V}_j \xi_j \right) \frac{\partial \xi_j}{\partial Y} \right] d\Omega \quad + \quad a_4 \int_\Omega \xi_j \xi_i d\Omega$$
$$+ a_2 \int_\Omega \left(\frac{\partial \xi_j}{\partial X}\frac{\partial \xi_i}{\partial X} + \frac{\partial \xi_j}{\partial Y}\frac{\partial \xi_i}{\partial Y} \right) d\Omega + a_5 \left[\sqrt{\left(\sum_{j=1}^{m} \widehat{U}_j \xi_j \right)^2 + \left(\sum_{j=1}^{m} \widehat{V}_j \xi_j \right)^2} \right]$$

$\int_\Omega \xi_j\xi_i d\Omega,$

$$\Upsilon_{ij}^{22} = a_6 \int_\Omega \left[\left(\sum_{j=1}^{m} \widehat{U}_j \xi_j \right) \frac{\partial \xi_j}{\partial X} + \left(\sum_{j=1}^{m} \widehat{U}_j \xi_j \right) \frac{\partial \xi_j}{\partial Y} \right] d\Omega + a_9 \int_\Omega \xi_j\xi_i d\Omega$$
$$+ a_7 \int_\Omega \left(\frac{\partial \xi_j}{\partial X}\frac{\partial \xi_i}{\partial X} + \frac{\partial \xi_j}{\partial Y}\frac{\partial \xi_i}{\partial Y} \right) d\Omega + a_{10} \left[\sqrt{\left(\sum_{j=1}^{m} \widehat{U}_j \xi_j \right)^2 + \left(\sum_{j=1}^{m} \widehat{V}_j \xi_j \right)^2} \right]$$
$$\int_\Omega \xi_j\xi_i d\Omega,$$

$$\Upsilon_{ij}^{44} = \int_\Omega \left[\left(\sum_{j=1}^{m} \widehat{U}_j \xi_j \right) \frac{\partial \xi_j}{\partial X} + \left(\sum_{j=1}^{m} \widehat{V}_j \xi_j \right) \frac{\partial \xi_j}{\partial Y} \right] d\Omega$$
$$+ a_{11} \int_\Omega \left(\frac{\partial \xi_j}{\partial X}\frac{\partial \xi_i}{\partial X} + \frac{\partial \xi_j}{\partial Y}\frac{\partial \xi_i}{\partial Y} \right) d\Omega,$$

$$\Upsilon_{ij}^{14} = -a_3 \int_\Omega \xi_j\xi_i d\Omega, \qquad \Upsilon_{ij}^{24} = -a_8 \int_\Omega \xi_j\xi_i d\Omega,$$

$$\mathbf{B}_1 = -\int_\Omega \frac{\partial \xi_i}{\partial X}\eta_j d\Omega, \qquad \mathbf{B}_2 = -\int_\Omega \frac{\partial \xi_i}{\partial Y}\eta_j d\Omega,$$

$$\mathbf{B}_1^{\mathrm{T}} = \int_\Omega \frac{\partial \xi_j}{\partial X}\eta_i d\Omega, \qquad \mathbf{B}_2^{\mathrm{T}} = \int_\Omega \frac{\partial \xi_j}{\partial Y}\eta_i d\Omega.$$

$$\Upsilon_{ij}^{12} = \Upsilon_{ij}^{21} = \Upsilon_{ij}^{33} = \Upsilon_{ij}^{34} = \Upsilon_{ij}^{41} = \Upsilon_{ij}^{42} = \Upsilon_{ij}^{43} = 0.$$

The system in Eq. (3.22) is representing a nonlinear set of algebraic equations having Laplace with nonlinear term matrix entries in diagonal. The entries at Υ_{ij}^{14} and Υ_{ij}^{24} have mass matrices. This discretized system is linearized by using fixed point iterative scheme. Finally, the linear system is solved by Gaussian elimination method to get approximate solution.

Stopping Criteria

The convergence of fixed point iterative scheme is ensured by selecting the tolerance value of dependent variables by using following stopping criterion.

$$\left| \frac{\bigoplus^{k+1} - \bigoplus^{k}}{\bigoplus^{k+1}} \right| \leq 10^{-6},$$

where the "$\bigoplus$" is for dependent variables $\widehat{U}$, $\widehat{V}$, $\widehat{P}$ and $\widehat{\theta}$ while "k" is showing the number of on going iteration.

3.5.3 Mesh Refinement

Mesh refinement in FEM is mostly applied to find the accurate solutions. In this process the existing elements are further divided which increases the number of local elements. **Fig.** 3.2 shows the grid collaboration for levels $l = 1, 2$ and 3. The coarsest level is designed by taking 9 elements at $l = 1$. Further refinement for level $(l + 1)$ is achieved by joining the midpoints of opposite faces of each elements into four more elements.

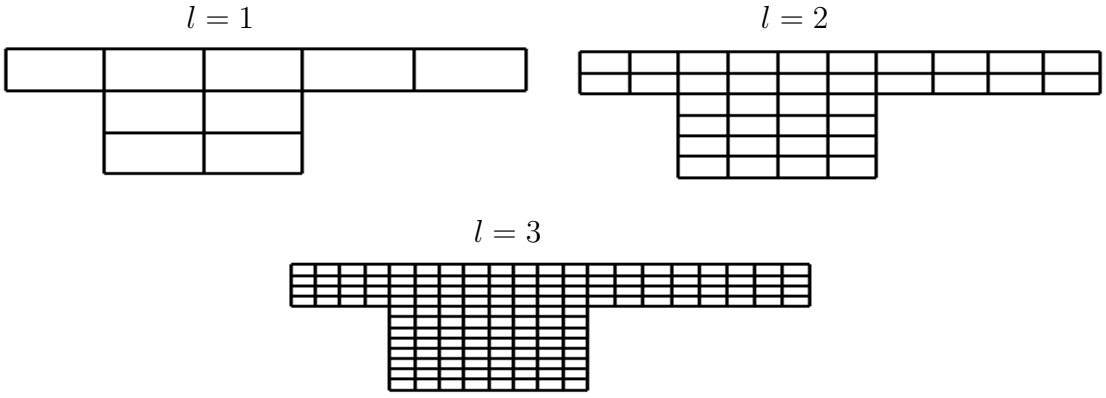

Figure 3.2: Spatial grid design for mesh levels $l = 1, 2$ and 3

3.5.4 Code Validation

The code validity of proposed problem is tested for the assisting forced flow, opposing forced flow and horizontal forced flow. The independency of solution is accomplished by studying the maximum temperature transfer (θ_{max}) at $0.01 \leq Ri \leq 100$ for forced, natural and mixed convective flow regimes. The comparison of θ_{max} values for the present study with those in referenced literature is given in **Table** 3.3. The results have shown a good verification to those in literature [19, 21, 22, 73].

Assisting forced flow

Ri	Hussain et al. [43]	[19]	[22]	[73]
0.01	0.57623	0.576	0.575	0.577
0.1	0.54379	0.544	0.549	0.545
1	0.42042	0.42	0.426	0.422
10	0.30294	0.303	0.306	0.305
100	0.20985	0.209	-	0.211

Opposing forced flow

Ri	Hussain et al. [43]	[19]
0.01	0.62331	-
0.1	0.62633	0.627
1	0.61660	0.617
10	0.23757	0.237
100	0.13155	0.132

Horizontal forced flow

Ri	Hussain et al. [43]	[19]	[21]
0.01	1.09456	-	-
0.1	1.06117	1.06	1.07
1	0.85609	0.856	0.871
10	0.61370	0.613	0.620
100	0.43698	0.437	-

Table 3.3: The comparison of θ_{max} (present study) to references [19, 21, 22, 73].

3.5.5 Grid Independence Test

The mesh convergence test is conducted in this section to check the refinement of grids. For this purpose the average Nusselt number is calculated for $Re = 100$, $Ri = 1$, $Da = 0.001$, $\gamma = 0°$ and $Pr = 6.2$. The outputs are recorded for levels $l = 1$ to 6 with the respective #DOFs and #EL for the velocity, pressure and temperature components. The compared results are shown below in **Table** 3.4.

Level	#EL	#DOFs	Nu_{avg}
1	9	186	1.484620639
2	36	639	2.446421253
3	144	2355	4.672907931
4	576	9027	7.676610502
5	2304	35,331	9.603780045
6	9216	139,779	10.25456938

Table 3.4: Grid independence test of present study.

3.6 Result Discussion

In this section the numerical results for mixed convective flow in an inclined channel with cavity with alumina-water nanofluid in porous medium are presented. The channel has a heating source at the left wall of cavity. The channel is tilting at different angles γ. To analyze flow behaviour for heat transport, different physical parameters are manipulated which include Reynolds number ($10 \leq Re \leq 200$), Richardson number ($0.01 \leq Ri \leq 10$), porosity ($0.2 \leq \epsilon \leq 0.8$) and inclination angle of cavity ($0^\circ \leq \gamma \leq 315^\circ$). Flow-velocity profiles are inspected in terms of streamline contours whereas flow-temperature distributions are visualized with the help of isothermal patterns. The average heat transport is determined by calculating average Nusselt number for governing parameters. The standard parameters for different nanofluid flow cases are taken as $Ri = 1$, $Re = 100$ $\gamma = 0^\circ$, $Da = 10^{-3}$, $\epsilon = 1$ and $\phi = 0.04$ at fixed Prandtl number, i.e., $Pr = 6.2$. Variation in quantities will be mentioned where needed. The graphical profiles for Nu_{avg} with Re, Ri, ϵ and γ are also expressed.

The behaviour of streamlines and isotherms with varying Reynolds number are investigated in **Fig**. 3.3. Initially for $Re = 10$, the flow enters into channel with low velocity due to evident viscous forces of fluid due to which weak flow movement is spotted for this small value of Re at the central cavity region. As Re varies

from 10 to 200, the intensity of flow seems stronger at the center of cavity. Visible expansion in streamline curves are inspected here. Actually increase in Re enhances the inlet velocity of flow as a result of which inertial forces of flow increases here. For the least value of Re, i.e., $Re = 10$ maximum number of isothermal lines are merged with the left heating wall. The expansion of thermal layers are found throughout the cavity which mainly seem to shift towards the outlet of channel. For greater values of Re, isothermal lines characterize the domination of shear forces due to which more adjacent heat layers are observed at the bottom boundary and towards the right wall of cavity. This assures the presence of heat layers at the bottom side and to the right corner of cavity. Hence maximum convective heat transfer is observed for greater values of Re.

Different modes of convection and their impacts on flow are investigated in terms of Richardson number in **Fig**. 3.4. Low Richardson number is responsible for forced convection. Shear forced-driven flow at $Ri = 0.01$ is responsible for weak inlet velocity, therefore maximum flow moves towards the outlet side of channel without moving into cavity. Hence a weak flow circulation is seen inside the cavity region. For mixed convective flow at $Ri = 1$, when the buoyancy forces and shear forces participate equally, a prominent flow activity is formed in cavity region as well as in channel region. Streamline curves are uniformly moving from the upper channel to the middle of cavity. As Ri increases from 0.01 to 10, free convection dominates and buoyancy forces become stronger than shear forces. Streamlines shift towards right wall of cavity. Hence a vivid flow circulation is seen inside cavity. Bulk of thermal layers are seen at the left and bottom wall of cavity region for $Ri = 0.01$ and $Ri = 1$. Here the shear force of fluid seems to compete for this thermal layer activity. As Richardson number increases up to $Ri = 10$, strong heat layers in the form of isotherms start shifting towards the right corner of cavity and outlet of channel due to high buoyancy force effects.

Fig. 3.5 interprets the effects of Darcy number on heat transport process by analyzing the flow streamlines and isotherms of heat. Darcy number is directly proportional to the permeability of porous medium. This implies that increasing

Darcy number produces increasing permeability of porous medium. Such situation favours more nanofluid to soak inside porous layers. Drag forces of porous matrix are responsible for greater internal resistance among fluid layers at low Darcy number, i.e., $Da = 10^{-6}$. It slows down the flow-velocity profiles inside the cavity region. More streamlines are present in the upper horizontal channel and few curves are detected closer to the left side of cavity for initial values of Da. As Darcy number ascends, the more permeability allows the streamlines to shift towards right region in cavity. For higher value, i.e., $Da = 10^{-3}$ greater permeability invokes less resistance between fluid layers which enhances the strength of flow inside open cavity. Similarly for higher values of Da, isotherms seem more restricted with the left heating wall of cavity. As the permeability strengthen for greater values of Da, the isothermal patterns and fluid layers are becoming closer to the bottom boundary of cavity. It leads to the presence of intense heat level in the bottom region of cavity due to weak strength of medium resistive forces.

The impact of porosity on heat transfer are represented by isothermal patterns and streamline contours in **Fig**. 3.6. For $\epsilon = 0.2$, which is taken as the lowest value of porosity, the streamlines illustrate that the most of the flow movement is confined to the upper channel from inlet side to outlet region. Due to which a weak flow movement is seen in the central region of cavity. Porosity is related to the presence of voids in porous matrix. Increasing porosity means greater number of voids (free spaces) which provides more space to absorb nanofluid into the porous layers. At $\epsilon = 0.8$, i.e., at higher value of porosity, a strong flow rotation is seen in the center of cavity. Isothermal patterns also constricted to the left wall of the cavity with high temperature for $\epsilon = 0.2$ which is gradually shifted towards the right wall as porosity approaches to $\epsilon = 0.8$. All these conclusions portray that the growth in voids of medium increases the temperature gradients and hence a visible convective heat transfer is observed at greater porosity.

Significant aspects of inclined channel in temperature distribution can be distinctly observed in the form of streamlines and isotherms in **Fig**. 3.7. The channel with no inclination at $\gamma = 0°$, a weak flow circulation is noticed in cavity as compared to the channel. For growing values of γ, a gradual strength in flow's movement

is seemed in cavity region which becomes maximum as γ ascends up to the value $\gamma = 135°$. For the values greater than $\gamma = 135°$, less flow lines are seen in cavity region and hence less convective heat transfer is noticed. At $\gamma = 0°$ the isotherms are more adjacent to the left heated wall of cavity. For the growth in inclination angles from $0°$ to $135°$, visible increments in temperature gradients are observed for maximum heat transfer. For angles greater than $\gamma = 135°$ weak convective heat transfer is happened. It is concluded that variations of certain values of γ give variations in buoyancy forces which intensify the thermal energy transport process.

The progress of average Nusselt number at different values of Reynolds and Richardson numbers are presented for pure fluid and nanofluid in **Fig.** 3.8. For two different values of nanoparticles volume fraction, i.e., $\phi = 0, 0.04$ a pronounced effect on average Nusselt number with increasing Re is shown in **Fig**. 3.8 (a). A maximum heat transfer is noticed for $Re = 100$ and $Re = 200$ at $\phi = 0$ and 0.04. Amplified convection is notable for nanofluid case because of the least influence of viscous forces. Opposite results are shown in **Fig**. 3.8 (b) for the incremented values of Ri at $\phi = 0, 0.04$. For higher value of $Ri = 10$ at $\phi = 0.04$, the domination of buoyancy forces is observed which gives least values of average Nu. Hence a less average heat transfer activity is seen in graph for high value of Ri.

The resluts for the influence of cavity inclination angles and porosity are displayed in **Fig**. 3.9. In **Fig**. 3.9(a) the maximum value of average Nu is noticed for $\gamma = 135°$. After cavity inclination $\gamma = 135°$, a gradual decrease in average Nu is observed. Plots for pure fluid ($\phi = 0$) and nanofluid ($\phi = 0.04$) in **Fig**. 3.9(a) show almost same trend for average heat transfer but a clear enhancement for average Nu is noticed for increased volume concentration $\phi = 0.04$ at $\gamma = 135°$. The increase in average Nu due to porosity is shown in **Fig**. 3.9(b). The consequences on ϵ for different values of ϕ depicts that maximum value of average Nu is recorded for $\phi = 0.04$ at $\epsilon = 0.8$. Hence augmentation in average convective heat transfer is discovered for higher value of porosity at $\phi = 0.04$.

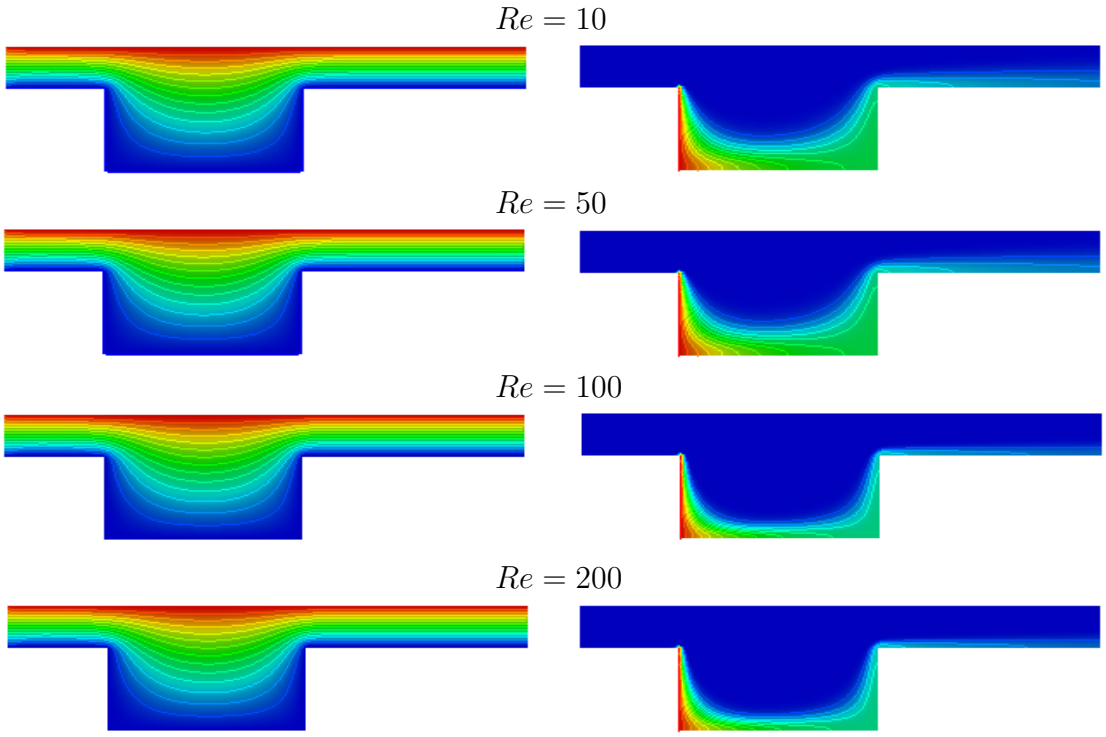

Figure 3.3: Depiction of isothermal pattern (Right) and streamline contours (Left) with rising Re.

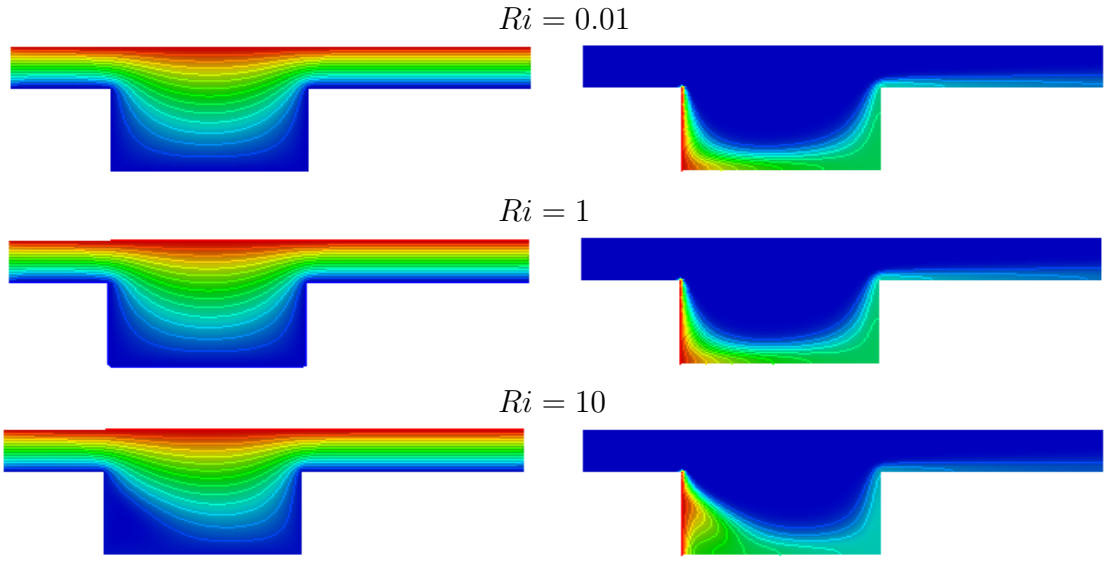

Figure 3.4: Depiction of isothermal pattern (Right) and streamline contours (Left) with rising Ri.

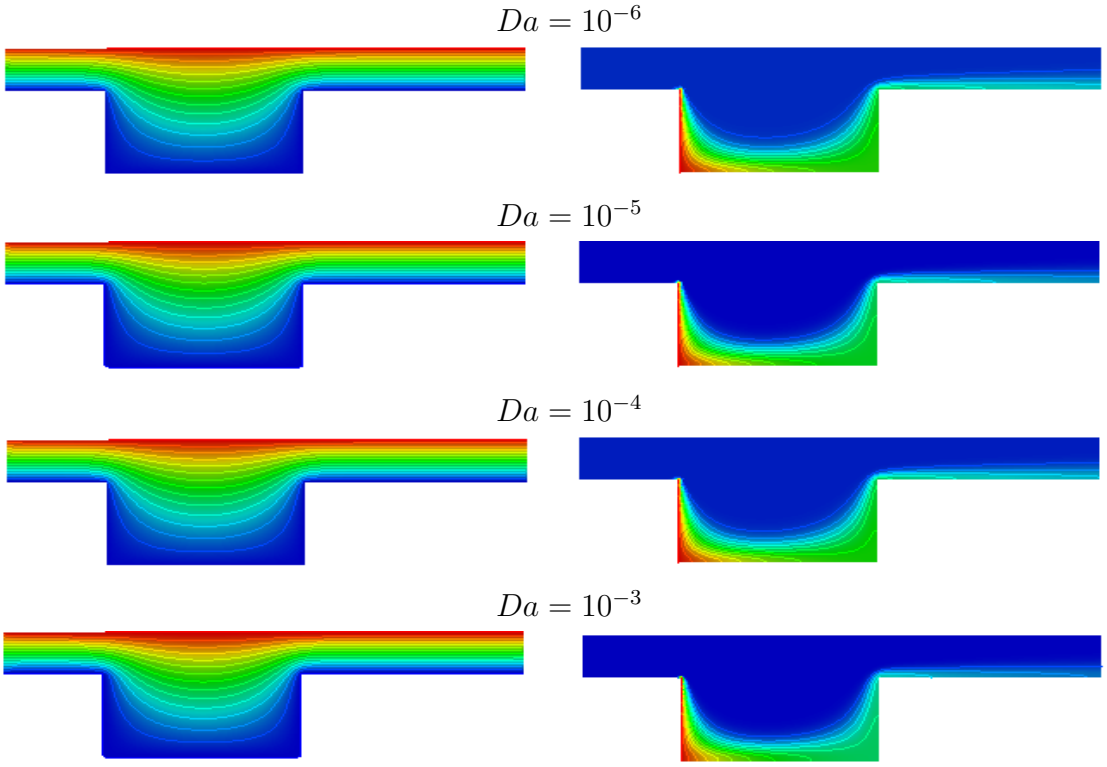

Figure 3.5: Depiction of isothermal pattern (Right) and streamline contours (Left) with rising Da.

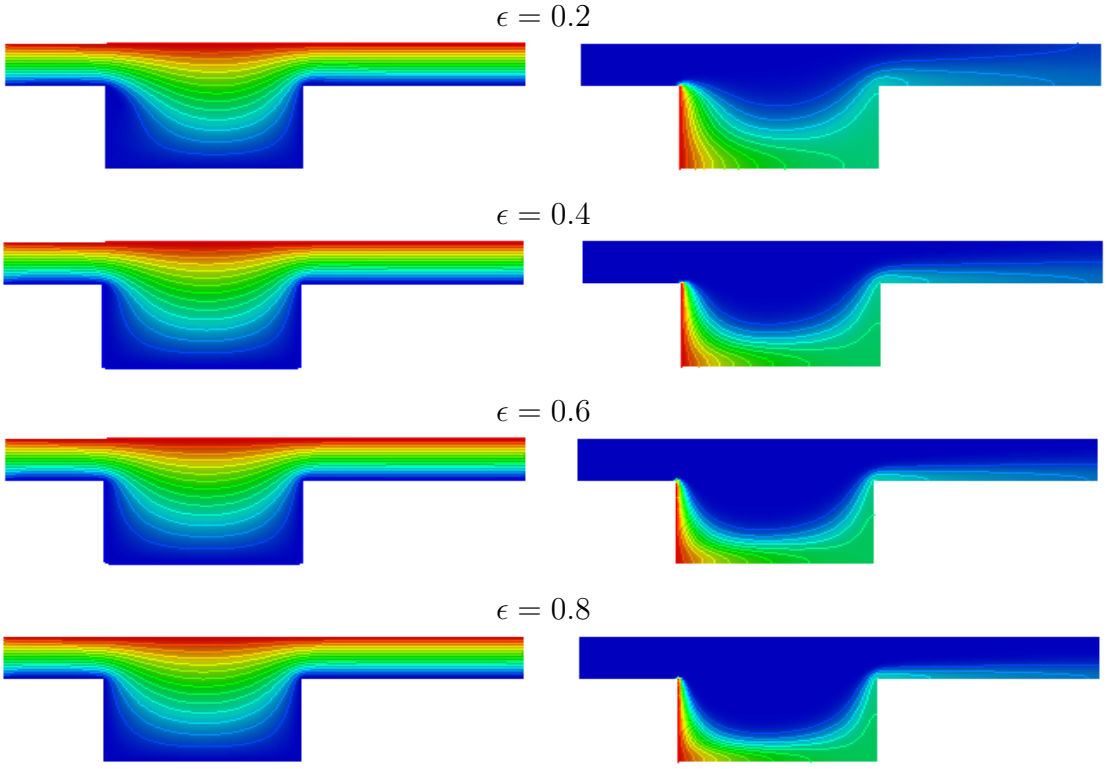

Figure 3.6: Depiction of isothermal pattern (Right) and streamline contours (Left) with rising ϵ.

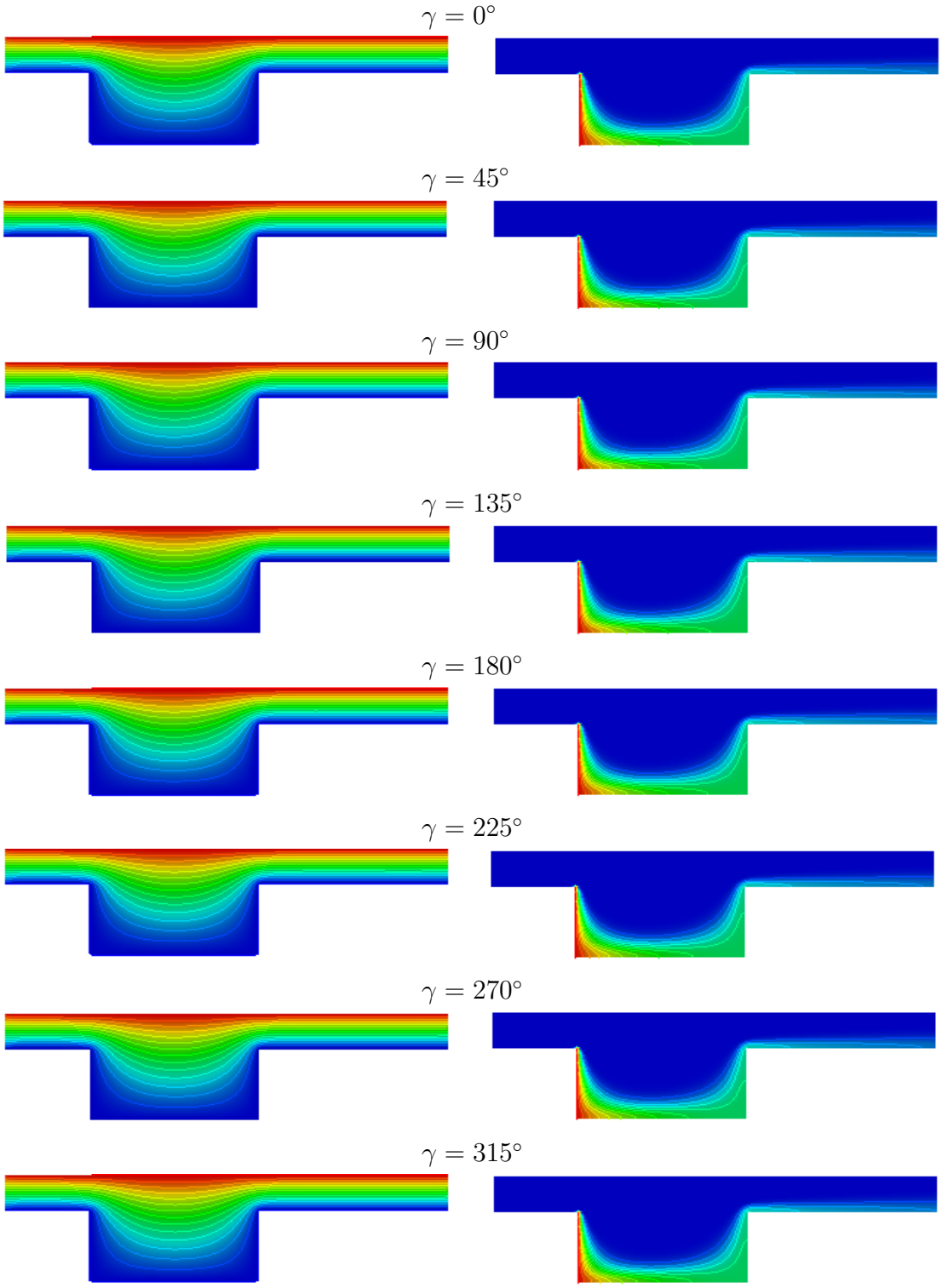

Figure 3.7: Depiction of isothermal pattern (Right) and streamline contours (Left) for channel orientations $\gamma°$.

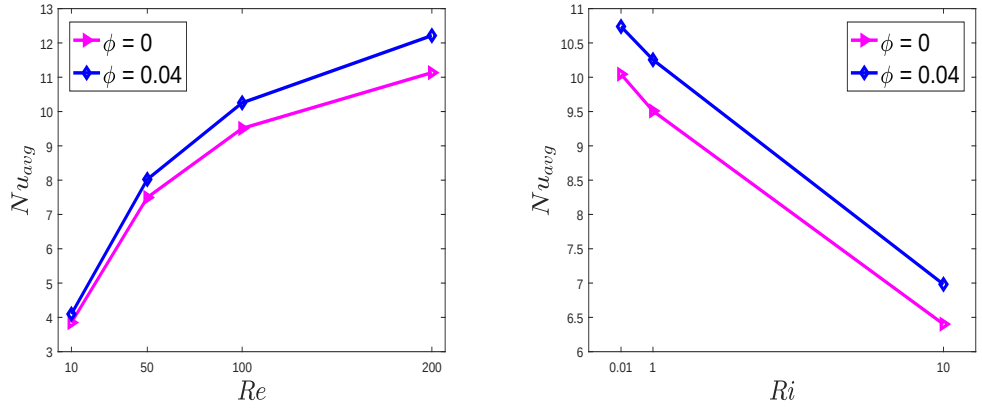

(a) (b)

Figure 3.8: Progress in Nu_{avg} on different Reynolds numbers (a) and Richardson numbers (b) for pure fluid and nanofluid.

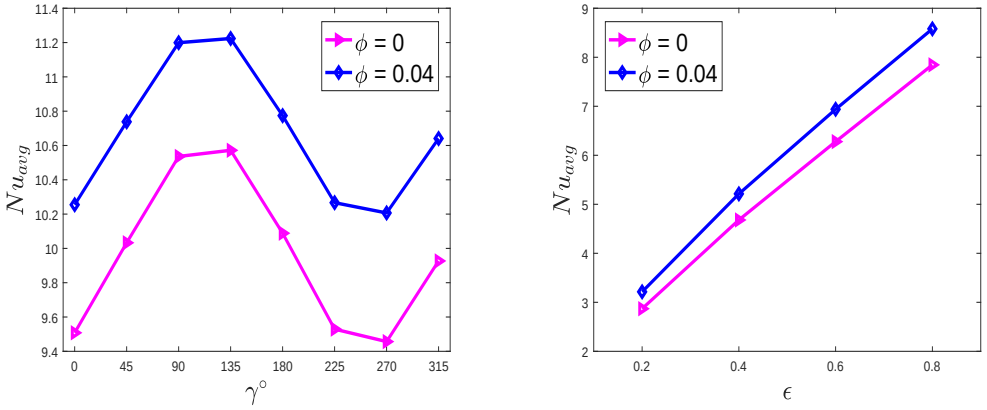

(a) (b)

Figure 3.9: Progress in Nu_{avg} at different cavity inclinations (a) and porosity (b) for pure fluid and nanofluid.

Chapter 4

Study of Magnetic Field Inclination and Joule Heating Effects on Mixed Convective Nanofluid Flow Problem

To control the fluid properties of interest is a challenging field in fluid mechanics. The use of magnetic field of moderate strength in this regard is contemporarily studied by the researchers since last many decades. Many electrically conducting fluids like plasma, liquid metals, salt water and electrolytes are studied in MHD field for effective heat transport purposes. The evident role of inclined magnetic field on fluid's domain produces a more managed and controlled convective heat transfer mechanism.

The main objective of this chapter is to extend the work presented by Hussain et al. [43] by introducing the inclined magnetic field and Joule heating effects in examining the thermal properties and flow behaviour of alumina-water nanofluid numerically. Numerical simulations have been performed by weighted residual GFEM. The pragmatic illustration of flow behaviour is elaborated in the form of streamlines and isothermal patterns.

4.1 Physical Interpretation of Problem

The schematic diagram of the proposed problem by considering the effects of magnetic field inclination and Joule heating on mixed convective nanofluid flow is presented in **Fig**. 4.1. A steady two-dimensional flow of alumina-water is considered in an open channel with cavity of dimensions H and $L = 2H$. The whole channel is inclined in counterclockwise direction at an angle γ. Channel is entirely embedded with porous medium for which Darcy-Brinkman-Forchheimer model is applied. MHD effects are added here by influencing an external uniform magnetic field of strength **B**. The magnetic field is also inclining in counterclockwise direction with angle ψ. The nanofluid inside the cavity is steady, laminar, incompressible and Newtonian. The inlet flow is at temperature T_c moving with uniform velocity u_0. The associated dimensions for channel are l and w while the height of inlet is taken as $\frac{H}{2}$. The left wall of cavity is at temperature T_h while remaining walls are kept thermally adiabatic. Another important assumption is that nanofluid and porous medium are in thermal equilibrium.

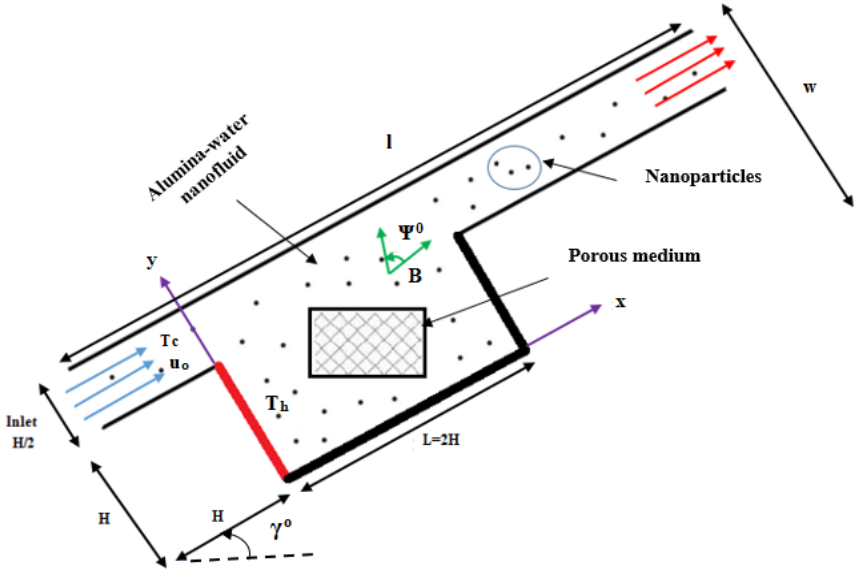

Figure 4.1: Schemed model of proposed problem.

The nanoparticles and base fluid are non-reactive to each other. Effects of Joule

heating are considered to investigate thermal power loses. The other heat dissipation effects like viscous dissipation by stresses and dissipation due to porous medium are ignored. Boussinesq approximation is used to analyze the influence of natural convection due to density variations in buoyancy force term.

4.2 Dimensional Governing Equations

In the light of above mentioned situation, the dimensional formulation of the steady, incompressible and Newtonian PDEs with Lorentz force effects are mentioned in this section. The system of dimensional PDEs comprises of mass, momentum and energy conservation equations. The strength of Lorentz force $\mathbf{F}$ is taken as $\mathbf{F} = \sigma\left(\tilde{V} \times \mathbf{B}\right) \times \mathbf{B}$. Here $\mathbf{B} = (\mathbf{B_x}, \mathbf{B_y})$ is external uniform magnetic field with magnitude B_0 and σ is termed as electrical conductivity of nanoparticles. Influence of Joule heating due to the presence of magnetic field effects in term of rate of work done in heat loss, i.e., $\dot{W} = \mathbf{F}.\tilde{V}$ is introduced in energy equation to measure the resistive heat production by nanoparticles.

Continuity Equation:

$$\frac{\partial \tilde{u}}{\partial x} + \frac{\partial \tilde{v}}{\partial y} = 0, \tag{4.1}$$

x-Component of Momentum Equation:

$$\begin{aligned}\frac{\rho_{nf}}{\epsilon^2}\left(\tilde{u}\frac{\partial \tilde{u}}{\partial x} + \tilde{v}\frac{\partial \tilde{u}}{\partial y}\right) = &-\frac{\partial p}{\partial x} + \frac{\mu_f}{\epsilon(1-\phi)^{2.5}}\left(\frac{\partial^2 \tilde{u}}{\partial x^2} + \frac{\partial^2 \tilde{u}}{\partial y^2}\right) \\ &+ (\beta\rho)_{nf}\, g\,(T - T_c)\sin\gamma - \frac{\mu_{nf}}{K}\tilde{u} \\ &- \frac{1.75\rho_{nf}}{\sqrt{150K}\epsilon^{3/2}}\left(\sqrt{\tilde{u}^2 + \tilde{v}^2}\right)\tilde{u} \\ &+ \sigma_{nf} B_0^2\left(\tilde{v}\sin\psi\cos\psi - \tilde{u}\sin^2\psi\right),\end{aligned} \tag{4.2}$$

y-Component of Momentum Equation:

$$\begin{aligned}\frac{\rho_{nf}}{\epsilon^2}\left(\tilde{u}\frac{\partial\tilde{v}}{\partial x}+\tilde{v}\frac{\partial\tilde{v}}{\partial y}\right) &= -\frac{\partial p}{\partial y}+\frac{\mu_f}{\epsilon(1-\phi)^{2.5}}\left(\frac{\partial^2\tilde{v}}{\partial x^2}+\frac{\partial^2\tilde{v}}{\partial y^2}\right)\\ &\quad+(\beta\rho)_{nf}\,g\,(T-T_c)\cos\gamma-\frac{\mu_{nf}}{K}\tilde{v}\\ &\quad-\frac{1.75\rho_{nf}}{\sqrt{150K}\epsilon^{3/2}}\left(\sqrt{\tilde{u}^2+\tilde{v}^2}\right)\tilde{v}\\ &\quad+\sigma_{nf}B_0^2\left(\tilde{u}\sin\psi\cos\psi-\tilde{v}\cos^2\psi\right), \qquad (4.3)\end{aligned}$$

Energy Equation:

$$\begin{aligned}\tilde{u}\frac{\partial T}{\partial x}+\tilde{v}\frac{\partial T}{\partial y} &= \alpha_{nf}\left(\frac{\kappa_m}{\kappa_{nf}}\right)\left(\frac{\partial^2 T}{\partial x^2}+\frac{\partial^2 T}{\partial y^2}\right)\\ &\quad+\frac{\sigma_{nf}B_0^2}{(\rho C_\rho)_{nf}}\left(\tilde{u}\sin\psi-\tilde{v}\cos\psi\right)^2. \qquad (4.4)\end{aligned}$$

The following conditions on boundaries are enforced for the schemed problem.

- On the inlet side of channel:

$$\tilde{u}(x,y)=u_0, \qquad \tilde{v}(x,y)=0, \qquad T=T_c.$$

- On left wall of cavity:

$$\tilde{u}(x,y)=0, \qquad \tilde{v}(x,y)=0, \qquad T=T_h.$$

- On the horizontal adiabatic walls of channel and cavity:

$$\tilde{u}(x,y)=0, \qquad \tilde{v}(x,y)=0, \qquad \frac{\partial T}{\partial y}=0.$$

- On the vertical adiabatic walls of channel and cavity:

$$\tilde{u}(x,y)=0, \qquad \tilde{v}(x,y)=0, \qquad \frac{\partial T}{\partial x}=0.$$

- On the outlet side of channel:

$$\frac{\partial \tilde{u}}{\partial x} = 0, \qquad \frac{\partial \tilde{v}}{\partial y} = 0, \qquad \frac{\partial T}{\partial x} = 0.$$

4.3 Dimensionless Governing Equations

Dimensionless analysis of the designed problem is accomplished by using the following physical relations:

$$X = \frac{x}{H}, \quad Y = \frac{y}{H}, \quad \widehat{U} = \frac{\tilde{u}}{u_0}, \quad \widehat{V} = \frac{\tilde{v}}{u_0}, \quad \widehat{\theta} = \frac{T - T_c}{T_h - T_c}, \quad \widehat{P} = \frac{p}{\rho_{nf} {u_0}^2},$$

$$Re = \frac{u_0 H}{\nu_f}, \quad Da = \frac{K}{H^2}, \quad Pr = \frac{\nu_f}{\alpha_f}, \quad Ri = \frac{Gr}{Re^2}, \quad Gr = \frac{g\beta_f \Delta T H^3}{\nu_f^2},$$

$$Ha = B_0 H \sqrt{\frac{\sigma_f}{\mu_f}}, \quad Ec = \frac{u_0^2}{(C_\rho)_f (T_h - T_c)}.$$

After applying the above mentioned relations the set of equations from Eqs. (4.1) to (4.4) can be transformed as follows:

Continuity Equation:

$$\frac{\partial \widehat{U}}{\partial X} + \frac{\partial \widehat{V}}{\partial Y} = 0, \tag{4.5}$$

x-Component of Momentum Equation:

$$\begin{aligned} \frac{1}{\epsilon^2}\left(\widehat{U}\frac{\partial \widehat{U}}{\partial X} + \widehat{V}\frac{\partial \widehat{U}}{\partial Y}\right) = &-\frac{\partial \widehat{P}}{\partial X} + \frac{1}{\epsilon Re}\frac{\rho_f}{\rho_{nf}}\frac{1}{(1-\phi)^{2.5}}\left(\frac{\partial^2 \widehat{U}}{\partial X^2} + \frac{\partial^2 \widehat{U}}{\partial Y^2}\right) \\ &+ Ri\frac{\rho_f}{\rho_{nf}}\left((1-\phi) + \phi\frac{\rho_p \beta_p}{\rho_f \beta_f}\right)\sin\gamma\,\widehat{\theta} \\ &- \frac{\mu_{nf}}{\rho_{nf}\nu_f}\frac{1}{ReDa}\widehat{U} - \frac{1.75}{\sqrt{150Da}\epsilon^{3/2}}\left(\sqrt{\widehat{U}^2 + \widehat{V}^2}\right)\widehat{U} \\ &+ \frac{\sigma_{nf}}{\sigma_f}\frac{\rho_f}{\rho_{nf}}\frac{Ha^2}{Re}\left(\widehat{V}\sin\psi\cos\psi - \widehat{U}\sin^2\psi\right), \end{aligned} \tag{4.6}$$

y-Component of Momentum Equation:

$$\frac{1}{\epsilon^2}\left(\widehat{U}\frac{\partial\widehat{V}}{\partial X}+\widehat{V}\frac{\partial\widehat{V}}{\partial Y}\right)=-\frac{\partial\widehat{P}}{\partial Y}+\frac{1}{\epsilon Re}\frac{\rho_f}{\rho_{nf}}\frac{1}{(1-\phi)^{2.5}}\left(\frac{\partial^2\widehat{V}}{\partial X^2}+\frac{\partial^2\widehat{V}}{\partial Y^2}\right)$$
$$+Ri\frac{\rho_f}{\rho_{nf}}\left((1-\phi)+\phi\frac{\rho_p\beta_p}{\rho_f\beta_f}\right)\cos\gamma\,\widehat{\theta}$$
$$-\frac{\mu_{nf}}{\rho_{nf}\nu_f}\frac{1}{ReDa}\widehat{V}-\frac{1.75}{\sqrt{150Da}\epsilon^{3/2}}\left(\sqrt{\widehat{U}^2+\widehat{V}^2}\right)\widehat{V}$$
$$+\frac{\sigma_{nf}}{\sigma_f}\frac{\rho_f}{\rho_{nf}}\frac{Ha^2}{Re}\left(\widehat{U}\sin\psi\cos\psi-\widehat{V}\cos^2\psi\right), \tag{4.7}$$

Energy Equation:

$$\widehat{U}\frac{\partial\widehat{\theta}}{\partial X}+\widehat{V}\frac{\partial\widehat{\theta}}{\partial Y}=\frac{1}{RePr}\frac{\alpha_{nf}}{\alpha_f}\frac{\kappa_m}{\kappa_{nf}}\left(\frac{\partial^2\widehat{\theta}}{\partial X^2}+\frac{\partial^2\widehat{\theta}}{\partial Y^2}\right)$$
$$+\frac{\sigma_{nf}}{\sigma_f}\frac{(\rho C_\rho)_f}{(\rho C_\rho)_{nf}}\frac{Ha^2}{Re}Ec\left(\widehat{U}\sin\psi-\widehat{V}\cos\psi\right)^2. \tag{4.8}$$

The corresponding boundary conditions for non-dimensional equations are given below:

- On the inlet side of channel:

$$\widehat{U}=1,\qquad \widehat{V}=0,\qquad \widehat{\theta}=0.$$

- On left wall of cavity:

$$\widehat{U}=0,\qquad \widehat{V}=0,\qquad \widehat{\theta}=1.$$

- On the horizontal adiabatic walls of channel and cavity:

$$\widehat{U}=0,\qquad \widehat{V}=0,\qquad \frac{\partial\widehat{\theta}}{\partial Y}=0.$$

- On the vertical adiabatic walls of channel and cavity:

$$\widehat{U}=0,\qquad \widehat{V}=0,\qquad \frac{\partial\widehat{\theta}}{\partial X}=0.$$

- On the outlet side of channel:

$$\frac{\partial \widehat{U}}{\partial X} = 0, \qquad \frac{\partial \widehat{V}}{\partial Y} = 0, \qquad \frac{\partial \widehat{\theta}}{\partial X} = 0.$$

Physical Quantities for Heat Transport

The analysis of heat transport mechanism is performed in terms of Nusselt number as mentioned in **Chapter** 3. Dimensionless Nu_{L} (local Nusselt number) is given by

$$Nu_{\mathrm{L}} = -\frac{\kappa_{nf}}{\kappa_f} \left| \left(\frac{\partial \widehat{\theta}}{\partial X} \right) \right|_{X=0},$$

Nu_{avg} over left heated wall can be computed as

$$Nu_{\mathrm{avg}} = \int_0^c Nu \, dY,$$

where c is the length of the enclosure's heated wall.

4.4 Solution Procedure

The system of nonlinear coupled PDEs from (4.5) to (4.8) is numerically solved by weighted residual based GFEM. Main steps for the solution methodology are further discussed below:

4.4.1 Strong Form of Governing PDEs

The set of differential equations from (4.5) to (4.8) with associated boundary conditions are known as the strong form of governing PDEs. This formulation can

be re-written as

$$a_1\left(\widehat{U}\frac{\partial\widehat{U}}{\partial X}+\widehat{V}\frac{\partial\widehat{U}}{\partial Y}\right)=-\frac{\partial\widehat{P}}{\partial X}+a_2\left(\frac{\partial^2\widehat{U}}{\partial X^2}+\frac{\partial^2\widehat{U}}{\partial Y^2}\right)+a_3\widehat{\theta}$$
$$-a_4\widehat{U}-a_5\widehat{U}+a_6\widehat{V}-a_7\widehat{U}, \tag{4.9}$$

$$a_8\left(\widehat{U}\frac{\partial\widehat{V}}{\partial X}+\widehat{V}\frac{\partial\widehat{V}}{\partial Y}\right)=-\frac{\partial\widehat{P}}{\partial Y}+a_9\left(\frac{\partial^2\widehat{V}}{\partial X^2}+\frac{\partial^2\widehat{V}}{\partial Y^2}\right)+a_{10}\widehat{\theta}$$
$$-a_{11}\widehat{V}-a_{12}\widehat{V}+a_{13}\widehat{U}-a_{14}\widehat{V}, \tag{4.10}$$

$$\frac{\partial\widehat{U}}{\partial X}+\frac{\partial\widehat{V}}{\partial Y}=0, \tag{4.11}$$

$$\widehat{U}\frac{\partial\widehat{\theta}}{\partial X}+\widehat{V}\frac{\partial\widehat{\theta}}{\partial Y}=a_{15}\left(\frac{\partial^2\widehat{\theta}}{\partial X^2}+\frac{\partial^2\widehat{\theta}}{\partial Y^2}\right)+J^*\left(\widehat{U}\sin\psi-\widehat{V}\cos\psi\right). \tag{4.12}$$

In the set of above equations the values of a's are written below:

$a_1=a_8=\frac{1}{\epsilon^2}$, $a_2=a_9=\frac{1}{\epsilon Re}\frac{\rho_f}{\rho_{nf}}\frac{1}{(1-\phi)^{2.5}}$,

$a_3=Ri\frac{\rho_f}{\rho_{nf}}\left((1-\phi)+\phi\frac{\rho_p\beta_p}{\rho_f\beta_f}\right)\sin\gamma$, $a_4=a_{11}=\frac{\mu_{nf}}{\rho_{nf}\nu_f}\frac{1}{ReDa}$,

$a_5=a_{12}=\frac{1.75}{\sqrt{150Da}\epsilon^{3/2}}\left(\sqrt{\widehat{U}^2+\widehat{V}^2}\right)$, $a_6=a_{13}=\frac{\sigma_{nf}}{\sigma_f}\frac{\rho_f}{\rho_{nf}}\frac{Ha^2}{Re}\sin\psi\cos\psi$,

$a_7=\frac{\sigma_{nf}}{\sigma_f}\frac{\rho_f}{\rho_{nf}}\frac{Ha^2}{Re}\sin^2\psi$, $a_{10}=Ri\frac{\rho_f}{\rho_{nf}}\left((1-\phi)+\phi\frac{\rho_p\beta_p}{\rho_f\beta_f}\right)\cos\gamma$,

$a_{14}=\frac{\sigma_{nf}}{\sigma_f}\frac{\rho_f}{\rho_{nf}}\frac{Ha^2}{Re}\cos^2\psi$, $a_{15}=\frac{1}{RePr}\frac{\alpha_{nf}}{\alpha_f}\frac{\kappa_m}{\kappa_{nf}}$,

$a_{16}=\frac{\sigma_{nf}}{\sigma_f}\frac{(\rho C_\rho)_f}{(\rho C_\rho)_{nf}}\frac{Ha^2}{Re}Ec$, $J^*=a_{16}\left(\widehat{U}\sin\psi-\widehat{V}\cos\psi\right)$.

4.4.2 Weak Formulation

For the achievement of numerical solution by using FEM, it is desirable to convert the PDEs from (4.9) to (4.12) into integral form to get the approximate solution. For this purpose, first we introduce test spaces ($\mathbf{W}$, Q) having infinite dimensions. Let $\widehat{U}$, $\widehat{V}$, $\widehat{P}$ and $\widehat{\theta}$ are the solution for both velocity components, pressure and

temerature fields. It is convenient to take $\mathbf{W} = [H_1(\Omega)]^3$ as test spaces for $\widehat{U}$-velocity, $\widehat{V}$-velocity and temperature components whereas $Q = L_2(\Omega)$ represents the test space for pressure field. Variational form is obtained by selecting test functions of type $\hat{w}\ \varepsilon\ \mathbf{W}$ and $\hat{q}\ \varepsilon\ Q$. Multiply the both momentum and energy equations with test functions $\hat{w}$ and similarly continuity equation with $\hat{q}$.
Find $(\widehat{U},\widehat{V},\widehat{\theta},\widehat{P})\ \varepsilon\ (\mathbf{W} \times Q)$ such that

$$a_1 \int_\Omega \left(\widehat{U}\frac{\partial \widehat{U}}{\partial X} + \widehat{V}\frac{\partial \widehat{U}}{\partial Y}\right)\hat{w}d\Omega - \int_\Omega \frac{\partial \widehat{P}}{\partial X}\hat{w}d\Omega + a_2 \int_\Omega \left(\frac{\partial^2 \widehat{U}}{\partial X^2} + \frac{\partial^2 \widehat{U}}{\partial Y^2}\right)\hat{w}d\Omega$$
$$- a_3 \int_\Omega \widehat{\theta}\hat{w}d\Omega + a_4 \int_\Omega \widehat{U}\hat{w}d\Omega + a_5 \int_\Omega \widehat{U}\hat{w}d\Omega - a_6 \int_\Omega \widehat{V}\hat{w}d\Omega$$
$$+ a_7 \int_\Omega \widehat{U}\hat{w}d\Omega = 0, \tag{4.13}$$

$$a_8 \int_\Omega \left(\widehat{U}\frac{\partial \widehat{V}}{\partial X} + \widehat{V}\frac{\partial \widehat{V}}{\partial Y}\right)\hat{w}d\Omega - \int_\Omega \frac{\partial \widehat{P}}{\partial Y}\hat{w}d\Omega - a_9 \int_\Omega \left(\frac{\partial^2 \widehat{V}}{\partial X^2} + \frac{\partial^2 \widehat{V}}{\partial Y^2}\right)\hat{w}d\Omega$$
$$- a_{10} \int_\Omega \widehat{\theta}\hat{w}d\Omega + a_{11} \int_\Omega \widehat{V}\hat{w}d\Omega + a_{12} \int_\Omega \widehat{V}\hat{w}d\Omega - a_{13} \int_\Omega \widehat{U}\hat{w}d\Omega$$
$$+ a_{14} \int_\Omega \widehat{V}\hat{w}d\Omega = 0, \tag{4.14}$$

$$\int_\Omega \left(\frac{\partial \widehat{U}}{\partial X} + \frac{\partial \widehat{V}}{\partial Y}\right)\hat{q}d\Omega = 0, \tag{4.15}$$

$$\int_\Omega \left(\widehat{U}\frac{\partial \widehat{\theta}}{\partial X} + \widehat{V}\frac{\partial \widehat{\theta}}{\partial Y}\right)\hat{w}d\Omega + a_{15} \int_\Omega \left(\frac{\partial^2 \widehat{\theta}}{\partial X^2} + \frac{\partial^2 \widehat{\theta}}{\partial Y^2}\right)\hat{w}d\Omega - J^* \sin\psi \int_\Omega \widehat{U}\hat{w}d\Omega$$
$$+ J^* \cos\psi \int_\Omega \widehat{V}\hat{w}d\Omega = 0, \tag{4.16}$$

for all $(\hat{w},\hat{q})\ \varepsilon\ (\mathbf{W} \times Q)$.
To obtain finite element equations, use Galerkin discretization to approximate infinite dimensional test and solution spaces to finite dimensional spaces. Let $(\widehat{U}_\hbar,\widehat{V}_\hbar,\widehat{P}_\hbar,\widehat{\theta}_\hbar) \approx (\widehat{U},\widehat{V},\widehat{P},\widehat{\theta})$ are the approximated solution components whereas $(\mathbf{W}_\hbar,\ Q_\hbar) \approx (\mathbf{W} \times Q)$ are the finite dimensional test spaces. Thus, the weak formulation of the problem at the discrete level reads the following:

Find $(\widehat{U}_\hbar,\widehat{V}_\hbar,\widehat{P}_\hbar,\widehat{\theta}_\hbar)\ \varepsilon\ (\mathbf{W}_\hbar,\ Q_\hbar)$ such that

$$a_1\int_\Omega\left(\widehat{U}_\hbar\frac{\partial\widehat{U}_\hbar}{\partial X}+\widehat{V}_\hbar\frac{\partial\widehat{U}_\hbar}{\partial Y}\right)\hat{w}_\hbar d\Omega \quad + \quad a_2\int_\Omega\left(\frac{\partial\widehat{U}_\hbar}{\partial X}\frac{\partial\hat{w}_\hbar}{\partial X}+\frac{\partial\widehat{U}_\hbar}{\partial Y}\frac{\partial\hat{w}_\hbar}{\partial Y}\right)d\Omega$$
$$-\int_\Omega\frac{\partial\widehat{P}_\hbar}{\partial X}\hat{w}_\hbar d\Omega \ - \ a_3\int_\Omega\widehat{\theta}_\hbar\hat{w}_\hbar d\Omega \ + \ a_4\int_\Omega\widehat{U}_\hbar\hat{w}_\hbar d\Omega \ + \ a_5\int_\Omega\widehat{U}_\hbar\hat{w}_\hbar d\Omega$$
$$-a_6\int_\Omega\widehat{V}_\hbar\hat{w}_\hbar d\Omega+a_7\int_\Omega\widehat{U}_\hbar\hat{w}_\hbar d\Omega=0, \tag{4.17}$$

$$a_8\int_\Omega\left(\widehat{U}_\hbar\frac{\partial\widehat{V}_\hbar}{\partial X}+\widehat{V}_\hbar\frac{\partial\widehat{V}_\hbar}{\partial Y}\right)\hat{w}_\hbar d\Omega \quad + \quad a_9\int_\Omega\left(\frac{\partial\widehat{V}_\hbar}{\partial X}\frac{\partial\hat{w}_\hbar}{\partial X}+\frac{\partial\widehat{V}_\hbar}{\partial Y}\frac{\partial\hat{w}_\hbar}{\partial Y}\right)d\Omega$$
$$-\int_\Omega\frac{\partial\widehat{P}_\hbar}{\partial Y}\hat{w}_\hbar d\Omega \ - \ a_{10}\int_\Omega\widehat{\theta}_\hbar\hat{w}_\hbar d\Omega \ + \ a_{11}\int_\Omega\widehat{V}_\hbar\hat{w}_\hbar d\Omega \ + \ a_{12}\int_\Omega\widehat{V}_\hbar\hat{w}_\hbar d\Omega$$
$$-a_{13}\int_\Omega\widehat{U}_\hbar\hat{w}_\hbar d\Omega+a_{14}\int_\Omega\widehat{V}_\hbar\hat{w}_\hbar d\Omega=0, \tag{4.18}$$

$$\int_\Omega\frac{\partial\widehat{U}_\hbar}{\partial X}\hat{q}_\hbar d\Omega+\frac{\partial\widehat{U}_\hbar}{\partial Y}\hat{q}_\hbar d\Omega=0, \tag{4.19}$$

$$\int_\Omega\left(\widehat{U}_\hbar\frac{\partial\widehat{\theta}_\hbar}{\partial X}+\widehat{V}_\hbar\frac{\partial\widehat{\theta}_\hbar}{\partial Y}\right)\hat{w}_\hbar d\Omega+a_{15}\int_\Omega\left(\frac{\partial\widehat{\theta}_\hbar}{\partial X}\frac{\partial\hat{w}_\hbar}{\partial X}+\frac{\partial\widehat{\theta}_\hbar}{\partial Y}\frac{\partial\hat{w}_\hbar}{\partial Y}\right)d\Omega$$
$$-J^*\sin\psi\int_\Omega\widehat{U}_\hbar\hat{w}_\hbar d\Omega+J^*\cos\psi\int_\Omega\widehat{V}_\hbar\hat{w}_\hbar d\Omega=0, \tag{4.20}$$

for all $(\hat{w}_\hbar,\hat{q}_\hbar)\ \varepsilon\ (\mathbf{W}_\hbar,\ Q_\hbar)$.

The finite element equations from (4.17) to (4.20) are approximated by using the following FEM approximated functions which are expressed as $\widehat{U}_\hbar=\sum_{j=1}^{m}\widehat{U}_j\xi_j$, $\widehat{V}_\hbar=\sum_{j=1}^{m}\widehat{V}_j\xi_j$, $\widehat{\theta}_\hbar=\sum_{j=1}^{m}\widehat{\theta}_j\xi_j$, and $\widehat{P}_\hbar=\sum_{j=1}^{l}\widehat{P}_j\eta_j$ which are trial functions for the corresponding solution spaces.

Similarly $\hat{w}_\hbar=\sum_{i=1}^{m}\hat{w}_i\xi_i$ and $\hat{q}_\hbar=\sum_{i=1}^{l}\hat{q}_i\eta_i$ are trial functions for the test spaces. In particular, the biquadratic Q_2-space is utilized to discretize the velocity and temperature components and discontinuous linear P_1^{disc}-finite element space is used for the pressure component under LBB-stability condition for finite element pair Q_2/P_1^{disc}. This condition leads to the third order accuracy of biquadratic Q_2-elements and second order accuracy of discontinous linear P_1^{disc}-elements in L_2-norm as discussed in **Chapter** 3.

Substitution of these approximations into Eqs. (4.17) to (4.20) leads to the following discrete system of nonlinear algebraic equations.

$$[A^*(\widehat{U},\widehat{V})]\{X^*\} = \{\bar{F}^*\}.$$

In matrix notation:

$$\underbrace{\begin{bmatrix} \Upsilon^{11} & \Upsilon^{12} & \mathbf{B}_1 & \Upsilon^{14} \\ \Upsilon^{21} & \Upsilon^{22} & \mathbf{B}_2 & \Upsilon^{24} \\ \mathbf{B}_1^{\mathrm{T}} & \mathbf{B}_2^{\mathrm{T}} & \Upsilon^{33} & \Upsilon^{34} \\ \Upsilon^{41} & \Upsilon^{42} & \Upsilon^{43} & \Upsilon^{44} \end{bmatrix}}_{A^*} \underbrace{\begin{bmatrix} \widehat{U} \\ \widehat{V} \\ \widehat{P} \\ \widehat{\theta} \end{bmatrix}}_{X^*} = \underbrace{\begin{bmatrix} \bar{F}^1 \\ \bar{F}^2 \\ \bar{F}^3 \\ \bar{F}^4 \end{bmatrix}}_{\bar{F}^*}. \tag{4.21}$$

Here the block stiffness matrix, block solution vector and block load vector are denoted by A^*, X^* and $\bar{F}^*$ respectively. The entries in block stiffness matrix for the respective local element are expressed in term of $(\xi - \eta)$ coordinates as

$$\begin{aligned}
\Upsilon_{\mathrm{ij}}^{11} =& a_1 \int_\Omega \left[\left(\sum_{j=1}^{m} \widehat{U}_j \xi_j \right) \frac{\partial \xi_j}{\partial X} + \left(\sum_{j=1}^{m} \widehat{V}_j \xi_j \right) \frac{\partial \xi_j}{\partial Y} \right] d\Omega + a_4 \int_\Omega \xi_j \xi_i d\Omega + a_5 \int_\Omega \xi_j \xi_i d\Omega \\
&+ a_2 \int_\Omega \left(\frac{\partial \xi_j}{\partial X}\frac{\partial \xi_i}{\partial X} + \frac{\partial \xi_j}{\partial Y}\frac{\partial \xi_i}{\partial Y} \right) d\Omega + a_7 \int_\Omega \xi_j \xi_i d\Omega, \\
\Upsilon_{\mathrm{ij}}^{12} =& - a_6 \int_\Omega \xi_j \xi_i d\Omega, \\
\Upsilon_{\mathrm{ij}}^{14} =& - a_3 \int_\Omega \xi_j \xi_i d\Omega, \\
\Upsilon_{\mathrm{ij}}^{21} =& - a_{13} \int_\Omega \xi_j \xi_i d\Omega, \\
\Upsilon_{\mathrm{ij}}^{22} =& a_8 \int_\Omega \left[\left(\sum_{j=1}^{m} \widehat{U}_j \xi_j \right) \frac{\partial \xi_j}{\partial X} + \left(\sum_{j=1}^{m} \widehat{U}_j \xi_j \right) \frac{\partial \xi_j}{\partial Y} \right] d\Omega + a_{11} \int_\Omega \xi_j \xi_i d\Omega + a_{12} \int_\Omega \xi_j \xi_i d\Omega \\
&+ a_9 \int_\Omega \left(\frac{\partial \xi_j}{\partial X}\frac{\partial \xi_i}{\partial X} + \frac{\partial \xi_j}{\partial Y}\frac{\partial \xi_i}{\partial Y} \right) d\Omega + a_{14} \int_\Omega \xi_j \xi_i d\Omega, \\
\Upsilon_{\mathrm{ij}}^{44} =& \int_\Omega \left[\left(\sum_{j=1}^{m} \widehat{U}_j \xi_j \right) \frac{\partial \xi_j}{\partial X} + \left(\sum_{j=1}^{m} \widehat{V}_j \xi_j \right) \frac{\partial \xi_j}{\partial Y} \right] d\Omega + a_{15} \int_\Omega \left(\frac{\partial \xi_j}{\partial X}\frac{\partial \xi_i}{\partial X} + \frac{\partial \xi_j}{\partial Y}\frac{\partial \xi_i}{\partial Y} \right) d\Omega, \\
\Upsilon_{\mathrm{ij}}^{24} =& -a_{10} \textstyle\int_\Omega \xi_j \xi_i d\Omega, \\
\Upsilon_{\mathrm{ij}}^{41} =& -J^* \sin\psi \textstyle\int_\Omega \xi_j \xi_i d\Omega,
\end{aligned}$$

$\Upsilon_{ij}^{42} = -J^* \cos\psi \int_\Omega \xi_j \xi_i d\Omega,$

where for the entries Υ_{ij}^{41} and Υ_{ij}^{42}, J^* can be written as

$$J^* = a_{16} \left[\left(\sum_{j=1}^{m} \widehat{U}_j \xi_j \right) \sin\psi - \left(\sum_{j=1}^{m} \widehat{V}_j \xi_j \right) \cos\psi \right].$$

Further, the entries Υ_{ij}^{13}, Υ_{ij}^{23}, Υ_{ij}^{31} and Υ_{ij}^{32} are the pressure matrices with their respective transposes. These are mentioned below

$$\mathbf{B}_1 = -\int_\Omega \frac{\partial \xi_i}{\partial X} \eta_j d\Omega, \qquad \mathbf{B}_2 = -\int_\Omega \frac{\partial \xi_i}{\partial Y} \eta_j d\Omega,$$
$$\mathbf{B}_1^{\mathrm{T}} = \int_\Omega \frac{\partial \xi_j}{\partial X} \eta_i d\Omega, \qquad \mathbf{B}_2^{\mathrm{T}} = \int_\Omega \frac{\partial \xi_j}{\partial Y} \eta_i d\Omega.$$

Inspite of above, $\Upsilon_{ij}^{33} = \Upsilon_{ij}^{34} = \Upsilon_{ij}^{43}$ are participating as null entries in global stiffness matrix.

The resulting discretized system of nonlinear algebraic equations includes the Laplace, mass and convective matrices along with nonlinear terms. Nonlinear terms are linearized by using fixed point iteration technique. Finally, the linearized algebraic system is then solved by using Gaussian elimination method to achieve final approximated results. The stopping criterion will remain same for this present case as mentioned in **Chapter** 3 to ensure the convergence of approximated solution.

4.5 Result Discussion

The effects of magnetic field inclination and Joule heating on mixed convective nanofluid flow in an inclined porous channel with cavity have been analyzed numerically. The channel is inclined at angle $\gamma = 45°$. The nanofluid is alumina-water which is viscous, laminar and Newtonian fluid. The left wall of cavity is heated in this case. The effects of magnetic field are controlled by rotating it in counterclockwise direction for different values of ψ. The numerical results are recorded in term of many physical parameters to study their influence on the behaviour of flow. These parameters along with ranges include ($0.01 \leq Ri \leq 10$),

$(0 \leq Ha \leq 200)$, $(10^{-5} \leq Da \leq 10^{-1})$, $(0.2 \leq \epsilon \leq 0.8)$ and $(0° \leq \psi \leq 90°)$ are mentioned where needed. The Prandtl number is fixed for this present study, i.e., $Pr = 6.2$. Visualization of resluts are displayed in terms of streamlines, isotherms and graphical plots for average Nusselt numbers.

The effects of Richardson number in terms of forced, mixed and natural convection on streamlines and isothermal patterns are presented in **Figs**. 4.2 and 4.3 for magnetic field inclination angles $\psi = 30°$ and $90°$ respectively. In **Fig.** 4.2, the streamlines (left) distinctly depicts the movement of flow for different modes of convection for $Ri = 0.01, 1$ and 10 at $\psi = 30°$. For $Ri = 0.01$, the forced convection leads at this low value of Richardson number. The inertial forces of fluid are activated for which streamlines seem more confined to the upper side of channel and a weak flow movement is noticed near the left wall of cavity. Mixed convection dominated flow is at $Ri = 1$ for which the strength of buoyancy forces and shear forces are equal. At this value all streamlines shift towards the central region of open cavity and then move towards the outlet region of channel with observable velocity. Hence a visible cluster of streamline curves is formed at the central portion of cavity. As Ri reaches to 10, the natural convection activates for this high value of Richardson number. The streamlines move from left side to the right side of cavity due to high buoyancy force effects and hence a fine flow circulation is detected inside the cavity region. Similar results have been noticed for isotherms (right) in **Fig.** 4.2. For $Ri = 0.01$, more fluid layers are restricted at the left heated wall of cavity due to high shear forces and as a result less thermal energy layers are bounded at the bottom wall of cavity. For natural convection at $Ri = 10$, intense thermal fluid layers are evidently observed in the bottom region of cavity which move to the right wall due to high buoyancy forces. **Fig.** 4.3 shows improved heat convection results for vertical magnetic field inclination $\psi = 90°$ as Ri ascends from 0.01 to 10. As Ri increases from 0.01 to 1, streamlines (left) expands more vigorously towards the central region of cavity due to weak effects of shear forces and increased strength of magnetic forces. At $Ri = 10$, the streamline curves intensely shifted towards the right corner of cavity. This happens due to the noticeable effect of bouyancy forces as compared to Lorentz force. In case of

isotherms (right), as Ri grows from 0.01 to 10, a very thin thermal boundary layer develops at the bottom wall of cavity due to high buoyancy fluid forces. Hence an observable free convective temperature gradient is located at the bottom wall and the right corner of cavity at $Ri = 10$.

The influence of different Hartmann numbers on flow's behaviour is portrayed in **Figs.** 4.4 and 4.5 for magnetic field inclination angles $\psi = 30°$ and $\psi = 90°$. In the absence of magnetic field at $Ha = 0$ (in both Figures), the maximum distribution of streamlines (left) is noticed inside the open cavity region while in isotherms (right), visible thin isothermal lines are observed at the bottom wall of cavity. For both cases this situation ensures the presence of maximum heat layers inside cavity region at $Ha = 0$. In **Fig.** 4.4 (left), as the strength of magnetic field is increased up to $Ha = 50$, the flow enters into the channel with increased velocity but the out flow velocity is decreased due to the presence of Lorentz force. Streamlines (left) seem to be merged at the left heating wall of cavity. Due to this effect a weak flow movement is viewed inside the open cavity region. Shear forces of fluid are reduced at magnetic field of strength $Ha = 100$. At this value, a thin cluster of streamlines is analyzed with the left wall of cavity. While an observable amount of fluid is confined to the upper horizontal channel moving towards the outlet side with decreased velocity due to high strength of Lorentz force. The strength of thermal layers in terms of isotherms for $Ha = 50$ and $Ha = 100$ at $\psi = 30°$ is presented in **Fig.** 4.4 (right). A noticeable temperature field is present with the left wall and middle of the bottom side of cavity which seem to be distorted at the right corner showing the presence of less amount of heat energy inside cavity. This effect is strengthen gradually for $Ha = 100$. At this highest strength of magnetic field, the influence of buoyancy force is reduced. Hence visible, thick and more deformed thermal layer distribution is obsreved from left to right wall of cavity. These heat layers gradually move towards the upper right side of channel due to strong effects of Lorentz force and leaving the decreased amount of heat in cavity region. For vertical position of magnetic field, i.e, $\psi = 90°$, evident thermal activity is noted for $Ha = 0, 50$ and 100 in **Fig.** 4.5. The average Nusselt number gradually increases for these values of Ha than previous case. For $Ha = 50$ and $Ha = 100$,

the combined strength of shear and buoyancy forces is greater than the effects of Lorentz force at $\psi = 90°$. Streamlines (left) are depicting that the flow enters into the channel and moves towards the cavity with distinct velocity. Similarly a distinguishable velocity of flow is analyzed clearly at the outlet of channel due to the decreased influence of Lorentz force. More amplified results are revealed for isotherms (right) at vertical position of magnetic field. For incremented value of Ha notable temperature distribution is seen inside the cavity. At $Ha = 100$, more integrated heat layers are formed at enclosure's left wall, which consequently move towards the enclosure's right side and to the upper right side of horizontal channel.

The impacts of magnetic field orientations to study the behaviour of heat transport on nanofluid flow with $Ha = 100$ have been presented in **Fig.** 4.6. Less convective heat transfer is observed for horizontal alignment of magnetic field, i.e., $\psi = 0°$. Streamlines (left) revealed that the flow is more concentrated in the upper horizontal channel without moving into the open cavity. Flow is passing with maximum velocity from the left inlet to the right outlet of channel with ceased flow motion inside open cavity region. A visible constriction of streamline curves along the left wall of cavity is viewed for inclined field angle $\psi = 30°$. At this magnetic field's layout, flow moves with decreased velocity from the channel due to the influence of Lorentz force. The strength of magnetic force is dominated here than shear forces of fluid. For tilted angle $\psi = 60°$ of magnetic field, most amplified convective heat transfer is analyzed. More fluid layers are entering into the channel and travel towards the open cavity region. Shear forces seem to lead the flow's movement from left wall to the central region of cavity. Hence the combined effects of shear and Lorentz force results in minimum outlet velocity. For horizontal magnetic field at $\psi = 0°$, isotherms (right) are allocated throughout the cavity assures the minimum presence of heat inside cavity. Isotherms for tilted angle $\psi = 30°$ seem more attached with the left heated wall of enclosure and deformed as progress towards right wall. Heat flow towards outlet is prominent in this case. Hence less heat dispension is observed inside the open cavity region. For magnetic field alignment at $\psi = 60°$, maximum heat layers are confined with the

left wall and at the bottom wall of cavity. So maximum thermal energy is noticed inside the cavity region. For vertical magnetic field, i.e., $\psi = 90°$, the impact of shear and bouyancy forces is eminant due to which isothermal lines are merged with left and bottom wall and a visible heat outflow occurs.

The significant impressions of Ri and Ha to analyze the convective heat distributions in terms of Nu_{avg} for different magnetic field inclinations is illustrated in **Figs.** 4.7 and 4.8. Reduction in convective heat transfer is viewed for the increasing values of Ri in **Fig.** 4.7. Forced convection at $Ri = 0.01$ seems to dominate in this regard for all magnetic field angles. With the augmentation in the orientation of magnetic field, increased values of Nu_{avg} are observed. Most enhanced heat transfer process is seen at $\psi = 90°$. Hence rise in magnetic field alignments produces much improved convective heat transport process. In **Fig.** 4.8, Nu_{avg} decreases progressively for increasing values of Ha from 0 to 200 at horizontal layout of magnetic field, i.e., $\psi = 0°$. More amplified results are noticed for inclined angle $\psi = 30°$ and vertical angle $\psi = 90°$ with growing values of Ha. At $Ha = 0, 50$ and 100, Nu_{avg} increases due to the least effects of magnetic force. The magnified values of Ha which are $Ha = 150$ and 200 produce decreased values of Nu_{avg} gradually due to maximized strength of magnetic force.

The diversification of Nu_{avg} for different magnetic field inclinations and porosity parameter is portrayed in **Figs.** 4.9 and 4.10. In **Fig.** 4.9, less convective heat transfer is seen for horizontally aligned magnetic field, i.e., $\psi = 0°$ for nanoparticles volume fraction $\phi = 0$. As the inclination approaches to $\psi = 60°$, augmented value of Nu_{avg} is noted. This situation leads to evident heat convection. This variation starts to drop down for magnetic field inclination greater than $\psi = 60°$. Reducing trend for heat distribution in pure fluid is observable at angles $\psi = 150°$ and $\psi = 180°$. Beside of this, intensified convective heat transfer is found for nanofluid case, i.e., $\phi = 0.04$ at the same magnetic field inclinations. The influence of increasing porosity parameter on Nu_{avg} is shown in **Fig.** 4.10. Minimum heat transfer is depicted on low values of porosity parameter, i.e., $\epsilon = 0.2$ due to high drag force effects of porous medium. As the porosity of medium rises up to $\epsilon = 0.8$, a distinguishable increase in Nu_{avg} has been analyzed. Overall, a

gradual augmentation in convection process is detected with the CCW rotations of magnetic field.

The effects of Ec on Nu_{avg} for different magnetic field inclinations and solid volume fractions in thermal energy distributions are inspected in **Figs.** 4.11 and 4.12. The average Nusselt number is slightly decreasing with the increasing variations in Eckert number in **Fig.** 4.11. Constant values of Nu_{avg} are seen at the smallest values of Ec, which are 10^{-5}, 10^{-4} and 10^{-3} and slightly decreasing values for $Ec = 10^{-2}$ and 10^{-1}. But as the field inclinations are progressing the ratio of convective heat transfer to heat transfer by conduction increases, i.e., Nu_{avg} enhances. As magnetic layouts are incrementing, the strength of magnetic force is also growing especially at $\psi = 90°$. This growing strength reduces the kinetic energy of flow although the Eckert numbers are rising. Hence for each magnetic field inclination pronounced convective heat transfer is noticed. Average Nusselt number is compared with different nanoparticles volume fraction (ϕ) for different Eckert numbers ($10^{-5} \leq Ec \leq 10^{-1}$) in **Fig.** 4.12. Average heat transfer increases with growing solid volume fraction of nanoparticles. Significant reduction in convection process is notified for rising Eckert numbers due to intensified activation of kinetic energy of fluid. At these values enhanced temperature distribution is occurred inside the whole cavity due to internal heating effects by the resistance of nanofluid's particles. Further, it favours in the least Nu_{avg} because internal heat seems more confined to the cavity region especially at $Ec = 10^{-1}$. The fact behind this seems that heat transfer process is dominated by thermal conduction at the rising Eckert numbers.

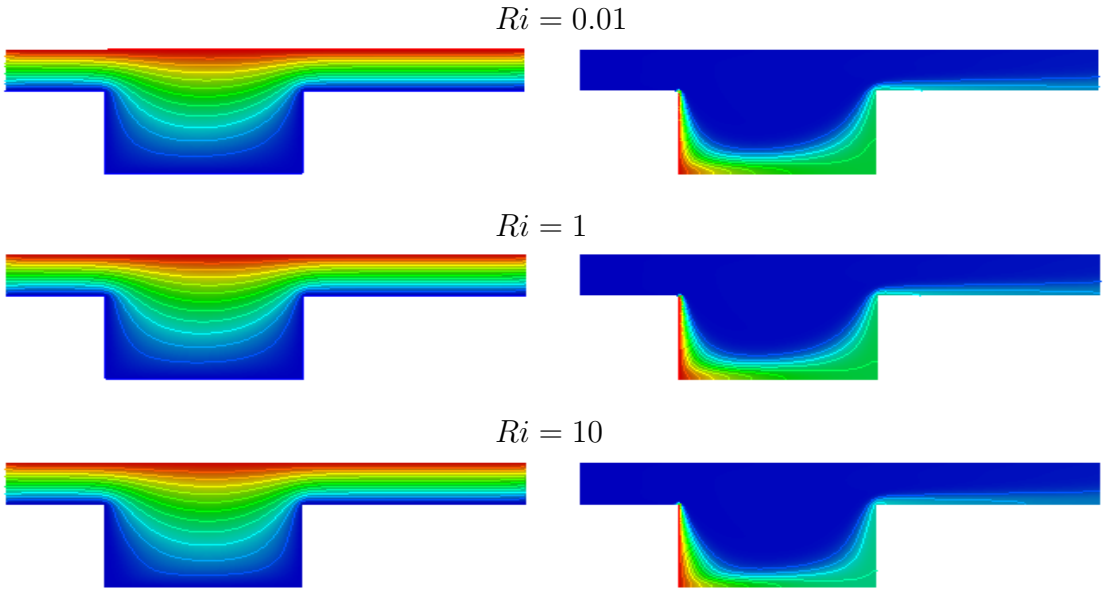

Figure 4.2: Depiction of isothermal patterns (Right) and streamline contours (Left) with increasing Ri at $\psi = 30°$.

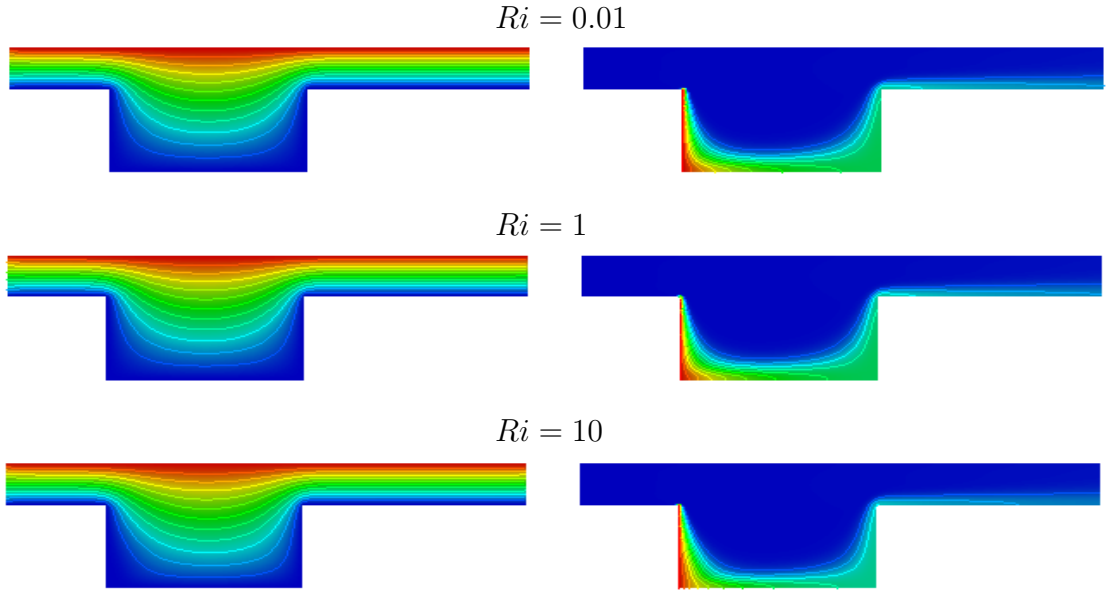

Figure 4.3: Depiction of isothermal patterns (Right) and streamline contours (Left) with increasing Ri at $\psi = 90°$.

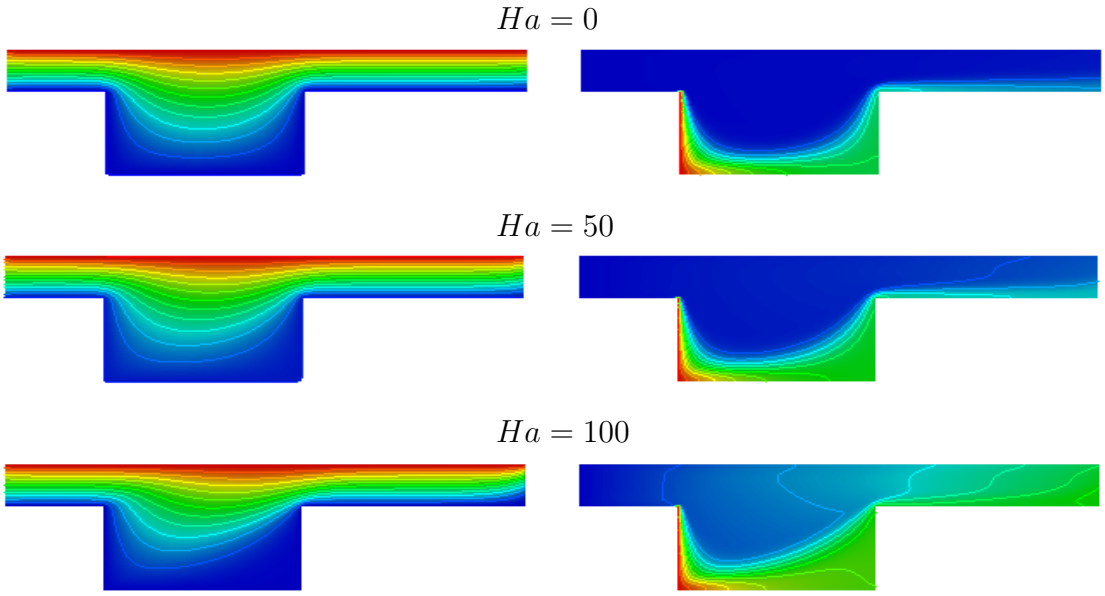

Figure 4.4: Depiction of isothermal patterns (Right) and streamline contours (Left) with increasing Ha at $\psi = 30°$.

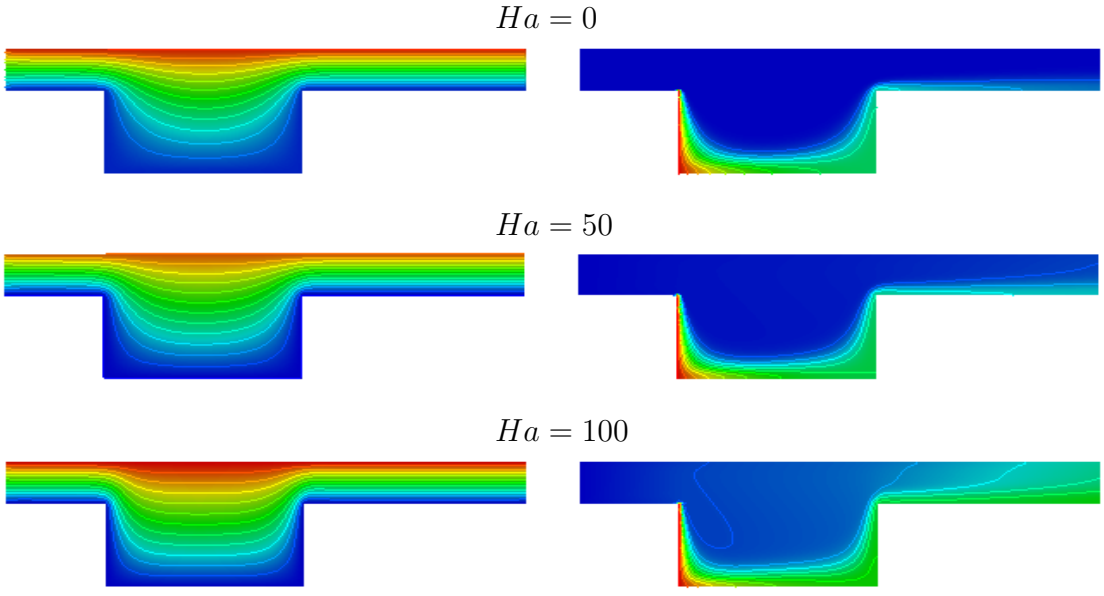

Figure 4.5: Depiction of isothermal patterns (Right) and streamline contours (Left) with increasing Ha at $\psi = 90°$

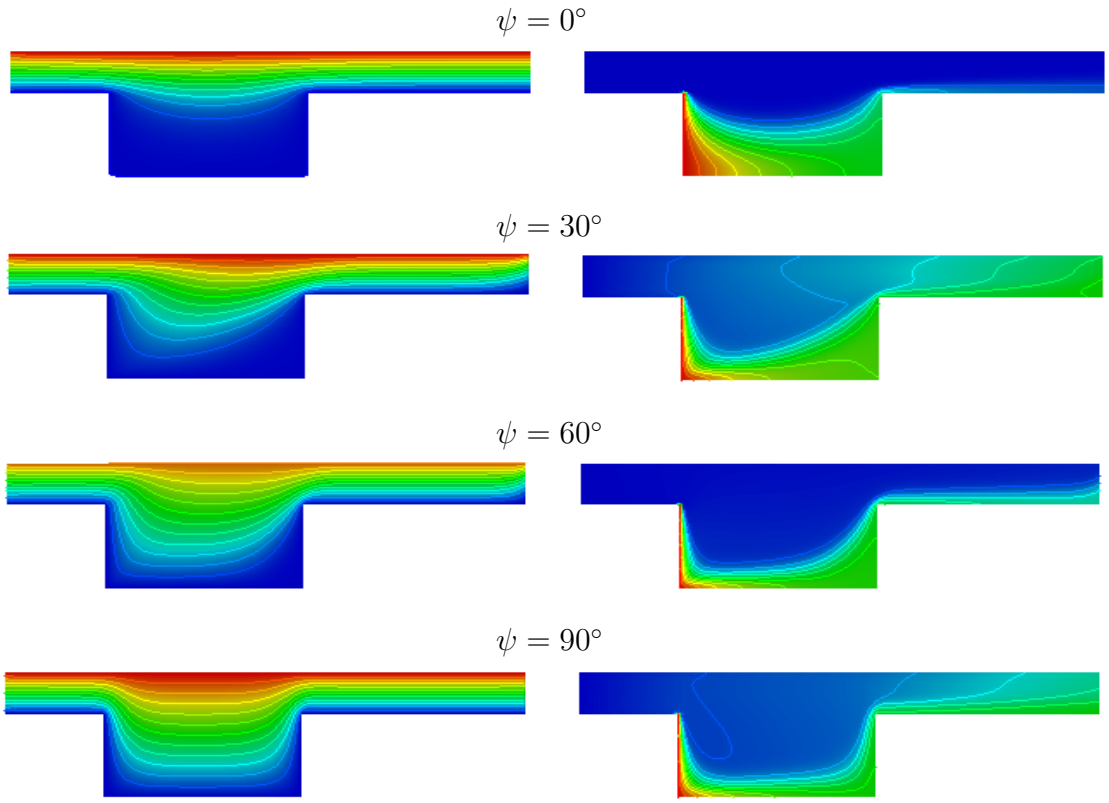

Figure 4.6: Depiction of isothermal patterns (Right) and streamline contours (Left) for different magnetic field rotations ψ at $Ha = 100$.

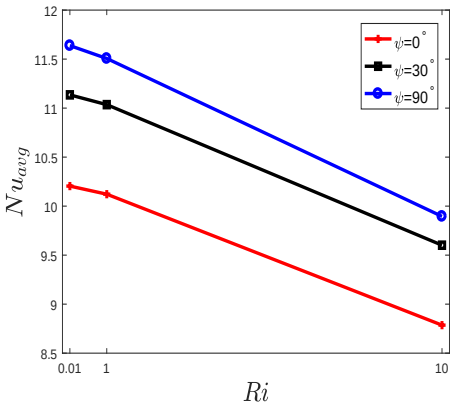

Figure 4.7: Contrast of Nu_{avg} with increasing Richardson number (Ri) for magnetic field angles (ψ°).

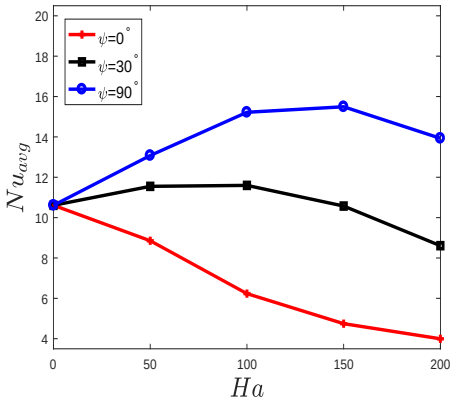

Figure 4.8: Contrast of Nu_{avg} with increasing Hartmann number (Ha) for magnetic field angles (ψ°).

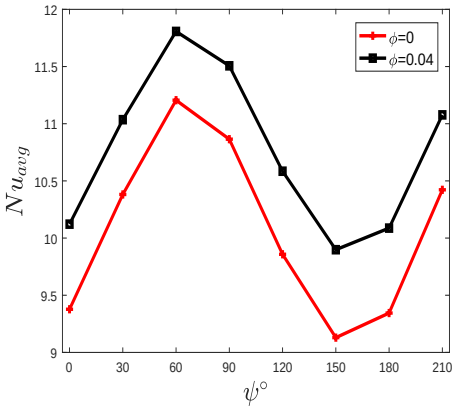

Figure 4.9: Contrast of Nu_{avg} with increasing magnetic field angles (ψ°) for pure fluid and nanofluid.

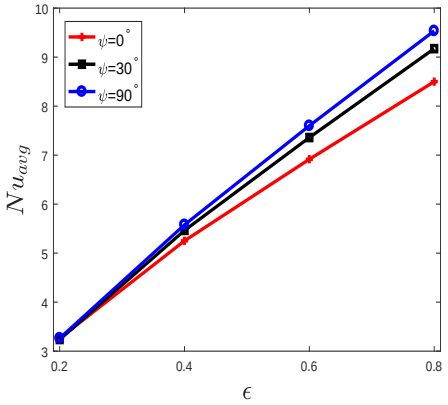

Figure 4.10: Contrast of Nu_{avg} with increasing porosity (ϵ) for magnetic field angles ($\psi°$).

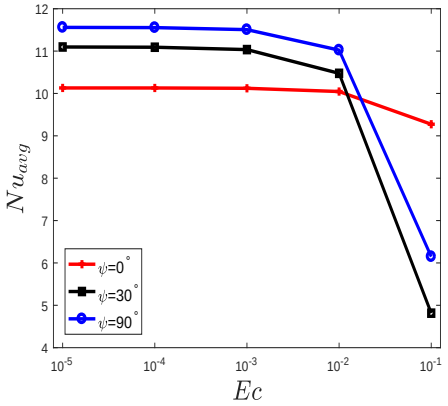

Figure 4.11: Contrast of Nu_{avg} with increasing Eckert number (Ec) for magnetic field angles ($\psi°$).

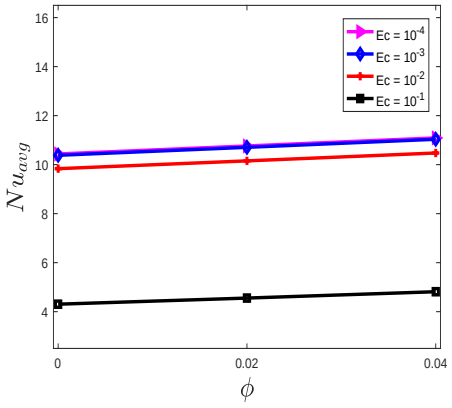

Figure 4.12: Contrast of Nu_{avg} with increasing solid particles volume fraction (ϕ) for different Eckert numbers (Ec).

Chapter 5

Conclusion

This research work is conducted to study about the effects of different inclination angles of an external magnetic field and role of Joule heating on mixed convective alumina-water nanofluid flow. The flow is moving through an open ended channel with an open cavity inside it. Heating source is attached with the left wall of this one sided open cavity of the horizontal channel. We are keen to explore the maximum thermal energy distribution in the cavity region. To analyze this temperature distribution, different thermophysical parameters are introduced to study heat flow impacts on the fluid flow. For this purpose porous medium is added to extravagant heat transport process. The DBF model for the porous medium is used to analyze its role in this heat governing phenomenon. The physical parameters which are productive in studying the impacts of convective heat transfer in flow are Richardson number, Reynolds number, Hartmann number, Darcy number, cavity inclinations, porosity parameter, magnetic field inclination, solid volume fraction of particles and Eckert number. Numerical simulations have been performed by using GFEM. Finite element approach is used for the discretization of solution fields. The space discretization of velocity, temperature and pressure field components is performed by utilizing higher order LBB-stable Q_2/P_1^{disc} finite element pair. Here biquadratic element space (Q_2) is utilized to discretize velocity and temperature components of governing system whereas discontinuous linear finite element space (P_1^{disc}) is used to discretize pressure field. This condition leads to the third order

accuracy of continuous biquadratic quadrilateral element (Q_2) while second order accuracy of discontinuous linear (P_1^{disc}) element in L_2 norm. Gaussian quadrature methods are used to solve integration of each elemental terms. At the end, the nonlinear discretized system is linearized by using fixed point iteration scheme.

The ongoing problem is the extension of exceptional work by Hussain et al. [43] by further focusing on the role of the magnetic field inclinations on flow's behavior. Moreover, the resistive heat occurrence by nanoparticles due to external magnetic field is added in energy equation in terms of Joule heating effect. In this proposed problem, the magnetic field of strength **B** is rotating externally in counterclockwise direction outside the whole channel. The magnetic field alignments are chosen as ($0° \leq \psi \leq 90°$). For this ongoing case, the channel inclination is fixed at $\gamma = 45°$. In addition to this, numerical results are shown in terms of streamlines and isothermal patterns to study flow-velocity behaviour and thermal energy distributions inside the whole channel. The variations in Nu_{avg} to view heat convection process is illustrated in the form of useful MATLAB plots.

Concluding Remarks

The significant exploration of this present research can be concluded as below:

- An augmentation in convective heat transfer has been observed for mixed convective regime at different magnetic field inclinations $0°, 30°$and $90°$ respectively for increasing Richardson number. Maximum rise in Nu_{avg} is noticed at the magnetic field alignment $\psi = 90°$ with high buoyancy force effect.

- Significant reduction in Nu_{avg} is inspected for flow patterns at the increasing Hartmann number. More intensified values of Nu_{avg} are found at CCW rotated magnetic field angles with increasing magnetic field strength.

- Increasing the magnetic field inclination, i.e., ($0° \leq \psi \leq 90°$) gives the enhanced results for convective heat transfer. Most amplified Nu_{avg} is viewed at $\psi = 60°$.

- Average Nusselt number grows for the increasing porosity parameter at different magnetic field inclinations. Notable augmentation in Nu_{avg} is seen at $\psi = 90°$.

- Reduced variations are analyzed in convective heat distribution with the increments in Eckert number. Amplified convection process is seen with CCW tilts of magnetic field for different Eckert numbers especially at vertical angle $\psi = 90°$.

- Exceptional convection is noticed for nanofluid at increasing solid volume fractions. Likewise, an evident decline in Nu_{avg} is observed for increasing Eckert number at different solid volume fractions.

Future Suggestions and Scope

The following are the few suggested directions to explore inventive areas in this present work:

- The above preceding study can be examined for un-steady nanofluid flow problem.

- Impacts of inclined magnetic field orientations on ferromagnetic nanoparticles for temperature distribution can be investigated.

- Opposing and horizontally heated flow can be inspected under the influence of inclined magnetic field.

- Higher order FEM can be employed for improved spatial discretization of governing PDEs.

- Many engineering obstacle problems dealing with such channels having hurdles like rotating cylinder, blocks, moveable plats, etc. can be inspected.

- Effects of sinusoidal temperature distributions can be analyzed on the same flow problem.

Bibliography

[1] Z. Zhai, "Application of computational fluid dynamics in building design: aspects and trends," *Indoor and Built Environment*, vol. 15, no. 4, pp. 305–313, 2006.

[2] R. Banerjee, X. Bai, D. Pugh, K. Isaac, D. Klein, J. Edson, W. Breig, and L. Oliver, "CFD simulations of critical components in fuel filling systems," Tech. Rep. 2002-01-0573, SAE Technical Paper, SAE 2002 World Congress, Detroit Michigan, pp. 1–19, March 2002.

[3] C. Zhang, M. Saadat, P. Y. Li, and T. W. Simon, "Heat transfer in a long, thin tube section of an air compressor: an empirical correlation from CFD and a thermodynamic modeling," in *American Society of Mechanical Engineers (ASME) 2012 International Mechanical Engineering Congress and Exposition*, vol. 7, (Houston Texas (USA)), pp. 1601–1607, 2012.

[4] B. Xia and D. W. Sun, "Applications of computational fluid dynamics (CFD) in the food industry: a review," *Computers and Electronics in Agriculture*, vol. 34, no. 1-3, pp. 5–24, 2002.

[5] X. Q. Wang and A. S. Mujumdar, "Heat transfer characteristics of nanofluids: a review," *International Journal of Thermal Sciences*, vol. 46, no. 1, pp. 1–19, 2007.

[6] S. U. S. Choi, "Nanofluid technology: current status and future research," Tech. Rep. ANL/ET/CP-97466,, Argonne National Lab.(ANL), Argonne, IL (United States), pp. 1–21, Oct.20,1998,.

[7] Y. Hwang, Y. Ahn, H. Shin, C. Lee, G. Kim, H. Park, and J. Lee, "Investigation on characteristics of thermal conductivity enhancement of nanofluids," *Current Applied Physics*, vol. 6, no. 6, pp. 1068–1071, 2006.

[8] Y. J. Hwang, J. Lee, C. Lee, Y. Jung, S. Cheong, C. Lee, B. Ku, and S. Jang, "Stability and thermal conductivity characteristics of nanofluids," *Thermochimica Acta*, vol. 455, no. 1-2, pp. 70–74, 2007.

[9] Y. Hwang, H. Park, J. Lee, and W. Jung, "Thermal conductivity and lubrication characteristics of nanofluids," *Current Applied Physics*, vol. 6, no. 1, pp. e67–e71, 2006.

[10] J. Buongiorno, "Convective transport in nanofluids," *Journal of Heat Transfer*, vol. 128, no. 3, pp. 240–250, 2006.

[11] S. Z. Heris, S. G. Etemad, and M. N. Esfahany, "Experimental investigation of oxide nanofluids laminar flow convective heat transfer," *International Communications in Heat and Mass Transfer*, vol. 33, no. 4, pp. 529–535, 2006.

[12] M. Mansour and S. E. Ahmed, "Mixed convection in double lid-driven enclosures filled with Al_2O_3–water nanofluid," *Journal of Thermophysics and Heat Transfer*, vol. 27, no. 4, pp. 707–718, 2013.

[13] A. Fereidoon, S. H. Saedodin, M. Esfe, and M. Noroozi, "Evaluation of mixed convection in inclined square lid-driven cavity filled with Al_2O_3/water nanofluid," *Engineering Applications of Computational Fluid Mechanics*, vol. 7, no. 1, pp. 55–65, 2013.

[14] A. Al-Amiri, K. Khanafer, J. Bull, and I. Pop, "Effect of sinusoidal wavy bottom surface on mixed convection heat transfer in a lid-driven cavity," *International Journal of Heat and Mass Transfer*, vol. 50, no. 9-10, pp. 1771–1780, 2007.

[15] M. Hossain and H. Takhar, "Radiation effect on mixed convection along a vertical plate with uniform surface temperature," *Heat and Mass Transfer*, vol. 31, no. 4, pp. 243–248, 1996.

[16] I. Kurtbas and N. Celik, "Experimental investigation of forced and mixed convection heat transfer in a foam-filled horizontal rectangular channel," *International Journal of Heat and Mass Transfer*, vol. 52, no. 5-6, pp. 1313–1325, 2009.

[17] S. Mirmasoumi and A. Behzadmehr, "Effect of nanoparticles mean diameter on mixed convection heat transfer of a nanofluid in a horizontal tube," *International Journal of Heat and Fluid Flow*, vol. 29, no. 2, pp. 557–566, 2008.

[18] S. Alchaar, P. Vasseur, and E. Bilgen, "Natural convection heat transfer in a rectangular enclosure with a transverse magnetic field," *Journal of Heat Transfer*, vol. 117, no. 3, pp. 668–673, 1995.

[19] O. Manca, S. Nardini, K. Khanafer, and K. Vafai, "Effect of heated wall position on mixed convection in a channel with an open cavity," *Numerical Heat Transfer: Part A: Applications*, vol. 43, no. 3, pp. 259–282, 2003.

[20] M. H. Esfe, M. Akbari, and A. Karimipour, "Mixed convection in a lid-driven cavity with an inside hot obstacle filled by an Al_2O_3–water nanofluid," *Journal of Applied Mechanics and Technical Physics*, vol. 56, no. 3, pp. 443–453, 2015.

[21] Z. Mehrez, M. Bouterra, A. El Cafsi, and A. Belghith, "Heat transfer and entropy generation analysis of nanofluids flow in an open cavity," *Computers & Fluids*, vol. 88, pp. 363–373, 2013.

[22] Z. Mehrez, A. El Cafsi, A. Belghith, and P. Le Quéré, "The entropy generation analysis in the mixed convective assisting flow of Cu–water nanofluid in an inclined open cavity," *Advanced Powder Technology*, vol. 26, no. 5, pp. 1442–1451, 2015.

[23] S. Hussain, S. Ahmad, K. Mehmood, and M. Sagheer, "Effects of inclination angle on mixed convective nanofluid flow in a double lid-driven cavity with discrete heat sources," *International Journal of Heat and Mass Transfer*, vol. 106, pp. 847–860, 2017.

[24] P. Kumar and V. Eswaran, "The effect of radiation on natural convection in slanted cavities of angle $\gamma = 45^0$ and 60^0," *International Journal of Thermal Sciences*, vol. 67, pp. 96–106, 2013.

[25] B. Ghasemi and S. Aminossadati, "Natural convection heat transfer in an inclined enclosure filled with a water-CuO nanofluid," *Numerical Heat Transfer, Part A: Applications*, vol. 55, no. 8, pp. 807–823, 2009.

[26] H. F. Oztop, K. Al-Salem, Y. Varol, I. Pop, and M. Fırat, "Effects of inclination angle on natural convection in an inclined open porous cavity with non-isothermally heated wall," *International Journal of Numerical Methods for Heat & Fluid Flow*, vol. 22, no. 8, pp. 1053–1072, 2012.

[27] F. Mabood, S. Shateyi, M. Rashidi, E. Momoniat, and N. Freidoonimehr, "MHD stagnation point flow heat and mass transfer of nanofluids in porous medium with radiation, viscous dissipation and chemical reaction," *Advanced Powder Technology*, vol. 27, no. 2, pp. 742–749, 2016.

[28] G. R. Machireddy and V. R. Kattamreddy, "Impact of velocity slip and Joule heating on MHD peristaltic flow through a porous medium with chemical reaction," *Journal of the Nigerian Mathematical society*, vol. 35, no. 1, pp. 227–244, 2016.

[29] M. Sheikholeslami and S. Shehzad, "Magnetohydrodynamic nanofluid convection in a porous enclosure considering heat flux boundary condition," *International Journal of Heat and Mass Transfer*, vol. 106, pp. 1261–1269, 2017.

[30] N. S. Gibanov, M. A. Sheremet, H. F. Oztop, and N. Abu-Hamdeh, "Effect of uniform inclined magnetic field on mixed convection in a lid-driven cavity having a horizontal porous layer saturated with a ferrofluid," *International Journal of Heat and Mass Transfer*, vol. 114, pp. 1086–1097, 2017.

[31] K. Mehmood, S. Hussain, and M. Sagheer, "Numerical simulation of MHD mixed convection in alumina–water nanofluid filled square porous cavity using KKL model: Effects of non-linear thermal radiation and inclined magnetic field," *Journal of Molecular Liquids*, vol. 238, pp. 485–498, 2017.

[32] R. Nasrin, S. Parvin, M. Alim, and A. J. Chamkha, "Non-Darcy forced convection through a wavy porous channel using CuO nanofluid," *Int. J. Energy Technol*, vol. 4, pp. 1–8, 2012.

[33] A. Hadim, "Numerical study of non-Darcy mixed convection in a vertical porous channel," *Journal of Thermophysics and Heat Transfer*, vol. 8, no. 2, pp. 371–373, 1994.

[34] S. Mahmud and R. A. Fraser, "Magnetohydrodynamic free convection and entropy generation in a square porous cavity," *International Journal of Heat and Mass Transfer*, vol. 47, no. 14-16, pp. 3245–3256, 2004.

[35] B. R. Kumar, P. Murthy, and P. Singh, "Free convection heat transfer from an isothermal wavy surface in a porous enclosure," *International Journal for Numerical Methods in Fluids*, vol. 28, no. 4, pp. 633–661, 1998.

[36] M. Sheikholeslami, "Numerical investigation of nanofluid free convection under the influence of electric field in a porous enclosure," *Journal of Molecular Liquids*, vol. 249, pp. 1212–1221, 2018.

[37] N. Makulati, A. Kasaeipoor, and M. Rashidi, "Numerical study of natural convection of a water–alumina nanofluid in inclined C-shaped enclosures under the effect of magnetic field," *Advanced Powder Technology*, vol. 27, no. 2, pp. 661–672, 2016.

[38] Y. Yirga and D. Tesfay, "Heat and mass transfer in MHD flow of nanofluids through a porous media due to a permeable stretching sheet with viscous dissipation and chemical reaction effects," *International Journal of Mechanical, Aerospace, Industrial, Mechatronic and Manufacturing Engineering*, vol. 9, no. 5, pp. 1–8, 2015.

[39] T. Grosan, C. Revnic, I. Pop, and D. Ingham, "Magnetic field and internal heat generation effects on the free convection in a rectangular cavity filled with a porous medium," *International Journal of Heat and Mass Transfer*, vol. 52, no. 5-6, pp. 1525–1533, 2009.

[40] M. Sheikholeslami, M. G. Bandpy, and D. D. Ganji, "Numerical investigation of MHD effects on Al_2O_3–water nanofluid flow and heat transfer in a semi-annulus enclosure using LBM," *Energy*, vol. 60, pp. 501–510, 2013.

[41] M. Sheikholeslami, M. G. Bandpy, R. Ellahi, and A. Zeeshan, "Simulation of MHD CuO–water nanofluid flow and convective heat transfer considering Lorentz forces," *Journal of Magnetism and Magnetic Materials*, vol. 369, pp. 69–80, 2014.

[42] N. Rudraiah, R. Barron, M. Venkatachalappa, and C. Subbaraya, "Effect of a magnetic field on free convection in a rectangular enclosure," *International Journal of Engineering Science*, vol. 33, no. 8, pp. 1075–1084, 1995.

[43] S. Hussain, K. Mehmood, M. Sagheer, and A. Farooq, "Entropy generation analysis of mixed convective flow in an inclined channel with cavity with alumina-water nanofluid in porous medium," *International Communications in Heat and Mass Transfer*, vol. 89, pp. 198–210, 2017.

[44] F. M.White, *Fluid Mechanics.* McGraw Hill, seventh ed., 2011.

[45] W. M. Rohsenow, J. P. Hartnett, and Y. I. Cho, *Handbook of Heat Transfer*, vol. 3. McGraw-Hill New York, third ed., 1998.

[46] F. Irgens, *Reology and Non-Newtonian Fluids.* Springer, 2014.

[47] Munson, Okiishi, Huebsch, and Rothmayer, *Fundamentals of Fluid Mechanics.* Jhon wiley and sons,inc., seventh ed., 2013.

[48] F. M.White, *Viscous Fluid Flow.* McGraw Hill, third ed., 2006.

[49] D. Tritton, *Physical Fluid Dynamics.* Van Nostrand Reinhold Company, first ed., 1977.

[50] A. C. Yunus and J. M. Cimbala, *Fluid Mechanics Fundamentals and Applications*, vol. 185201. International Edition, McGraw Hill Publication, first ed., 2006.

[51] H. O. Patrick and N. David, *Introduction to Convective Heat Transfer Analysis*. McGraw-Hill Companies Inc, first ed., 1999.

[52] M. H. Chaudhry, *Open-Channel Flow*. Springer Science & Business Media, second ed., 2007.

[53] R. P. Chhabra and J. F. Richardson, *Non-Newtonian Flow and Applied Rheology: Engineering Applications*. Butterworth-Heinemann, second ed., 2011.

[54] Y. Xuan and Q. Li, "Heat transfer enhancement of nanofluids," *International Journal of Heat and Fluid Flow*, vol. 21, pp. 58–64, 2000.

[55] R. Saidur, K. Leong, and H. Mohammad, "A review on applications and challenges of nanofluids," *Renewable and Sustainable Energy Reviews*, vol. 15, no. 3, pp. 1646–1668, 2011.

[56] N. Ali, J. A. Teixeira, and A. Addali, "A review on nanofluids: Fabrication, stability, and thermophysical properties," *Journal of Nanomaterials*, vol. 2018, pp. 1–33, 2018.

[57] M. Pakdemirli, "The boundary layer equations of third-grade fluids," *International Journal of Non-Linear Mechanics*, vol. 27, no. 5, pp. 785–793, 1992.

[58] A. Bejan, *Convection Heat Transfer*. John wiley & sons, fourth ed., 2013.

[59] S. Sureshkumar and M. Muthtamilselvan, "A slanted porous enclosure filled with Cu-water nanofluid," *The European Physical Journal Plus*, vol. 131, no. 4, pp. 1–95, 2016.

[60] D. A. Nield, A. Bejan, *et al.*, *Convection in Porous Media*, vol. 3. Springer, fifth ed., 2006.

[61] I. Pop and D. B. Ingham, *Transport Phenomena in Porous Media II*. Elsevier, first ed., 2002.

[62] R. Givler and S. Altobelli, "A determination of the effective viscosity for the Brinkman–Forchheimer flow model," *Journal of Fluid Mechanics*, vol. 258, pp. 355–370, 1994.

[63] J. H. Lienhard(IV/V), *A Heat Transfer Textbook*. Phlogiston Press, third ed., 2008.

[64] J. Kunes, *Dimensionless Physical Quantities in Science and Engineering*. Elsevier, first ed., 2012.

[65] C. Johnson, *Numerical Solution of Partial Differential Equations by the Finite Element Method*. Courier Corporation, 2012.

[66] H. Brinkman, "The viscosity of concentrated suspensions and solutions," *The Journal of Chemical Physics*, vol. 20, no. 4, pp. 571–571, 1952.

[67] J. Koo and C. Kleinstreuer, "A new thermal conductivity model for nanofluids," *Journal of Nanoparticle Research*, vol. 6, no. 6, pp. 577–588, 2004.

[68] J. Koo and C. Kleinstreuer, "Laminar nanofluid flow in microheat-sinks," *International Journal of Heat and Mass Transfer*, vol. 48, no. 13, pp. 2652–2661, 2005.

[69] N. S. Akbar, M. Raza, and R. Ellahi, "Peristaltic flow with thermal conductivity of $H_2O + Cu$ nanofluid and entropy generation," *Results in Physics*, vol. 5, pp. 115–124, 2015.

[70] J. C. Maxwell, *A Treatise on Electricity and Magnetism*, vol. 1. Oxford: Clarendon Press, 1873.

[71] J. Li and C. Kleinstreuer, "Thermal performance of nanofluid flow in microchannels," *International Journal of Heat and Fluid Flow*, vol. 29, no. 4, pp. 1221–1232, 2008.

[72] S. Hussain, F. Schieweck, and S. Turek, "Efficient Newton-multigrid solution techniques for higher order space–time Galerkin discretizations of incompressible flow," *Applied Numerical Mathematics*, vol. 83, pp. 51–71, 2014.

[73] S. M. Aminossadati and B. Ghasemi, "A numerical study of mixed convection in a horizontal channel with a discrete heat source in an open cavity," *European Journal of Mechanics-B/Fluids*, vol. 28, no. 4, pp. 590–598, 2009.